The Messenger

No. 155 – March 2014

Laser Guide Star Facility upgrade
VUDS — VIMOS Ultra Deep Survey
HUGS — HAWK-I ultra deep survey
Celebrating ESO's 50 years in Chile

ISAAC. An Appreciation

Jason Spyromilio[1]
Jean-Gabriel Cuby[2]
Chris Lidman[3]
Rachel Johnson
Andreas O. Jaunsen[4]
Elena Mason[5]
Valentin D. Ivanov[1]
Linda Schmidtobreick[1]

(The ISAAC Instrument Scientists in chronological order)

[1] ESO
[2] Laboratoire d'astrophysique de Marseille, Université Aix-Marseille & CNRS, Marseille, France
[3] Australian Astronomical Observatory, Epping, Australia
[4] Institute of Astrophysics, University of Oslo, Norway
[5] INAF–Osservatorio Astronomico de Trieste, Italy

ISAAC was switched off, almost certainly for the final time, on 12 December 2013. The last observing block executed was OB1030962, the target, Supernova 2013ct, for a programme whose principal investigator just happened to be the first instrument scientist for ISAAC. "All constraints were respected and spectra of the target detected" are the public comments in the log. A short history of ISAAC, from the instrument scientists' viewpoint, is presented.

Building ISAAC

The Infrared Spectrograph And Array Camera, ISAAC, was the second instrument mounted on the Very Large Telescope (VLT), following the FOcal Reducer and low dispersion Spectrograph (FORS1). The Principal Investigator (PI) of ISAAC was Alan Moorwood. Although various appreciations of Alan have already been made (e.g., de Zeeuw, 2011; Leibundgut et al., 2011) and it is certain that he made profound contributions to all aspects of ESO, ISAAC was one of his proudest creations. ISAAC was one of two first generation instruments for the VLT built in-house at ESO Garching by a team of people working for Alan in a deeply personal and motivating atmosphere (the other instrument was the Ultraviolet and Visible Echelle Spectrograph [UVES]).

Although much of the discussion on the instrumentation suite for the VLT took place prior to the approval of the project in 1987, the definitive instrumentation plan was authored by Sandro D'Odorico and Alan in June 1989. It appears prescient today, since almost all first generation instruments had their genesis in that document. ISAAC in effect was the outcome of option E4 for a combined spectrometer/imager exploiting a single detector. It should also be recalled that even in 1989 the choice of site for the VLT had not been settled. Vizchachas next to La Silla with four Unit Telescopes in a linear configuration was still the default option for the VLT, with Paranal being considered as an alternate site.

At the time of ISAAC's design design, and even in the early construction period, the instrument was baselined on 256 by 256 pixel detectors. It should be recalled that the first infrared camera: IRCAM on the UK Infra Red Telescope (UKIRT) only had first light in 1986 with a 62 × 58 indium antimonide (InSb) detector (McLean et al., 1986). By the time the instrument was deployed on Paranal in 1998, the short wavelength arm had a fancy new 1024 × 1024 HgCdTe detector, but the long wavelength detector was still a 256 × 256 pixel InSb device.

The team assembled by Alan to build ISAAC relied very much on the instrumentation experience at ESO, based on the immediate previous generation of instruments (IRSPEC on the New Technology Telescope [NTT] and the two infrared cameras on the MPG/ESO 2.2-metre telescope). Alan had already brought an infrared heritage to ESO in the Geneva days, from his work at ESA and flying balloons with infrared payloads at University College London. Under his leadership and a series of ever more successful instruments, an effective team had been created.

The optical design, as with almost all instruments at the VLT, came from the trusted hands of Bernard Delabre. Gotthard Huster designed the mechanical system with help from Ralf Gonzelmann. Jean-Louis Lizon and Armin Silver built the instrument. The mass and size of the monster were daunting. Cooling the instrument required the use of a pre-cooling circuit, prototyped on IRSPEC and now common in most infrared instruments deployed at the VLT. In 1996, during the big-bang upgrade of the NTT, IRSPEC was retired and its cryostat was used to test many of the mechanical functions of ISAAC.

As the PI was fond of saying, ISAAC had diamond-turned-nickel-coated-post-polished mirrors. The cold structure where the instrument optics were mounted was particularly complex and would have been almost impossible to machine from a single block. Two cast aluminium structures were made at a local foundry and the huge vacuum vessel came from France. The bearings used to turn the massive gratings and filter wheels were off the shelf. They were disassembled by Jean-Louis down to their smallest components and then reassembled without the outgassing and freeze-prone lubricants and were equipped with new rolling elements. The bearings for the ISAAC filter wheels are comparable in size to an entire IRAC (the IR camera for the 2.2-metre telescope commissioned in 1994) filter wheel.

With the high number of functions in ISAAC, the traditional warm motor with a feed through to the vacuum vessel was not an option. A development programme inside ESO converted commercial stepper motors to function in cryogenic conditions. For ESO, ISAAC was also the first instrument equipped from the start with closed-cycle coolers. The original Leybold compressor outlasted the instrument, with more than 100 000 hours of continuous operation. The enormous platform which carried the powered co-rotator and electronics (a feature that became a common solution for instruments at Paranal) arose as the only viable option as the instrument proceeded through the construction phase.

To cool down such a massive load, a custom ESO cryogenic control system was constructed by Joar Brynnel, who also built the electronics that would drive the instrument functions using early versions of the, then, ESO standard MACCON motor controllers. The pre-

Figure 1. Jean-Louis Lizon, who powered ISAAC up in 1998, switches the instrument off for the last time in December 2013.

Figure 2. A younger Jean-Louis Lizon than in Figure 1 checks the ISAAC cold structure #1 during the construction phase in 1995.

cooling accelerated the cool down, a process that came in very handy in testing, but also in operations when a stuck function had to be unstuck!

Gert Finger was in charge of the detector system, with Manfred Meyer building the readout electronics. During the programme Jorg Stegmeier and Leander Mehrgan joined the detector group to make the first generation of IRACE (Infra-Red Advanced Controller Electronics) controllers. Giana Nicolini helped with the characterisation of detectors and prepared the upgrade of the Santa Barbara Research Corporation (SBRC) 256 × 256 pixel InSb array to the brand new 32-channel Aladdin 1K × 1K InSb array. Transputers formed the basis of the readout electronics, while the IRACE platform, in a shift from the VLT standards of VxWorks on 68030 processors, moved to the newfangled Sparc machines that were all the rage. In a minor panic during the early years of operation, the remaining worldwide supply of T2 and T8 transputer chips were procured by ESO so as to have sufficient spares for ISAAC and, of course, the other infrared instruments that followed in its path.

Peter Biereichel who had written much, if not all, the software for the early infrared instruments led the control software effort and along the way brought in Thomas Herlin and Jens Knudstrup to help. Much effort was needed to tame the early versions of the VLT common software. Anton Van Dijsseldonk project-managed all this effort before the days when he would have been called project manager.

Getting ISAAC to the sky

Following some design review (there were not so many of them in those days), Alan was convinced to hire an instrument scientist to support the commissioning of the instrument and the development of data reduction tools. The first author of this appreciation was hired in 1993 for this post and was succeeded by the second author after less than 18 months on the job, and long before the instrument ever went to sky. The third author took over after commissioning, etc, etc. The list of ISAAC instrument scientists is hopefully identical to the authorship of this article. Many large and small problems needed to be resolved, such as how the instrument interacted with the telescope, calibration challenges, observing sequences, etc, etc. For example, chopping via a synchronised timing signal, rather than a hardware connection, may be a trivial issue today, but the ISAAC controller, mentioned above, was not compatible with the VLT standard hardware for timing. A simple solution of a hardware trigger from the TIM board (a VxWorks custom board built by ESO for timing synchronisation across the VLT) was used.

The ISAAC software innovation stable provided the three state buttons that continue to plague the VLT control panels and the Real Time Display (RTD). The VLT standards forbade dedicated hardware to connect the data acquisition system in the dome with the control room. As a minimum for target acquisition there was a need for a networked workstation display that allowed astronomers to interact with the data live, rather than waiting for a data reduction system to digest a FITS file. In the days before requirements documents, a conversation between the instrument scientist and Thomas Herlin to flesh out the idea of a display that would stop astronomers looking at finding charts through lamps to get the right orientation, provide trivial zooming and scaling and allow the instantaneous data as well as the integrated frame to appear in real time, resulted. Envisaged from the very start to have an application interface to allow plug-ins, the RTD was a wild success and is not only used for all detector systems on the VLT but in various incarnations also formed the basis for the *skycat* tool, the FORS Instrumental Mask Simulator (FIMS), and ended up in wide use by many observatories. Every acquisition at ESO's optical telescopes relies on the RTD to click the target or the guide star!

For infrared astronomers, prescription observing per templates was a significant psychological challenge to overcome. However, ISAAC was in many ways responsible for bringing the concepts of templates into VLT operations. Erik Allaert was critical in making the toolkit to manage scripted observations in a sensible manner: the resulting tool is now used

ubiquitously at Paranal, as the Broker for Observation Blocks, BOB. As an aside, his inclusion of positively poor sound choices also resulted in the silencing of BOB on most consoles. Copying from the Infrared Space Observatory (ISO) operations, the idea of templates was introduced into the ISAAC draft user manual in 1995 and was taken into the operations scheme as the building block for OBs by the Data Flow Project Team, co-ordinated by Preben Grosbøl, including, amongst others, Michèle Peron, Dietrich Baade and Bruno Leibundgut. ISAAC was the first VLT instrument with a full instrument observing simulator with panels and displays talking to code that generated pseudo-realistic data and simplistic pipelines.

The original proper ISAAC pipeline was developed by Nicolas Devillard and Yves Jung under the tutelage of Pascal Ballester and instrument scientists 2, 3, etc. The fixes, upgrades and updates, etc, are too numerous to mention. However, at some point after much discussion, we did get the sky subtraction right. Pascal also provided the early exposure time calculators.

Offspring and early days

Jean-Louis Lizon was expeditious in the assembly of the instrument in Garching and, with Unit Telescope 1 (UT1) first light slipping to 1998, Alan decided to use the expertise developed with ISAAC to rapidly develop an instrument for the soon to be upgraded NTT. Launched as a project in 1996, SofI, the Son of ISAAC, was in effect one imaging arm of ISAAC with a grism wheel providing the spectroscopic capabilities.

While the correct name for SofI obviously should have been JACOB (Jean-Gabriel's and Alan's Camera for OBserving) or for that matter ESAU (ESO Array Unit), pronunciation and modesty issues prevailed to leave us with SofI.

SofI went to the NTT in 1997 and was successfully commissioned by the PI, the construction team and instrument scientist number 2, while at the same time bringing up to speed the future instrument scientist number 3. The commissioning went ahead with very few problems, thereby testing not only the instrument, but also the bulk of the ISAAC software. By mid-1998, with UT1 in full swing of commissioning, Jean-Louis arrived on Paranal to begin the re-integration of ISAAC.

Figure 3. ISAAC *JHKs* colour combination mosaic image of the Galactic HII region and star-forming complex M16 (NGC 6611). H_2 emission knots show in red.

It is worth recalling that the instrument laboratory in the control room at that time had plastic sheets instead of windows and many facilities were sorely lacking. Alan oft would debate whether the occasional stuck filter wheel in ISAAC came from dust in the early days of integration. It is true that Jean-Louis has been to Paranal many times to keep the old dog going well past the design lifetime of three years continuous operation.

Commissioning of ISAAC was successful, even if interrupted by a stuck altitude motor cover on UT1 in February 1999, a complete demolition of the control room while instrument scientist number 2 debugged software and a disconnected telescope cooling hose that washed the whole Nasmyth platform down. ISAAC, together with FORS1, were incidentally the first instruments to be brought into the QC0 (Quality Control) and QC1 processes.

ISAAC observations

With over 850 papers to its name, ISAAC is almost certainly amongst the most productive infrared instruments. It is especially difficult to pick particular science results and our apologies are public and up-front. We have picked a few that entertained us.

Messier 16

Mark McCaughrean was a regular Christmas visitor observer at UT1 in the first years of operation. His kind, beautifully handwritten appreciation letters were

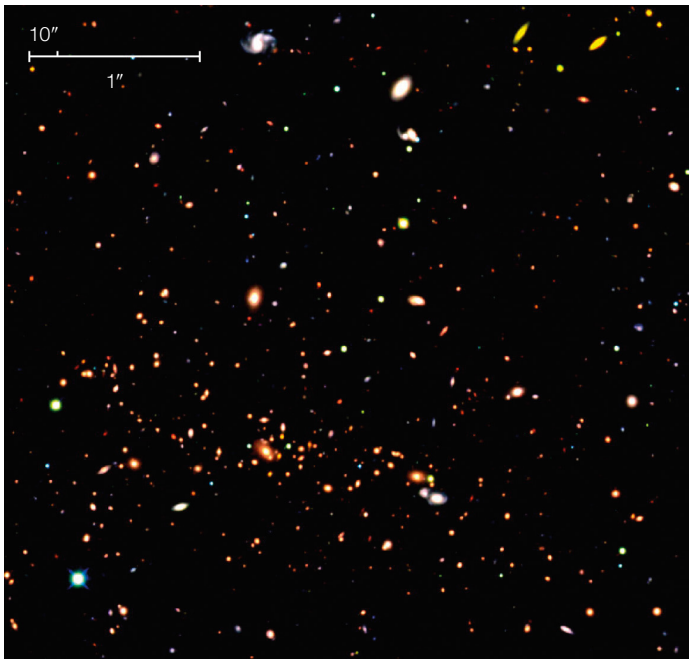

Figure 4. Three-colour composite image of the field around the massive galaxy cluster MS 1054-03 (z = 0.83) taken as part of FIRES. ISAAC *Js* and *Ks* and HST WFPC2 F814W images were combined as green, red, blue respectively. From Förster Schreiber et al. (2006).

posted on the whiteboard behind what was the UT1 console (now the VLT Interferometer), and his spectacular images of various nebulae (one is shown in Figure 3) have been icons of infrared astronomy since the very first images of Orion with IRCAM at UKIRT.

Faint Infrared Extragalactic Survey (FIRES)

Marijn Franx pestered the observatory into improving its efficiency of operations and calibration until we finally agreed that he was right all along. A 26.5-hour total integration time in *Ks*, 25.9 hr in *Js* and 24.4 hr in *H*, provided one of the most impressive deep fields from the ground.

The image quality of the data was truly spectacular with the final combined images below 0.52 arcseconds. An image from the FIRES programme is shown in Figure 4.

Spectroscopy of high-redshift galaxies

In the early days of the VLT quite a lot of catch-up with Keck was necessary. One of the best compliments to the instrument was the excellent dataset collected on high-redshift Lyman-break galaxies by Max Pettini, Alan, instrument scientist number 2 and Max's California and East Coast based collaborators. An example of a long-slit spectrum of a Lyman-break galaxy at z = 3.234 is shown in Figure 5.

Observing through the limb of Jupiter

Some observations simply don't fit the template package. Measuring, amongst others, the temperature profile of the Jovian atmosphere by taking spectra of HIP 9369 during an occultation by the limb of Jupiter was certainly one of the most memorable observations made. Keeping the slit orientation parallel to the limb in real time while everything is moving and turning was an observational *tour de force*. The results were published by Raynaud et al. (2003).

Acknowledgements

While it is probable that we have missed some of the people who participated in building ISAAC, it is wellnigh impossible to count and name all the staff at the La Silla Paranal Observatory who have worked (almost) every day for the past 15 years to keep the instrument going. But it would be impossible to conclude without attempting to thank some of them: Hans Gemperlein, Gustavo Rahmer, Markus Kissler-Patig, Vanesa Doublier, Steen Skole, Andreas Kaufer, Gianni Marconi, Claire Moutou, Eline Tolstoy, Ueli Weilenmann, Roberto Castrillo, Pablo Barriga, Gordon Gillet, Pedro Mardones, Massimilliano Marchesi, Eduardo Bendek, Alfredo Leiva, Jorge Jimenez, Nicolas Haddad and the rest of the cast, especially the instrument operation team members over the past 15 years. Many scientists in the Data Management Division in Garching, and observing at Paranal, have had the pleasure of interacting with ISAAC: Paola Amico, Mario van den Ancker, Tom Broadhurst, Fernando Comerón, Danuta Dobrzycka, Lowell Tacconi-Garman, Christian Hummel, Wolfgang Hummel, Sabine Mengel, Palle Møller, Monika Petr-Gotzens, Almudena Prieto, Francesca Primas, Martino Romaniello, David Silva, Elena Valenti, Markus Wittkowski and Bodo Ziegler have all had to live with the flips of the orientation of the slit and the rotations, the occasional glitch and the hundreds of users.

The instrument science team of Rolf Chini, George Miley, Tino Oliva and Jean-Loup Puget followed the instrument through the trials and tribulations of construction, picking filters and resolutions, and provided constant support.

Our final thanks must be reserved for Alan.

References

Andersen, M. et al. 2004, A&A, 414, 969
de Zeeuw, P. T. 2011, The Messenger, 145, 49
Förster Schreiber, N. M. et al. 2006, AJ, 131, 1891
Leibundgut, B. et al. 2011, The Messenger, 145, 50
McLean, I. et al. 1986, SPIE, 627, 430
Pettini, M. et al. 2001, ApJ, 554, 981
Raynaud, E. et al. 2003, Icarus, 162, 344

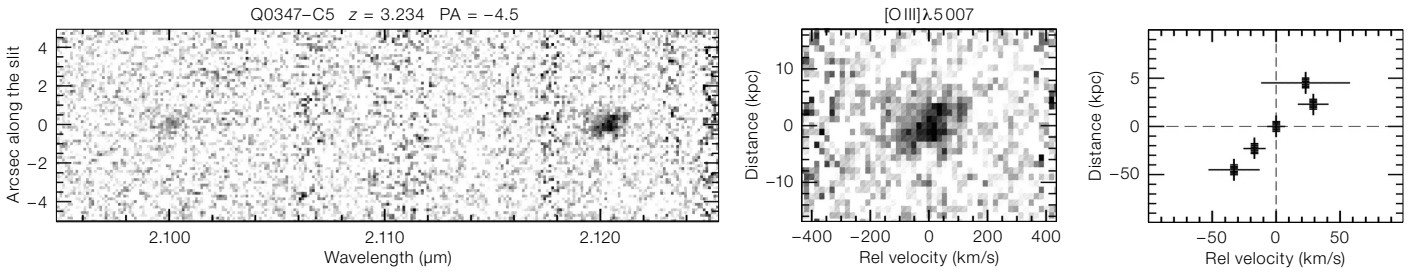

Figure 5. ISAAC long-slit spectra of the quasar Q0347-C5 taken by Max Pettini in 1999 (from Pettini et al., 2001). The left panel shows the two-dimensional spectrum with the [O III] 4959 Å and 5007 Å emission lines, the central panel an enlargement of the 5007 Å line kinematics and the right panel the fitted radial velocity along the slit.

Laser Guide Star Facility Upgrade

Steffan Lewis[1]
Domenico Bonaccini Calia[1]
Bernard Buzzoni[1]
Philippe Duhoux[1]
Gerhard Fischer[1]
Ivan Guidolin[1]
Andreas Haimerl[1]
Wolfgang Hackenberg[1]
Renate Hinterschuster[1]
Ronald Holzlöhner[1]
Paul Jolley[1]
Thomas Pfrommer[1]
Dan Popovic[1]
Jose-Luis Alvarez[1]
Juan Beltran[1]
Julien Girard[1]
Laurent Pallanca[1]
Miguel Riquelme[1]
Fréderic Gonte[1]

[1] ESO

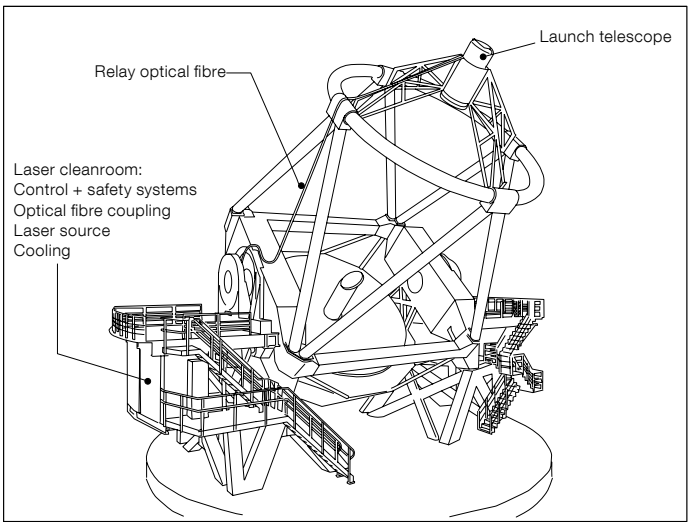

Figure 1. Sketch of VLT UT4 showing the main parts of the Laser Guide Star Facility.

The Laser Guide Star Facility is part of VLT Unit Telescope 4 and provides a single centre-launched sodium beacon for the two adaptive optics instruments SINFONI and NACO. The original facility, installed in 2006, employed a high-power dye laser source, PARSEC, producing an output beam that was delivered via a single-mode optical fibre to launch optics located behind the telescope secondary mirror. We recently installed a new prototype laser source, PARLA, based on Raman optical fibre technology. Requirements for the new laser include start-up times compatible with flexible observing, an output beam appropriate for the existing fibre-delivery system and an on-sky power of up to 7 watts. This is the first time that this type of laser has been deployed at a major observing facility, and it has a pathfinder role for future adaptive optics systems. Reported here are the main results of the development, deployment and early operation since the resumption of science operation in February 2013.

The Laser Guide Star Facility

The main parts of the Laser Guide Star Facility (LGSF) installed on the Very Large Telescope Unit 4 (VLT UT4, Yepun) and described by Bonaccini Calia et al. (2006), are shown in Figure 1. These include a laser cleanroom below the Nasmyth platform, an optical fibre beam relay and a launch optical system behind the telescope secondary mirror.

The laser cleanroom contains the bulk of the control and safety electronics, the optical fibre coupling system, and the laser source. In the original facility, the laser source was a dye laser system, PARSEC (Rabien et al., 2003), specified to produce a single-frequency spectral line centred on the sodium D_{2a} line at wavelength of 589.2 nm. The output beam from this laser was transmitted to the input of the relay optical fibre via a free-space beam relay on the laser bench. The role of this beam relay is to format the beam spatially and spectrally, and to actively stabilise the beam position and direction in order to maintain the optical fibre coupling efficiency during operation. Spectral formatting consists of broadening the laser line using a phase modulator in order to increase the total power that can be transmitted through the relay optical fibre.

A large mode area solid-core photonic crystal optical fibre transports the high-power visible laser beam from the laser cleanroom to the launch optics located behind the VLT UT4 secondary mirror. This optical fibre has a length of 27.5 metres, a core mode field diameter of approximately 14 µm and a numerical aperture of 0.04. Transmission losses, excluding input coupling, are approximately 10 %.

The launch optics, mounted behind the secondary mirror of the main telescope, receive the visible-light output from the relay fibre and propagate a nearly collimated 50 cm diameter beam onto the sky. They provide beam expansion, focusing, tip-tilt beam stabilisation and diagnostic functionality.

The scope of the upgrade reported here was to install a new prototype laser source. Other subsystems of the LGSF are essentially unchanged.

Sodium excitation

A sodium laser guide star (LGS) is formed by resonantly back-scattering laser light from atomic sodium in the upper mesosphere and lower thermosphere (abbreviated MLT). Optimisation of the laser format to maximise the return flux is being actively studied (Holzlöhner et al., 2010).

Optical radiation at 589 nm was first observed in the night-sky spectrum by V. M. Slipher in 1929 (Slipher, 1929). This radiation was later attributed to emission from neutral sodium atoms occurring mainly in the upper mesosphere (Bernard, 1939), excited by solar radiation. Lying above the range of aircraft, but below the altitude of orbiting spacecraft, the mesosphere is one of the least accessible and most poorly characterised regions of the Earth's atmosphere. Typically it is studied with sounding rockets or observed remotely using laser light detec-

tion and ranging (LIDAR) systems, and from satellites.

The region where atomic sodium is present lies at an altitude range of around 80–120 kilometres with some seasonal variation as well as latitude dependencies. The MLT is one of the coldest regions on Earth, at a temperature of around 180 K. This region is characterised by a number of other features including strong zonal winds, atmospheric tides and overturning gravity waves. Amongst the metals present there are Fe, K, Ca and Na, and it is generally held that this layer of metal atoms and ions is replenished by micrometeors in the microgram range, that is, interplanetary dust particles that are incident on the Earth and ablated in the upper atmosphere.

Although Fe is the most abundant metal atom in this region, Na is used for LGS applications because it has the highest product of abundance and optical transition cross-section at an accessible laser wavelength. Its mean column density is 4×10^9 cm^{-2}, which is a factor of 10^{-8} of the number for air molecules present in that region. At the lower boundary of the sodium layer, the concentration of oxygen radicals, which originate from ozone, is high enough to form products of sodium hydroxyl and other molecules, and thus remove atomic sodium. Above a temperature-dependent threshold, this process appears to be very efficient and the lower edge of the sodium layer is more sharply defined than the upper edge, where ablated sodium ions recombine with electrons from the ionosphere and from Solar radiation to form atomic sodium.

The sodium *D*-line, which is split into a fine structure doublet D_1 and D_2 at vacuum wavelengths of 589.76 nm and 589.16 nm respectively, contributes to the atmospheric air-glow and is responsible for the familiar orange–yellow light from high-pressure sodium street-lamps. The D_2-transition is approximately twice as strong as the D_1, and it is therefore the most efficient target for LGS generation. Despite this, the sodium layer is optically thin and on average only 4 % of the incident laser light is actually absorbed, with most of the remainder propagating into outer space. As a further complication, the D_2 line is hyperfine split into a closely spaced doublet known as D_{2a} and D_{2b} with a ratio of transition strengths of 5:3. These two transitions are separated by about 1.77 GHz, and under mesospheric conditions they partially overlap due to Doppler broadening of each line to a full width half maximum of about 1.07 GHz. There are many additional factors influencing the return flux, such as the laser temporal, spectral and polarimetric format as well as the Earth's geomagnetic field. Calculations of sodium return flux typically make extensive use of computer simulation. Nevertheless, most deployed laser systems to date have concentrated on exciting the D_{2a}-transition, simply because it has the highest peak transmission cross-section.

For the particular case of the LGSF, simulations also suggest that a single narrow line at the peak of the D_{2a} line would be the optimum format to maximise return flux per watt of launched optical power. In practice, the photonic crystal relay fibre is an important factor determining the optical power and launched laser format. This optical fibre does not preserve the polarisation state of the laser beam and stimulated Brillouin scattering, a nonlinear optical effect, limits the maximum power spectral density that it can transmit to approximately 2.7 watts per spectral line, for lines that are sufficiently well separated. Therefore, the single-frequency line produced by the PARLA laser was spectrally broadened using a sinusoidal phase modulator in order to launch a greater number of spectral lines into the existing relay optical fibre and hence more optical power onto the sky. The phase modulation is characterised by the modulation frequency and the amplitude of the peak phase shift measured in radians. The resulting broadened laser spectrum consists of multiple lines forming a frequency comb inside an overall intensity envelope, where the power of each individual line is required to remain below the limit for the relay optical fibre. The comb spacing is equal to the 110 MHz frequency of the phase modulator, and the width of the amplitude envelope and the number of lines in the final laser spectrum increases monotonically with the peak phase shift.

The optimum phase shift for the laser beam is a trade-off between the total power transmitted through the fibre and the overlap between the broadened multi-line laser spectrum and the sodium D_{2a} atomic transition. The overlap decreases progressively from 100 % at zero peak phase shift to 67 % at a peak phase shift of 3.76 rad, which is close to the maximum accessible with our equipment. A peak phase shift of around 2.6 rad, corresponding to five spectral lines, was selected for the installed system for a total power of 7 watts exiting the relay fibre. During laboratory tests it was also verified that the spectrum did not change measurably after propagation through the relay fibre and no signal was measured at longer wavelengths where one would expect to find spectral components due to Raman scattering in the glass optical fibre if they were present.

PARLA laser system

The PARLA laser source is based on similar technology to systems that are under development for other ESO projects, which have been described in detail elsewhere (see Bonaccini Calia et al., 2010; Arsenault et al., 2006; and Kaenders et al., 2010). Key elements include a seed laser, a high-power Raman optical fibre amplifier and an efficient frequency doubling scheme. The main optical train is shown in Figure 2. Requirements for the system include flexible observing, high availability, excellent beam quality and stability compatible with the existing optical fibre beam relay.

The laser system includes an electronics cabinet and a laser head which emits a free-space TEM_{00} laser beam with a maximum output power of 20.5 watts at 589 nm. Although this is a 20-watt-class system, the final operating point of the laser source in the installed system is only around 11 watts to achieve the required 7 watts launched power on sky. The laser line-width is specified to be less than 20 MHz, and the centre frequency is tuneable around the centre of the sodium D_2 atomic transition.

Downstream from the laser head, a periscope, phase modulator, and a beam expander unit relay the optical beam to the existing optical fibre coupling system (see Figure 2). The laser includes a stand-alone computer-controlled system that is

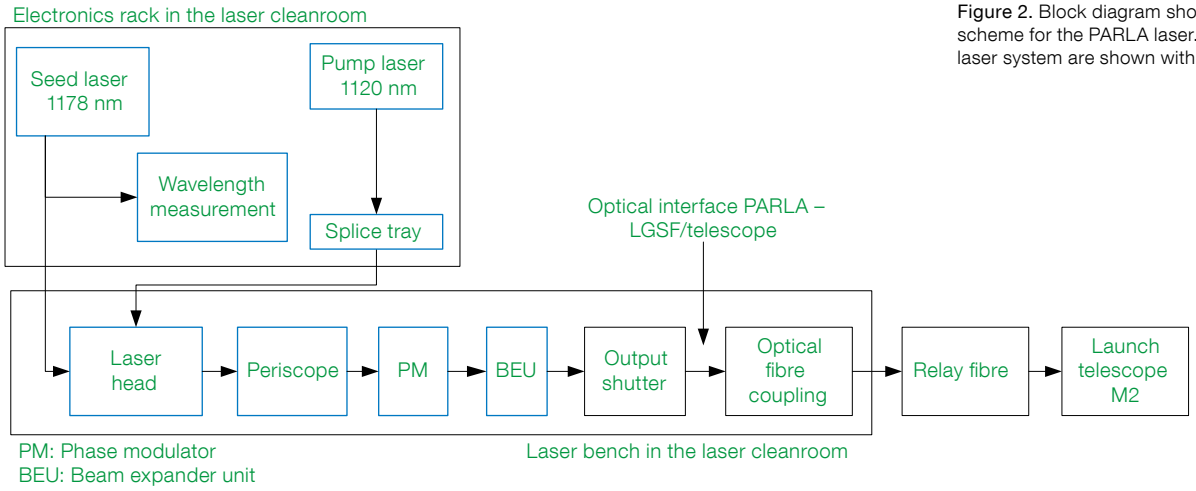

Figure 2. Block diagram showing the main optical scheme for the PARLA laser. The parts of the new laser system are shown with a blue outline.

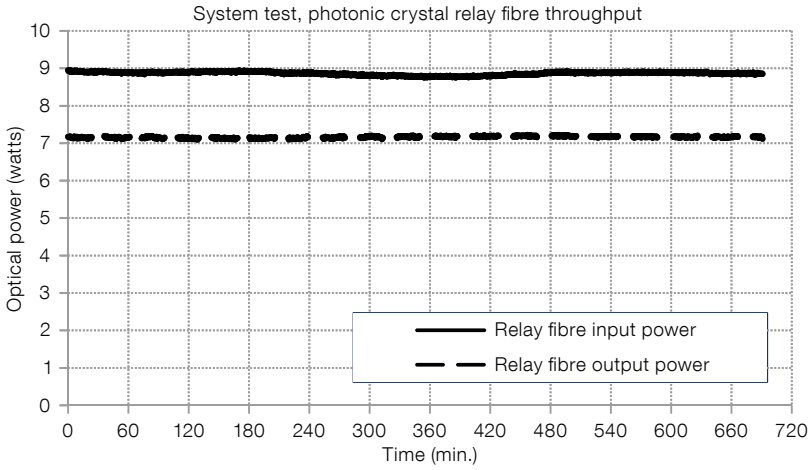

Figure 3. The input and output optical power measured through the relay fibre during the test in the laboratory in Europe is plotted. The average throughput is 80.8%.

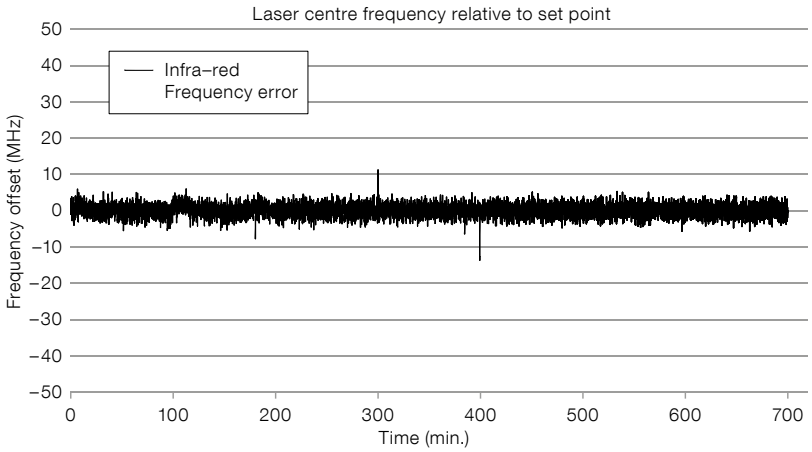

Figure 4. Variation of the laser central frequency measured during the test in Europe is plotted for a period of nearly 12 hours.

connected via a point-to-point Ethernet link to a VLT local control unit (LCU). This interface makes it possible, in a very simple way, to integrate the PARLA laser into the standard VLT control system at the Paranal Observatory.

Results from laboratory system tests, carried out in Europe, are shown in Figures 3 and 4. The laser was tested with a spare relay optical fibre in order to replicate the optical interface to the telescope. The duration of this particular test was 12 hours. Figure 3 shows the optical power at the input and output of the relay fibre. The output power was measured with a bolometer, and the fibre input power was measured using a calibrated pick-off mirror at the fibre input. During this test, the direction and lateral position of the laser beam at the input to the relay optical fibre were actively stabilised using an automated closed loop system, as is the case at the telescope. The average power at the input to the relay fibre was 8.86 watts, the output power 7.16 watts, and the average optical fibre throughput was 80.8%. The throughput includes both the transmission losses of the relay optical fibre (approximately 10%) and the input coupling losses, implying an input coupling efficiency of around 90%.

The infrared laser wavelength was also measured and logged during the test and Figure 4 shows the measured frequency error, in MHz, from the nominal set point during the test. The deviation is within a few MHz, which meets the goal

ESO/G.Hüdepohl (atacamaphoto.com)

Figure 5. Image of VLT UT4 (Yepun) during the PARLA commissioning, taken on 14 February 2013.

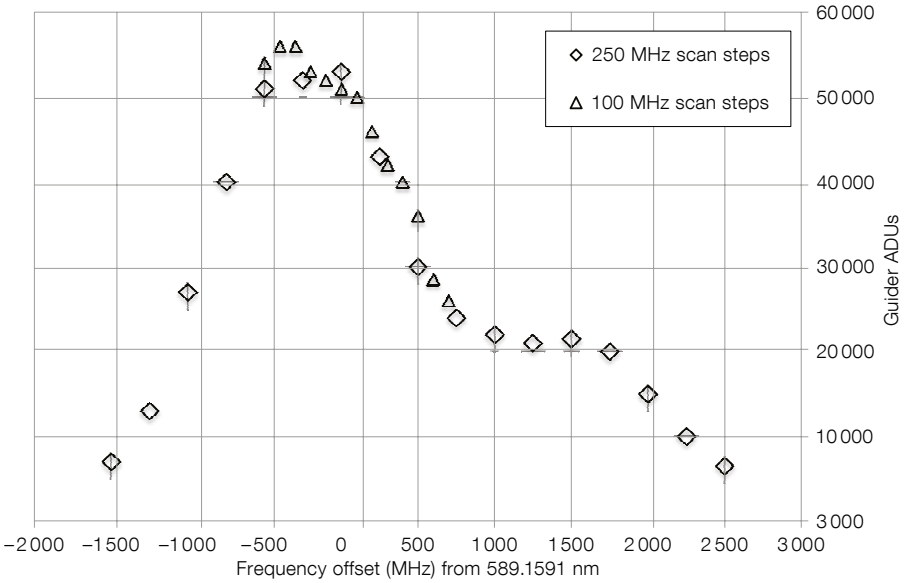

Figure 6. A wavelength scan through the sodium D_2 doublet taken during commissioning.

of 20 MHz. In addition to the selected optical characteristics described above, the laser system was subject to a comprehensive set of performance and functional tests, including the control system and interface to the VLT control software.

Installation and commissioning

The laser was installed on the telescope at the start of 2013, and commissioning took place in February 2013. The commissioning process included standalone tests of the LGSF with the new laser subsystem, and commissioning and science verification (SV) with the complete observing system and the two adaptive optics instruments, SINFONI and NACO. Figure 5 shows a photograph of UT4 taken during the commissioning in February 2013.

The LGS was first commissioned in a standalone mode, before the start of observations and SV tests with the instruments. To verify the correct output wavelength, the centre frequency of the laser system was scanned in steps of 250 MHz and 100 MHz around the nominal centre of the sodium D_{2a} transition and the relative return flux (brightness) of the LGS was measured using the UT4 guider camera. The guider output is in analogue-to-digital units (ADU) which are nominally linear with the flux. Figure 6 shows the plot of return flux versus laser wavelength taken during on-sky calibration. The measured line shape is a convolution of the laser spectrum and the Doppler-broadened sodium D_2 transition; the doublet is therefore not fully resolved. The main peak corresponds to the D_{2a} transition and the broad shoulder in the high frequency side corresponds to the sodium D_{2b} transition. The laser was tuned to the peak of the D_{2a} line, determined on sky in the final configuration.

The angular size subtended by the LGS was measured using the telescope guide camera at different altitudes and is listed in Table 1. Images of a natural guide star were taken before each LGS measurement and used to infer the seeing. The exposure time for the LGS images was approximately 2 seconds. This exposure duration averages the majority of the seeing effect, but formally

speaking is too short to qualify as a true long-exposure measurement of the spot size.

The return flux, and apparent magnitude, of the LGS were not measured photometrically. However, the counts from the SINFONI wavefront sensor, which is based on photon-counting avalanche photodiodes, were accessible. The wavefront sensor counts and the system performance during SV were the two metrics used to verify that the return flux was sufficient to meet the operational requirements. Measurements of the apparent LGS magnitude were made using SINFONI at different altitudes and at different times during the commissioning period. Typically the flux measured on the wavefront sensor equated to around 6 million counts per second. The optical power launched onto the sky was between 6 and 7 watts during these tests. This level of photon return was found to be sufficient to achieve good closed-loop adaptive optics performance during SV.

At the time of commissioning further measurements needed to be done before a definitive comparison could be made between the measured and theoretical return flux for this system. The principal uncertainty is the sodium abundance, which has been shown to vary by a factor of four seasonally (Simonich et al., 1979) and by a factor of up to two during a single night. Frequent measurements taken at different times of the year are therefore necessary.

Table 1. Measurements of the natural guide star (NGS) and laser guide star angular size.

Zenith angle (deg)	NGS size (arcsec)	LGS size (arcsec)
19.4	0.55	1.16
19.4	0.68	1.28
24.6	0.66	1.34
36.2	0.92	1.59
41.7	0.88	1.79
54.9	0.90	1.62

Science verification

The observing targets selected for SV are given in Table 2. These were repeats of existing and already published observations.

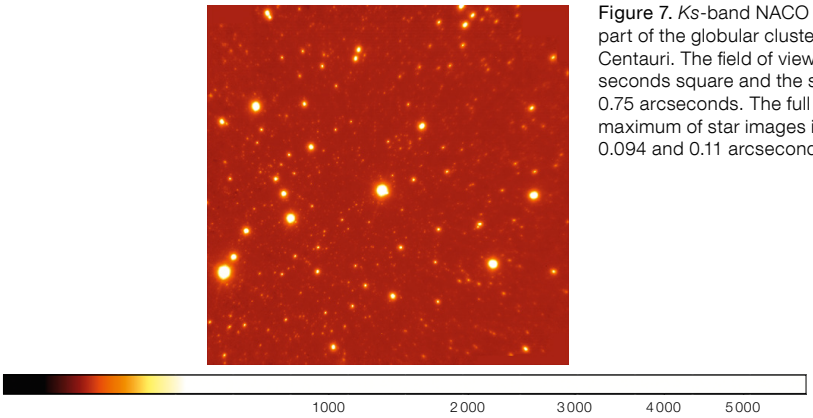

Figure 7. *Ks*-band NACO image of part of the globular cluster Omega Centauri. The field of view is 37 arcseconds square and the seeing was 0.75 arcseconds. The full width half maximum of star images is between 0.094 and 0.11 arcseconds.

Instrument	Object name	Description
NACO	NGC 3621	Bulgeless galaxy
NACO	Centaurus A	Active galactic nucleus
NACO	NGC 5139	Globular cluster, Omega Centauri
SINFONI	Haumea (TNO136108)	Trans-Neptunian object
SINFONI	NGC 36210.90	Bulgeless galaxy

Table 2. Science verification targets.

The observations selected for NACO were successfully executed during the commissioning nights. Observations were mainly made with the 7 × 7 wavefront sensor, and the adaptive optics loop remained closed without problems down to an altitude of 30 degrees during standard operation tests. The instrument was operated in a number of different configurations: tip-tilt correction only, high-order correction only, and with full correction. On the night of 17 February 2013 with full correction, Strehl ratios in the range 15.6–37 % in the *Ks*-band were measured in seeing ranging from 0.76 to 0.99 arcseconds, as recorded by the differential image motion monitor (DIMM) at 500 nm. Figure 7 shows an image of the cluster in Omega Centauri taken on another commissioning night. The field of view is 37 by 37 arcseconds, the seeing was 0.75 arcseconds and the coherence time τ_0 = 3.7 ms. The full width half maximum of the stars is between 0.094 and 0.11 arcseconds with full adaptive optics correction.

The observations of Haumea and NGC 3621 with SINFONI were also completed successfully. SINFONI was able to work stably in closed loop with the laser during standard operation tests. When observing the trans-Neptunian object Haumea, it was possible to observe up to the twilight limit without problem. For the last two nights of the planned commissioning period the system was handed back to science operations for service observing.

Operation

At the time of writing, the LGSF has been operating with the PARLA laser for almost one year.

One of the goals of the laser upgrade was to enable flexible observing. By this it is meant that the laser can be available for science observation within a short period of time, formally specified as 30 minutes, should the need or opportunity arise for a laser-supported observation. To achieve this aim, an idle state was defined in which the laser waits in a low-power configuration. In this scheme, the lifetime of the high-power optical components is extended by reducing their usage outside of actual observing time, while still ensuring that the system is available at short notice. This is a significant change from the original laser system which ran continuously at high power when it was available. In the new implementation, the telescope operator can wake up the laser using an automated script from the control room and be ready for operation in approximately ten minutes. Figure 8 shows the availability of the LGSF in hours per month for the first six months of operation after the upgrade.

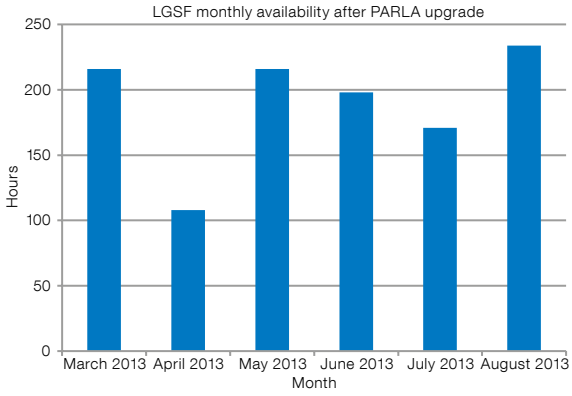

Figure 8. Availabilityof the LGSF for the first six months of science operation after the upgrade is plotted, in hours per month.

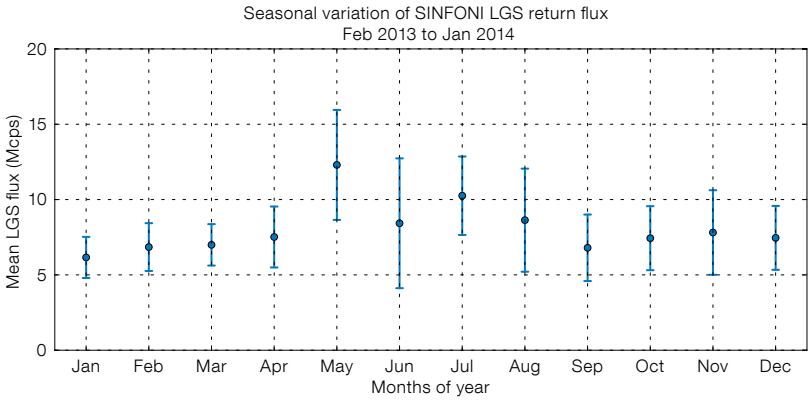

Figure 9. Monthly means and standard deviations of the counts, recorded by the SINFONI wavefront sensor, for the laser guide stars over the period of the upgraded LGSF.

After some months of operations with PARLA, the scientific use of the LGSF has increased very significantly to about 35 hours per month on average (SINFONI only). Remaining non-availability (see Figure 8) has a < 15 % impact on the total LGSF scientific use. The reliability of PARLA has made it possible to tackle other control issues, especially for SINFONI Multi-Applications Curvature Adaptive Optics (MACAO). Observations with the LGSF are now performed with significantly fewer overheads and in a more reliable way, providing that the atmospheric conditions are suitable.

The photon return flux, defined as the number of photons per unit area per second returning from the LGS, is also of interest over long timescales due to the large seasonal variability of this parameter (Holzlöhner et al., 2010; Simonich et al., 1979). Automated logging of the number of counts on the SINFONI wavefront sensor can be used as a relative measure, although instrumental effects preclude a photometric analysis. Figure 9 shows the mean and standard deviations of the wavefront sensor counts in a monthly time series. These values include contributions from the complete observing system and there is not necessarily a direct correspondence with the atmospheric sodium column abundance.

Prospects

The LGSF at the Paranal Observatory has been upgraded with a prototype laser source based on Raman fibre laser technology. This is the first time that this type of laser has been operated as part of a major astronomical observing facility. Results from almost one year of science operation have shown that the LGSF can be used more flexibly and with significantly higher availability after the upgrade. Experience with this system is providing valuable feedback for the ESO Adaptive Optics Facility, currently under development, which will deploy four complete LGS units on the centrepiece of VLT UT4.

Acknowledgements

We would like to acknowledge the support of Roberto Tamai for this project. We would also like to thank Nadine Neumayer and Yazan Al Momany for processing and reducing the science images and Jared O'Neal for work on system performance monitoring. We would like to thank the following companies for their support: Toptica Photonics AG, MPB Communications Inc. and Mitsubishi Cable.

References

Arsenault, R. et al. 2006, The Messenger, 123, 6
Bernard, R. 1939, ApJ, 89, 133
Bonaccini Calia, D. et al. 2006, SPIE, 6272, 627207
Bonaccini Calia, D. et al. 2010, SPIE, 7736, 77361U-1
Holzlöhner, R. et al. 2010, A&A, 510, A20
Kaenders, W. G. et al. 2010, SPIE, 7736, 773621
Rabien, S. et al. 2003, SPIE, 4839, 393
Simonich, D., Clemesha, B. & Kirchhoff, V. 1979, J. Geophys. Res.: Space Phys., 84, 1543
Slipher, V. M. 1929, PASP, 41, 262

A colour image of the polar ring galaxy NGC 4650A is shown. The image was formed by colour-coding the MUSE spectral cube (range 4800–9300 Å) obtained during the instrument commissioning run in February 2014. See Release eso1407 for more details.

Speckle Imaging with VLT/NACO No-AO Mode

Sridharan Rengaswamy[1]
Julien Girard[1]
Willem-Jan de Wit[1]
Henri Boffin[1]

[1] ESO

Long-exposure stellar images recorded with large ground-based telescopes are blurred due to the turbulent nature of the atmosphere. The VLT employs active and adaptive optics (AO) systems to compensate for the deleterious effects of the atmosphere in real time. The speckle imaging technique provides an alternative way to achieve diffraction-limited imaging by post-processing a series of short-exposure images. The use of speckle imaging with the no-AO mode of NACO at the VLT is demonstrated. Application of this technique is particularly suited to the *J*-band and it provides versatile high angular resolution imaging under mediocre conditions and/or in imaging extended objects. The implementation of this mode underlines the continuing attractiveness of NACO at the VLT.

Astronomical speckle imaging

The invention of speckle interferometry (Labeyrie, 1970) has revolutionised the field of high-resolution imaging with ground-based telescopes. In speckle interferometry, a series of short-exposure images of the object of interest (for example, a spectroscopic binary star) is recorded with a spectral filter whose bandwidth is smaller than the mean wavelength (quasi-monochromatic conditions). The modulus-squared Fourier transform of the images averaged over the ensemble (a quantity generally referred to as the energy spectrum) preserves the information up to the diffraction limit of the telescope. Deconvolving this average with a similarly obtained average of an isolated single star, close in time and angular distance to the target, removes the effects of the atmosphere and the telescope on the energy spectrum, leaving behind the energy spectrum of the object of interest. A subsequent Fourier transform of the energy spectrum provides the diffraction-limited autocorrelation of the object of interest. In the case of binary stars, the binary nature can be visually identified from the peaks of the autocorrelation.

Speckle interferometry has made significant contributions to the field of binary star research by creating several binary star catalogues (e.g., Mason et al., 2013). Since the energy spectrum does not preserve the Fourier phase information, it is not possible to obtain an image of the object apart from the autocorrelation. Hence there is a 180-degree ambiguity in the position angle of the binary star. In 1977, Gerd Weigelt showed, experimentally, that the phase of the complex triple product of the Fourier transform of the images at three spatial frequencies (the third frequency being the sum of the first two) averaged over the ensemble, provides the sum of the Fourier phases of the object at those three frequencies. This complex product, called the bi-spectrum, is immune to atmospheric turbulence (as the random phase errors introduced by the atmosphere are completely cancelled in the bi-spectrum) and provides a way to retrieve the Fourier phases of the object.

It should be noted that the phase of the bi-spectrum is the same as the "closure phase", a term coined by Jennison (1958) in radio astronomy and used first by Rogstad (1968) for optical imaging through turbulence. Combining the phase information with the energy spectrum obtained from the speckle interferometry, an image of the object of interest can be reconstructed. This technique is known as speckle imaging.

The no-AO mode of NACO

The Very Large Telescope (VLT) instrument NAOS–CONICA (NACO; Lenzen et al., 2003) was built at the end of the 1990s and its deformable mirror has a total of 185 actuators (Rousset et al., 2003). The no-AO mode of NACO (Girard et al., 2010), essentially bypasses the adaptive optics module NAOS and uses CONICA's "burst mode" to record a series of short-exposure images, exploiting the detector's windowing capability. There are different ways in which these short-exposure images can be processed. Holographic imaging of crowded fields was pioneered and presented by Rainer Schödel (Schödel & Girard, 2012; Schödel et al., 2013). Here we demonstrate how the NACO non-AO mode, coupled with the aforementioned speckle image processing technique, can be exploited to obtain near diffraction-limited images of objects of interest. We have developed the required pipeline data reduction tool (Rengaswamy, Girard & Montagnier, 2010) for reconstructing an image from the speckle data[1].

Imaging binary stars

The study of binary stars is an important branch of astrophysics. It is the most common way by which stellar masses are determined. Multi-epoch images of a binary system enable the calculation of the orbital elements of the binary. A typical long-exposure image does not resolve very close binary stars, i.e., those at sub-arcsecond separation, as the resolving power is impaired by the atmospheric turbulence. Short-exposure images (freezing the atmosphere) can be post-processed to resolve the binary. The bottom left panels of Figure 1 show images of the binary star HIP24800, reconstructed from a series of 900 speckle images recorded in NACO no-AO mode in January 2010. The top panels show the best and the worst images of the series. The best image is identified as the one for which the sum of the fourth power of the mean subtracted pixel intensities is the highest. The bottom right panel shows the long-exposure image, a simple mean of all the short exposures. The separation between the components of the binary is 161 milliarcseconds (mas) and their brightness ratio is about 2.3.

Imaging near-Earth objects

The no-AO mode of NACO also makes the imaging of fast-moving near-Earth objects at high angular resolution feasible. The near-Earth passage of the asteroid 2005 YU_{55} in November 2011 provided an excellent opportunity to test this. As the adaptive optics could not lock onto this fast-moving object, data were recorded in the no-AO mode in the *Ks*-band. Figure 2 shows the resulting

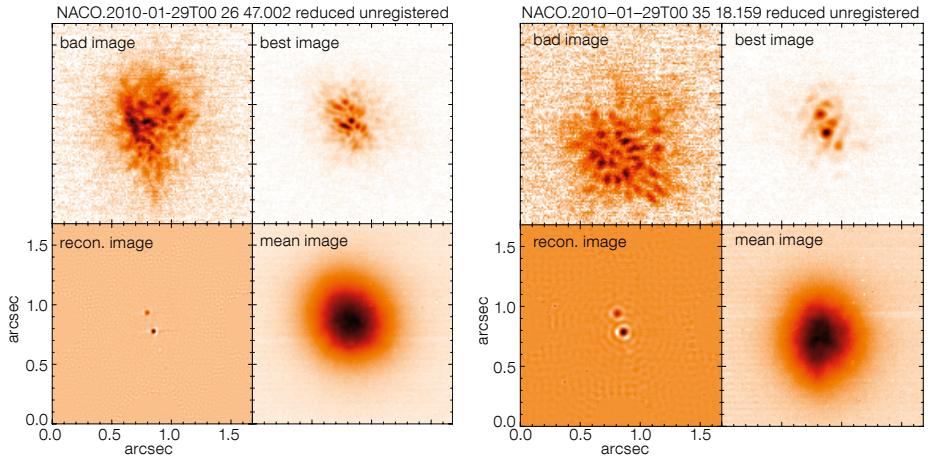

Figure 1. Speckle reconstructed images based on NACO no-AO observations of the binary HIP 24800 in *J*- (left) and *Ks*- (right) bands (low left panels). The top panels show the worst and best images of the recorded series. The lower right panels show the mean image.

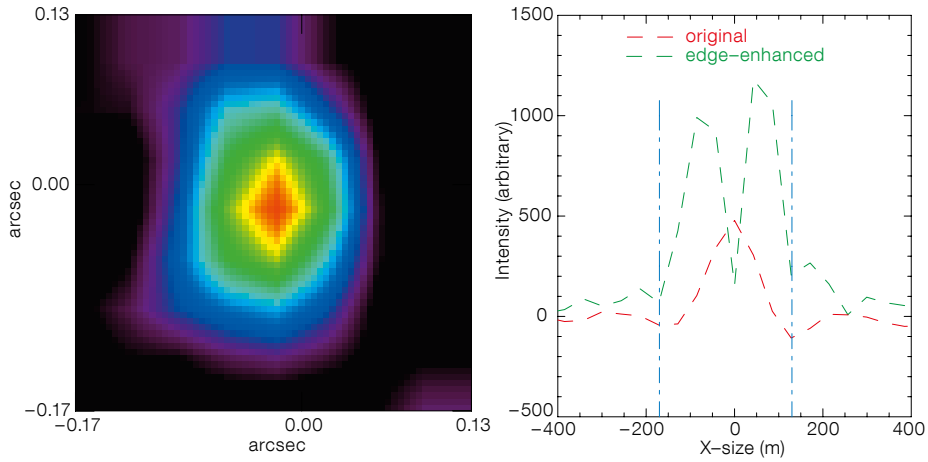

Figure 2. Reconstructed image of asteroid 2005 YU_{55} (left) and its horizontal cross-section (right). The red line indicates the cross-section before applying an edge detection operator to the reconstructed image. The green line indicates the cross-section after applying the edge detection operator. The blue lines indicate the size.

average reconstructed image of the asteroid. The nominal angular resolution of 60 mas at the *Ks*-band corresponds to a linear resolution of 95 metres at the distance (329 900 km) of the asteroid. The dimensions of the asteroid were much larger than this resolution and thus the technique allowed the asteroid to be spatially resolved. The cross-sections of the image, subjected to an edge enhancement operator (Prewitt edge enhancement operator of the IDL software) to retrieve the asteroid dimensions, indicated a size of (261 ± 20) × (310 ± 30) metres. For comparison, tri-axial diameters of 337 × 324 × 267 metres, with uncertainties of 15 metres in each dimension, were estimated for the size of the asteroid from the Keck adaptive optics system, six hours before our observations. Accounting for the time difference, and the 18-hour rotation period of the asteroid, our results are in good agreement with those of the Keck AO system, despite the mediocre observing conditions (seeing of 1.2 to 1.5 arcseconds at 550 nm and atmospheric coherence time of two milliseconds). These observations demonstrate the robustness of the no-AO mode and the speckle imaging technique.

Imaging circumstellar envelopes around evolved stars

L2 Pup (HD 56096, HR 2748) is a semi-regular pulsating red giant star in the constellation of Puppis with an angular diameter of 17 milliarcseconds. Figure 3 shows speckle-reconstructed images of L2 Pup at 2.27 µm observed with the

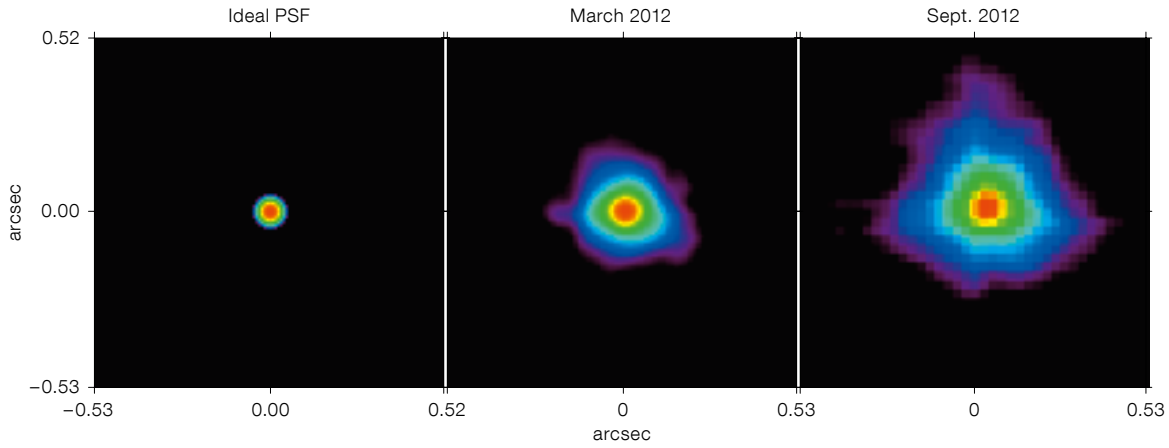

Figure 3. Speckle image reconstruction of the circumstellar envelope of L2 Pup, observed in March and September 2012. The theoretical (ideal) PSF is shown for comparison.

no-AO mode. The nominal resolution at this intermediate band is about 60 mas. While the stellar continuum is unresolved, the extended circumstellar emission from this star is visible in the reconstructed images. We have suppressed the features with intensity values less than 5 % of the maximum intensity in generating this figure. The circumstellar envelope appears enlarged in the second reconstruction, obtained six months after the first one. This is perhaps due to the 140-day pulsation period of the star or due to its high mass-loss rate. The panel on the left is the ideal point spread function at 2.27 μm. The middle and right panels indicate speckle reconstructions obtained from the March and September 2012 data, respectively. These images serve first and foremost as extremely valuable information on the dynamical evolution of the circumstellar envelope at high angular resolution. Secondly, they can serve as a good starting point for even higher angular resolution investigations with, for example, the Very Large Telescope Interferometer.

Allen et al. (1972) alluded to the possible presence of dust shells around carbon-rich Wolf–Rayet stars (WC stars) based on the near-infrared excess inferred from photometric observations. This was initially a surprising result, as the dust particles would be expected to be destroyed by the strong stellar winds from these stars. Therefore, these observations indicated the continuous formation of dust somewhere within the environment of these stars. With the advent of aperture masking interferometry, direct imaging of nearby Wolf–Rayet stars became feasible. A dusty pinwheel nebula structure was discovered around two persistently dust-forming WC stars, *viz*. WR 104 (WC9d + B0.5V) and WR 98a (WC8-9vd) (Monnier et al., 1999; Tuthill et al., 1999). Although these systems could be explained if the dust can be formed at the downstream regions of the shockfront formed by the colliding winds of the WR star and an associated secondary star of type OB, this has never been conclusively proven.

In an effort to clarify whether the dust formation in WC stars occurs at the colliding wind region or in the self-shadowing regions of the clumpy winds

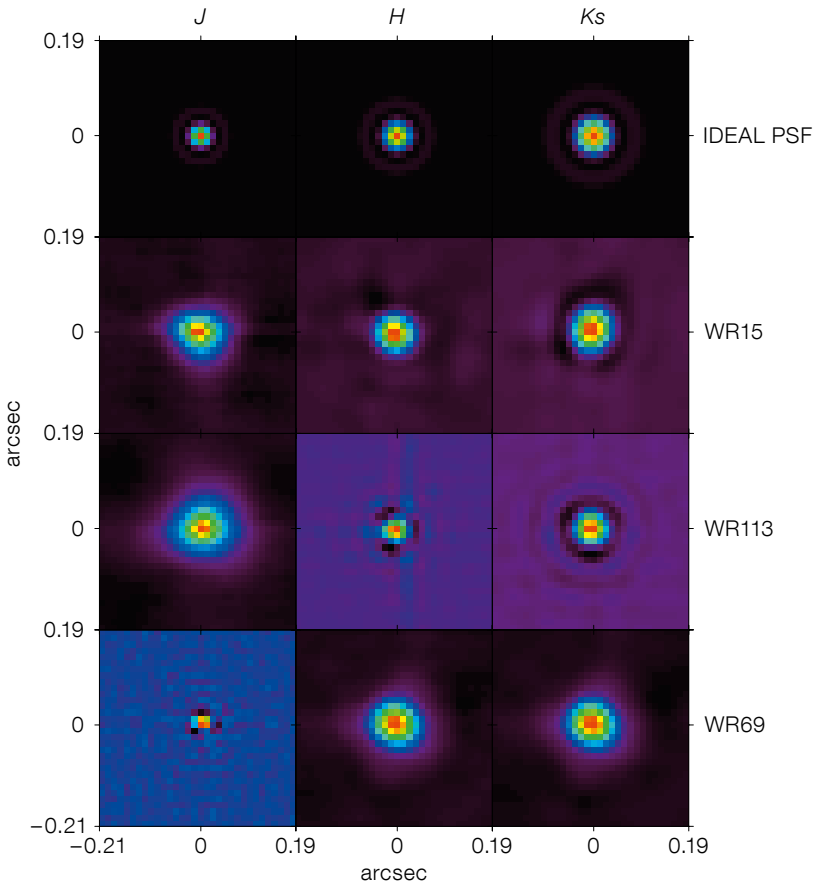

Figure 4. Reconstructed images of WR 15, WR 113 and WR 69 in *J*-, *H*- and *Ks*-bands. The top row shows theoretical (ideal) point spread functions in *J*-, *H*- and *Ks*-bands.

of an isolated star, we executed a pilot survey of six WC stars, consisting of three putative binaries and three isolated single stars. Figure 4 shows the speckle-reconstructed images of WR 113 and WR 69 (supposedly binaries) and WR 15 (a single star) in the *JHKs*-bands. The circumstellar envelope shows extended emission confirming the presence of the dust. By resolving the dust emission in several WC stars, at multiple epochs in *J*-, *H*-, *K*- and *L'*-bands, one can trace the temperature of the dust distribution and thus distinguish between the two scenarios of the dust formation.

Comparison between speckle-reconstructed and AO-corrected images

In an effort to assess the performance of speckle imaging, AO-corrected images were recorded nearly simultaneously along with the speckle datacubes in the case of the binary star shown in Figure 1. Figure 5 shows good comparison between the speckle-reconstructed images obtained with the NACO no-AO mode and the corresponding AO-corrected images in *J*- (left panel) and *Ks*- (right panel) bands. The speckle-reconstructed images have been rescaled (between 0 and 255) and the contrast has been reversed for the sake of display. Qualitatively, they match very well.

In order to have a quantitative comparison, we estimated the Strehl ratios of the binary components from the reconstructed images. It should be noted that speckle reconstruction yields the "object" intensity distribution on the sky (of course sampled at the spatial sampling of the detector). This is quantitatively different from the "image" intensity distribution (i.e., the object convolved with the response of the telescope) or the point spread function (PSF) obtained in normal or adaptive optics imaging. Thus,

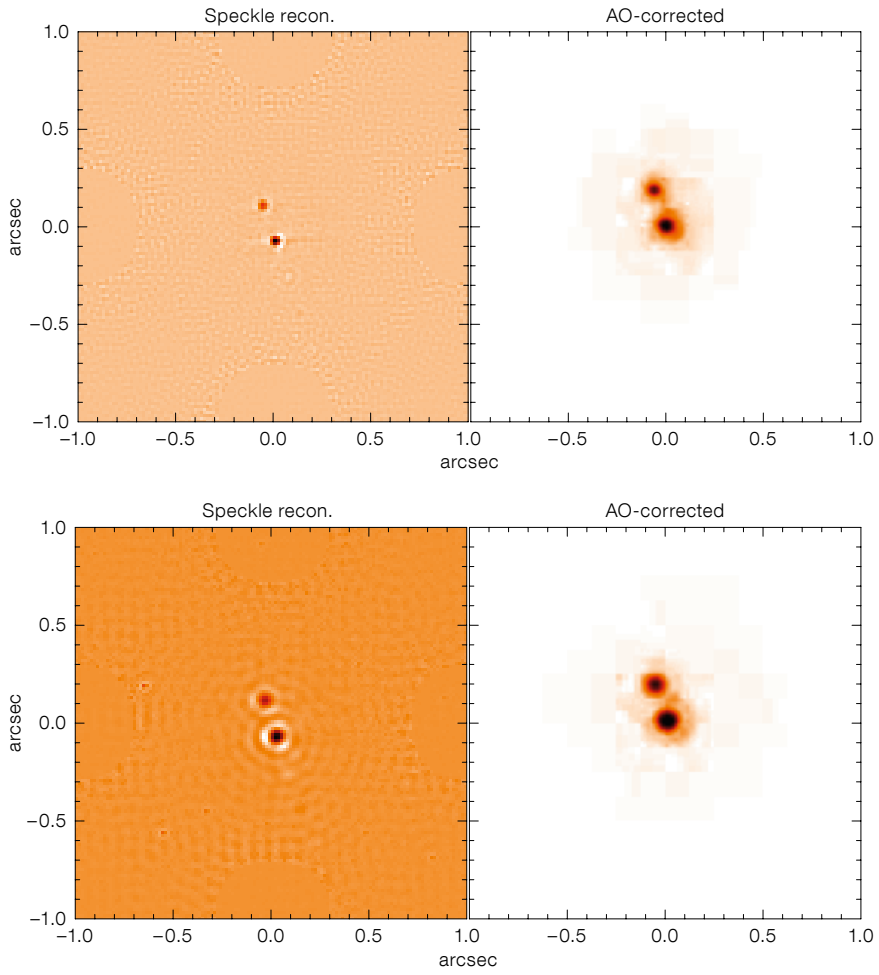

Figure 5. Comparison between speckle-reconstructed images and the images obtained with AO corrections at the telescope in *J*- (upper) and *Ks*- (lower) bands.

prior to estimating the Strehl ratios, we convolved the speckle reconstructions with an ideal synthesised PSF of the telescope. We estimated the Strehl ratio as the ratio of volume under the transfer function (Fourier transform of the PSF) of the reconstructed image (binary components in this case) to the volume under the transfer function of an ideal (synthesised) PSF. Strehl ratios were obtained with a window size of 16 × 16 pixels.

The average Strehl ratios of ten consecutive measurements in *J*- and *Ks*-bands were about 70 % and 90 % respectively under very good conditions (0.5–0.6 arcseconds seeing) observing close to the zenith. We clearly see that speckle imaging tends to provide a higher Strehl ratio than AO (typically 60 % Strehl in *Ks*-band and less at shorter wavelengths), under good conditions. This could be interpreted as follows: as speckle image reconstruction "corrects" for the phase aberrations up to infinite order (unlike adaptive optics imaging, which corrects the phase aberrations up to a finite order of equivalent Zernike modes), we obtain higher Strehl ratios than adaptive optics imaging or normal imaging.

When to use speckle imaging with the no-AO mode

It is important to consider when to use NACO no-AO instead of AO. In general, speckle imaging with the no-AO mode is more beneficial in the *J*-band where the AO fails to perform well due to its limited number of wavefront sensing/correcting elements. Further, it may not be always possible to lock the AO loop on fast-moving, extended, near-Earth objects even under favourable conditions (since AO performs best on point sources) and speckle imaging is extremely valuable for imaging such objects (e.g., asteroid 2005 YU_{55}).

AO stands out gloriously when it is required to image faint targets with long exposures (deep imaging). It minimises confusion in crowded fields (e.g., the Galactic Centre) by separating close sources. Its use is inevitable for high-resolution spectroscopy and should be preferred when the observing conditions are excellent. However, there could be situations where AO cannot be used efficiently. For example, when an object is very bright (e.g., L2 Pup with *Ks* = –2.3) long exposures will saturate the detector and thus short exposures with the no-AO mode should be preferred.

Another advantage of speckle imaging is the possibility of excluding bad images that correspond to highly turbulent states of the atmosphere. In other words, one can select the best images from the recorded series of images and then obtain a speckle-reconstruction from them. This is in line with the concept of "lucky imaging", where typically 10 % of the best images are used with a simple shift-and-add method to obtain a high-resolution image.

In our speckle processing, we use 90 % of the frames when all images in the recorded sequence have similar contrast. However we discard more than 50 % of the frames when the contrast of the frames shows significant variations, which occurs particularly under mediocre conditions. This flexibility facilitates speckle imaging under a wide variety of conditions. For example, the reconstructions of L2 Pup were obtained from the data recorded under 1.2–1.6 arcsecond seeing and one millisecond coherence time, after discarding nearly 80 % of the frames, thanks to the ability to record a few thousand frames. But the AO loop will not be stable under highly varying conditions. Further, the quality of the AO correction may not be good under unstable atmospheric conditions, while it would still be possible to obtain a speckle reconstruction after excluding frames with degraded image quality.

Additional benefit of the No-AO mode

An additional use of this mode is the ability to ascertain the proper tracking of the telescope (under wind shake, vibrations and occurrences of the primary mirror [M1] passive support motions). A burst of 8000 images of a bright target, each of 20 mas exposure spans 160 seconds. A software-based image registration process (cross correlation using Fourier transform [FCC]) can generate a plot of image motion as a function of time (as shown in Figure 6). Any slowly varying jitter with large amplitude (a few arcseconds) could be attributed to the residual tracking errors of the telescope. The estimated root mean square (rms) jitter for the case shown in Figure 6 is about 113 mas over 2.5 minutes with peak-to-peak jitter of about 0.6 arcseconds. There were no passive support motions in M1 which could momentarily increase the amplitude of the jitter. The estimated jitter is compatible with the expected (as per design specifications) rms tracking error for the VLT Unit Telescopes of 100 mas over 30 minutes.

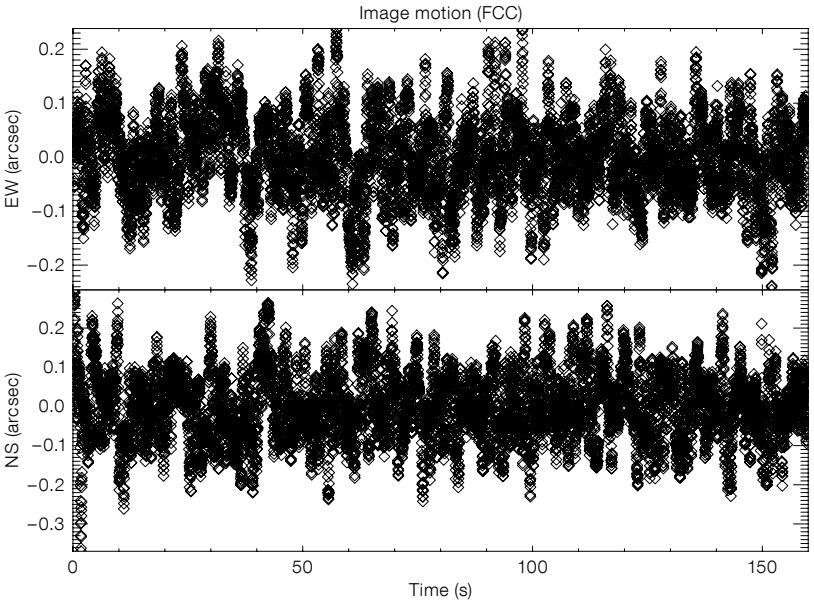

Figure 6. Image jitter estimated by cross-correlating the speckle frames with a reference frame. The rms jitter can be used to assess the quality of the tracking. Wind shake and the M1 passive support motions can cause a momentary increase in the magnitude of the jitter.

References

Allen, D. A., Harvey, P. M. & Swings, J. P. 1972, A&A, 20, 333
Girard, J. H. et al. 2010, SPIE, 7736, 77362N
Jennison, R. 1958, MNRAS, 118, 276
Labeyrie, A. 1970, A&A, 6, 85
Lenzen, R. et al. 2003, SPIE, 4841, 944
Mason, B. D., Hartkopf, W. I. & Hurowitz, H. M. 2013, AJ, 146, 56
Monnier, J. D., Tuthill, P. G. & Danchi, W. C. 1999, ApJ, 525, L97
Rengaswamy, S., Girard, J. H. & Montagnier, G. 2010, SPIE, 7734, 77341B
Rogstad, D. H. 1968, Appl. Opt., 7, 585
Rousset, G. et al. 2003, SPIE, 4839, 140
Schödel, R. & Girard, J. H. 2012, The Messenger, 150, 26
Schödel, R. et al. 2013, MNRAS, 429, 1367
Tuthill, P. G., Monnier, J. D. & Danchi, W. C. 1999, Nature, 398, 487
Weigelt, G. P. 1977, Optics Communications, 21, 55

Links

[1] The speckle imaging data reduction tool can be obtained on request to: srengasw@eso.org

Sunset over Paranal on 5 July 2012, the date of the very low precipitable water vapor event as described in the following article. The photo was taken by ESO Photo Ambassador Gabriel Brammer, who found the scene to be extraordinarily clear and beautiful. Little did he know that the following night would be one of the driest on record. See Picture of the Week for 3 February 2014 for details.

Antarctic Air Visits Paranal — Opening New Science Windows

Florian Kerber[1]
Harald Kuntschner[1]
Richard R. Querel[2,3]
Mario van den Ancker[1]

[1] ESO
[2] National Institute of Water & Atmospheric Research (NIWA), Lauder, New Zealand
[3] Universidad de Chile, Santiago, Chile

Extremely low humidity (precipitable water vapour [PWV] of ~ 0.1 mm) in the atmosphere above Paranal has been measured by a water vapour radiometer over a period of about 12 hours. PWV values < 0.2 mm are usually only found at very high altitude or in Antarctica. In fact a pocket of Antarctic air has been shown to be responsible for this phenomenon and it may occur a few times per year at Paranal. We highlight the science opportunities — created by new atmospheric windows — that arise in such conditions. The community is invited to provide feedback on how to make best use of low PWV with the VLT.

The dry episode over Paranal

The humidity in the atmosphere is measured in the form of precipitable water vapour — a measure of atmospheric water content. It is the amount (or depth) of water vapour in a column of the atmosphere if it were all to condense and fall as rain. The water vapour content of the atmosphere can be measured using the strong water line at 183 GHz. At the Paranal Observatory these measurements are made by the Low Humidity and Temperature Profiling radiometer (LHATPRO), manufactured by Radiometer Physics GmbH[1] and described by Kerber et al. (2012).

Given Paranal's sub-tropical location at 24.5 degrees latitude south it sounds far-fetched [pun intended] that Antarctic air would ever pass over Paranal, but this is exactly what happened on 5 July 2012. During that night LHATPRO recorded an episode of extremely low (~ 0.1 mm) PWV that lasted for more than 12 hours. While a beautiful panorama of Paranal taken at sunset (Figure on p. 16) on 5 July 2012 doesn't show anything unusual to the human eye, atmospheric conditions were in fact anything but ordinary. Located in the Atacama Desert at 2635 metres above sea level, Paranal is a very dry place. Its median PWV is about 2.4 mm with some seasonal variations, but on this particular night it experienced a "dry episode" that was truly remarkable (Kerber et al., 2014). In Figure 1 the temporal evolution of the humidity is displayed as measured by the LHATPRO radiometer and the two spectrographs CRIRES and X-shooter at the Very Large Telescope (VLT). The spectroscopic observations were taken in support of routine science operations and the PWV was deduced from an analysis of their spectra using an atmospheric model (Querel et al., 2011). Such dry conditions are more commonly expected at sites at much higher altitude, such as the Atacama Large Millimeter/submillimeter Array (ALMA[2]) on the Chajnantor Plateau (5050 metres above sea level, median PWV 1.2 mm) or other particularly dry sites, such as locations in Antarctica (the median PWV at Dome C, 3233 metres above sea level, during winter is around 0.2 mm), which offer excellent atmospheric transparency for infrared and (sub-)millimetre astronomy.

Service mode and low PWV

This dry episode is the first such event at a major observatory that has been fully documented in terms of atmospheric and meteorological conditions. Other relevant ambient conditions (seeing, temperature, wind, etc.) were around, or below, their median values. Hence, the excellent atmospheric transparency at infrared wavelengths offered by the low humidity would have offered ideal conditions for infrared (IR) observations.

In this context it is worth noting that for service-mode observations with several IR instruments at the VLT (e.g., CRIRES and VISIR), PWV can be specified as a user-defined observing constraint. The PWV measurements from the PWV monitor are available in real-time in the control room of the VLT, allowing decisions on which observations to conduct in service mode to be taken with great flexibility. This schema allows potentially very demanding observations requiring a very low (< 0.5 mm) column of water vapour to be scheduled when very dry and stable conditions occur, such as the episode of extremely dry air described.

A careful analysis of meteorological conditions involving numerical models showed that on that date Antarctic air passed over Paranal, driven far to the north by an unusual combination of weather patterns; details are given in Kerber et al. (2014). Is this a freak or a once-in-ten-years event? In all likelihood it isn't: based on archival data produced by VLT spectrographs, similarly dry conditions (PWV < 0.2 mm) occur very rarely — one or two nights per year, while PWV less than 0.5 mm is encountered about 2 % of the time, and less than 1 mm is found 15 % of the time.

On account of the sparse nature of these observations the duration of events in the past remains unknown. Are such conditions also predictable in advance? Conditions for excursions of Antarctic air are certainly special, but weather forecasting with a focus on astronomical conditions is a field of active research (Sarazin et al., 2013) and the predictive power of atmospheric models is clearly improving.

What kind of science is enabled by low PWV?

As already mentioned, atmospheric transparency in the infrared is dramatically enhanced in such dry conditions beyond the standard windows (*J*-, *H*-, *K*-, *L*-, *M*-, *N*-, and *Q*-bands) in the 1–25 μm range that are routinely used for ground-based astronomy. We have identified a number of astrophysically important lines (Kerber et al., 2014) that benefit particularly from such conditions.

A case in point is the hydrogen Paschen-α (Pa-α) line at 1875 nm, which is unobservable (transmission less than 2 %) under median PWV conditions on Paranal. This

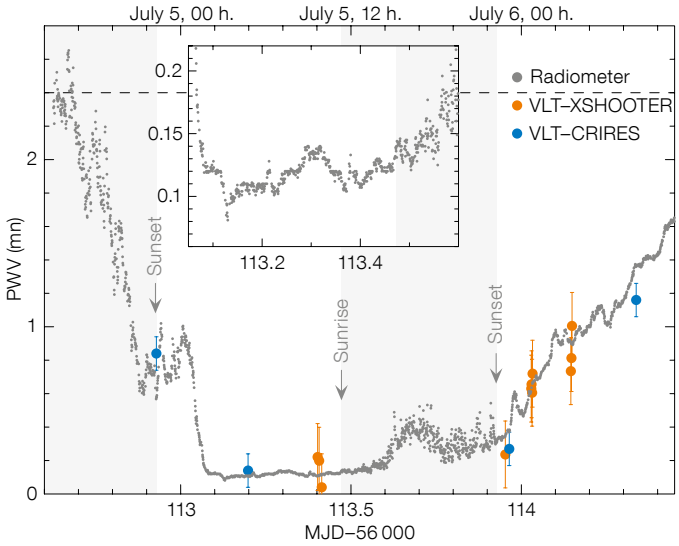

Figure 1. Time series of the PWV measured above Paranal from 5–6 July 2012. The data points in black are from the LHATPRO radiometer, while PWV measurements derived from VLT instruments are overplotted. The dashed line indicates the Paranal overall night-time median PWV (2.4 mm). Times of sunrise and sunset (see Figure on p. 16) are indicated; note the larger variability of PWV during daytime. Insert: Enlarged view of the dry episode showing the high level of stability during the 12-hour period as well as the extremely high precision of the radiometer data. The larger number of VLT measurements taken on 6 July (after MJD 56113.5) are in response to the very low PWV recorded the previous night. Figure from Kerber et al., 2014.

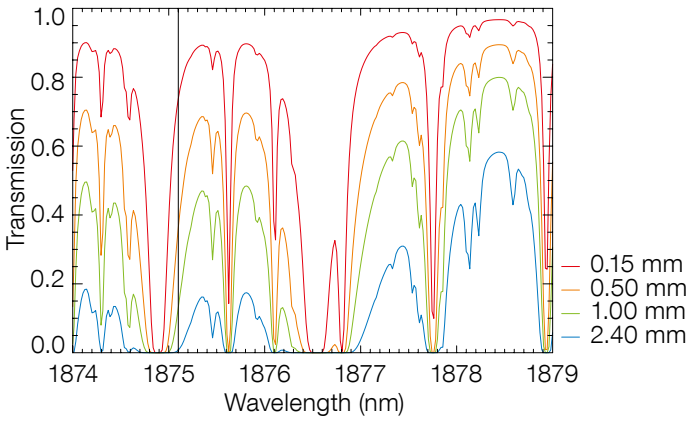

Figure 2. Transmission of the Earth's atmosphere in the region of the Pa-α line at 1875.1 nm. At PWV = 0.5 mm a transmission of 35 % is reached. Note that for extragalactic sources even higher transmission will be achievable due to redshift and PWV as high as 1 mm may offer usable conditions (modified from Kerber et al., 2014).

intrinsically strong line is prevalent in many astrophysical sources, is less affected by dust extinction than Hα, and, due to its wavelength, benefits significantly from adaptive optics. At low PWV atmospheric transmission improves rather dramatically (Figure 2), and reaches more than 75 % under the conditions encountered on 5 July 2012. This is why such observations are currently either done from space or at very high altitude. The University of Tokyo operates a camera (Motohara et al., 2008) equipped with Pa-α filters at its 1-metre telescope on Cerro Chajnantor (5640 metres) and recently the First Light Infrared Test Experiment CAMera (FLITECAM) on the Stratospheric Observatory for Infrared Astronomy (SOFIA) received similar filters (McLean et al., 2012).

This of course begs the question of how such new science could be enabled by making use of these extraordinary conditions on Paranal. The VLT, with its user-specified constraints on atmospheric conditions, is already prepared to accept very demanding scientific programmes in service mode that can only be performed during a small fraction of the time. Low-PWV science takes this one step further, but for spectroscopic observations. No additional investment in hardware is required to conduct low-PWV science using existing spectrographs (in fact, a first spectroscopic observation of Pa-α in a young stellar object has already been secured under very good but not excellent conditions and will be the subject of a future publication). This demonstrates that current VLT spectrographs can take advantage of such conditions and deliver new and exciting science.

In terms of imaging, the VLT offers telescopes with an 8-metre primary mirror and instruments with adaptive optics providing exceptional image quality. However, a small investment in hardware may be necessary to enable low-PWV science with existing and planned imagers. Narrowband filters for Pa-α — and an off-band wavelength — would have to be procured. One imager that would combine these qualities could be ERIS[3], currently under design by ESO and external partners from the Max-Planck Institute for Extraterrestrial Physics (with contributions from ETH Zürich) and INAF–Arcetri Astrophysical Observatory.

The authors would like to encourage the ESO community to send their feedback on low-PWV science with the VLT and their thoughts about Pa-α or other filters in the context of instrument development or upgrades[4].

Acknowledgements

Richard Querel acknowledges funding from Conicyt through Fondecyt grant 3120150.

References

Kerber, F. et al. 2014, MNRAS, in press
Kerber, F. et al. 2012, The Messenger, 148, 9
McLean, I. S. et al. 2012, Proc. SPIE, 8446, 844619
Motohara, K. et al. 2008, Proc. SPIE, 7014, 70142T
Querel, R. R., Naylor, D. A. & Kerber, F. 2011, PASP, 123, 222
Sarazin, M., Kerber, F. & De Breuck, C. 2013, The Messenger, 152, 17

Links

[1] Radiometer Physics GmbH, Germany: http://www.radiometer-physics.de
[2] ALMA Observatory: http://www.almaobservatory.org
[3] ERIS: http://www.eso.org/sci/facilities/develop/instruments/eris.html
[4] Comments for low PWV science with ESO instrumentation to: lowpwv@eso.org

The Calibration of ALMA using Radio Sources

Ed Fomalont[1]
Tim van Kempen[2]
Ruediger Kneissl[3]
Nuria Marcelino[4]
Denis Barkats[3]
Stuartt Corder[1]
Paulo Cortes[1]
Richard Hills[5]
Robert Lucas[6]
Alisdair Manning[3]
Alison Peck[4]

[1] National Radio Astronomy Observatory, Santiago, Chile
[2] Leiden University, Leiden, the Netherlands
[3] ESO
[4] National Radio Astronomy Observatory, Charlottesville, VA, USA
[5] Cavendish Laboratory, Cambridge, UK
[6] Institut d'Astrophysique de Grenoble, Grenoble, France

For ALMA to produce high quality images of astronomical objects with sub-arcsecond resolution at frequencies above 85 GHz, the radio signals must be combined from up to 66 antennas spread over 15 km with a maximum path length delay difference of about 0.025 mm. This accuracy requires precise antenna structures, stable electronics, compensation for many temporal changes in the system and the measurement of the path-changing water vapour emission in the line of sight. The final stage of path length calibration is provided by frequent observations of relatively strong, point-like distant radio sources, quasars, that lie within a few degrees of the astronomical object. The ALMA Quasar Catalogue was implemented to provide a database that contains the essential parameters for hundreds of quasars and their brightness variations at several frequencies as a function of time. This paper describes the filling of the catalogue and the use of these quasar test signals to provide the path length accuracy needed for the imaging of radio sources.

The Atacama Large Millimeter/submillimeter Array (ALMA) is an array of up to 66 antennas, placed in configurations with baselines (antenna-to-antenna vectors) up to 16 kilometres, and located in the Atacama Desert in Northern Chile. Each of the antennas receives the electromagnetic waves from a celestial source in the submillimetre (submm) to millimetre (mm) wavelength range. These faint signals (sensitivity of tens of μJy; 1 Jansky = 10^{-26} W m^{-2} Hz^{-1}) are transported to a central point where they are combined at a virtual focus. The complex digital processing device that focuses the signals is the correlator. In order to produce a high quality image, the signals from each antenna must be combined with a phase difference that is less than about 0.5 radian. At a frequency of 950 GHz with a wavelength of 0.3 mm, this phase difference corresponds a path delay accuracy of about 0.025 mm or 0.08 picosecond in relative time delay.

There are several relevant time scales associated with the delay changes. The short-term path length noise (less than one second) depends on the coherence properties of the ALMA electronics which meet the needed tolerance. The longer-term change of path delay, caused by the slowly changing properties of many ALMA components, is in excess of the tolerance, although some aspects can be monitored and their effects removed. Finally, the variable path delay associated with the propagation of the radio waves in the atmosphere above each antenna is one of the major contributors to the defocusing of the signal at the correlator, from time scales of one second to several hours.

In order to monitor the changes in path length during an observation, test signals with known properties can be propagated through the entire ALMA system — from above each antenna to the correlator — and the variable delay from each antenna can be suitably adjusted (both online and offline) before the image is formed.

Accurate and convenient test signals are provided by point-like radio sources in the sky, most of them distant quasars, typically brighter than about 0.1 Jy, with accurately known positions. A short observation of a quasar for a few minutes with ALMA provides the test data needed to determine the path length adjustments to improve the array imaging. The optimum coupling of the quasar calibrator and science target observations to produce high fidelity images are discussed below.

The filling of the ALMA Quasar Catalogue

Quasar emission is produced near the nucleus of an associated massive galaxy which may contain a black hole. The emission is variable because of the interaction of material with magnetic fields near the black hole, and often leads to the ejection of material in narrow radio jets. The changes in the emission from these objects have been widely studied (e.g., Antonucci, 1993), especially with very long baseline interferometric techniques. But, their significant variability in intensity is a complication in their use as amplitude (gain) calibrators. However, these quasars are sufficiently far away that most of their emission is contained in a region that is less than 0.01 arcseconds in projected size, so that their variability has little effect on their use to monitor path length changes.

In order to compile and store the information for hundreds of quasars, a source catalogue for ALMA was implemented in 2010. The initial content of the catalogue was taken from several low frequency catalogues from other observatories which used them for similar calibration purposes[1,2,3]. However, the strength of these quasars at the ALMA frequency range of 85 to 900 GHz was unknown except for those monitored at these high frequencies by the Submillimeter Array[4], the Wilkinson Microwave Anisotropy Probe[5] and the Herschel Space Observatory[6]. On account of the great sensitivity of ALMA, a much larger calibrator database would be needed. With the ability of ALMA to determine radio positions at the milliarcsecond level, the quasar positions were obtained from several Very Long Baseline Catalogues[7,8,9].

The special ALMA calibration observations began in early 2011 when many hundreds of sources were checked for their intensities. From these observations and other observatory monitoring at or above 85 GHz, about forty strong and relatively stable sources, well-distributed over the sky, were chosen to be observed

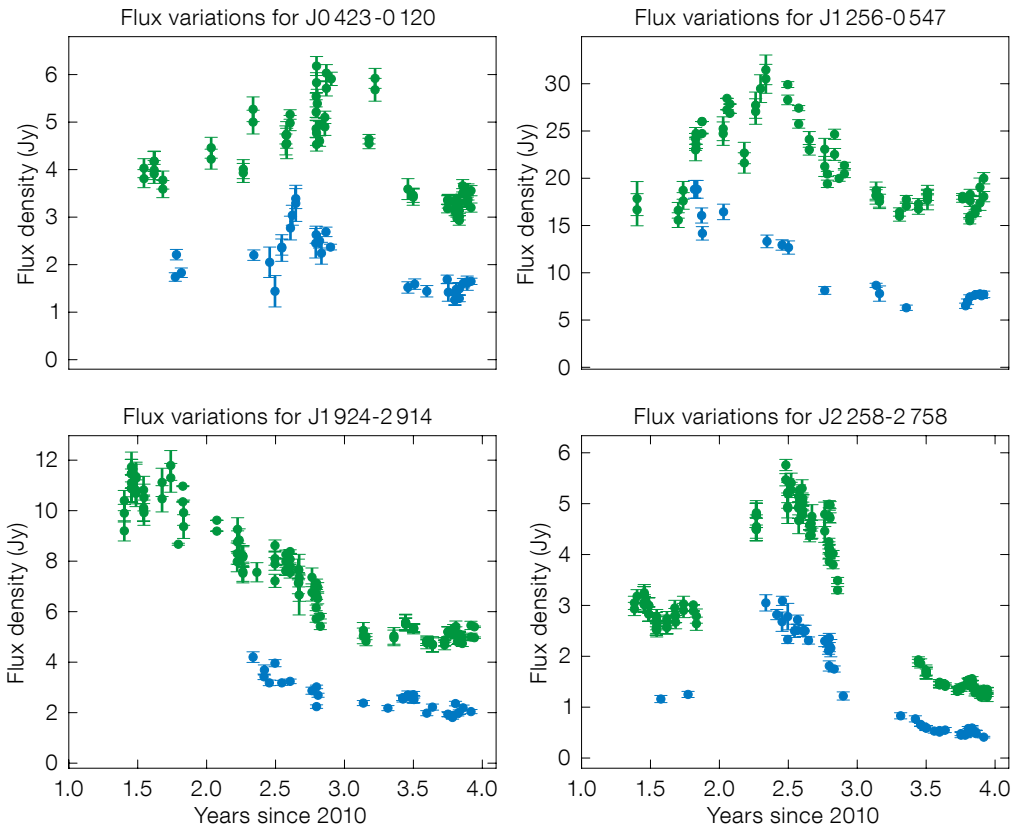

Figure 1. The flux variations of selected quasars are shown. The flux densities for J0423-0120, J1256-0547 (3C279), J1924-2914, J2258-2758 at Band 3 (100 GHz) in green and Band 7 (350 GHz) in blue are shown in the four panels. The observations cover the period from January 2011 to January 2014. The estimated uncertainties are shown by the error bars from each observation. The gaps in monitoring occur when the sources are near the Sun and not monitored regularly during the daytime.

by ALMA at 90 GHz and 350 GHz periodically. This sample is called the grid sample because at least one of them is visible at any time in the sky from ALMA and is usually within 30 degrees of any science target. These sources are sufficiently strong that the calibration across all narrowband frequency channels can be determined to a few percent accuracy.

Each ALMA grid session takes about 40 minutes and consists of one scan of about eight sources. In order to determine the flux density scale of the observations, a scan of a Solar System object is included. These objects have been well studied by many groups over the years, so that their strength is accurately known to about 5% in the ALMA frequency range. But, because of the high resolution of ALMA and the wandering of these bodies around the sky, they are not always available for use as flux density standards. The objects with sufficiently accurate models, but not larger than about 5 arcseconds in angular size are Mars, Uranus, Neptune, and the moons Titan, Ganymede and Callisto (Europa and Io are often too close to Jupiter), the asteroids Pallas, Juno and Vesta and the dwarf planet Ceres.

Examples of the variability at 100 and 350 GHz of four selected quasars are shown in Figure 1. These plots display the range of variability properties and were chosen because they have the most extensive monitoring history so far. The data histories for these and others show that their emission generally changes smoothly with a typical variation of 10% per month. Hence, a flux density measurement every two or three weeks, tied to a Solar System object, should provide a flux density estimate accurate to < 10% at any time. This accuracy is sufficient for the goals of most ALMA projects. But occasional outliers, which vary strongly over less than one month (e.g., J0423-0120 and J1256-0547), do occur. Changes in a factor of two over yearly periods are common, and the content of the grid source list will be modified accordingly.

The relatively constant ratio between the 100 and 350 GHz flux densities reflects the small range of quasar spectral slope around $\nu^{-0.7}$, although flares occur at somewhat different times at the two frequencies. Thus, the interpolation of a quasar flux density between 100 and 350 GHz is accurate to about 10%, if the two flux density measurements were made within two weeks. Extrapolation to 500 and 900 GHz is somewhat more uncertain, at the 15% level. Occasional simultaneous observations at three frequencies of these quasars show that many have a spectral curvature between 100 and 400 GHz that is sufficiently small not to impact significantly on the simple linear spectral index extrapolation to higher frequencies. Since the good observing conditions necessary for > 600 GHz observations are at a premium, calibrator measurements have lower priority than science observations. However, flux density estimates obtained from science projects are entered into the ALMA catalogue and provide some check of the extrapolation accuracy[10].

Finally, catalogue data-filling observations of weaker sources are also continuing in

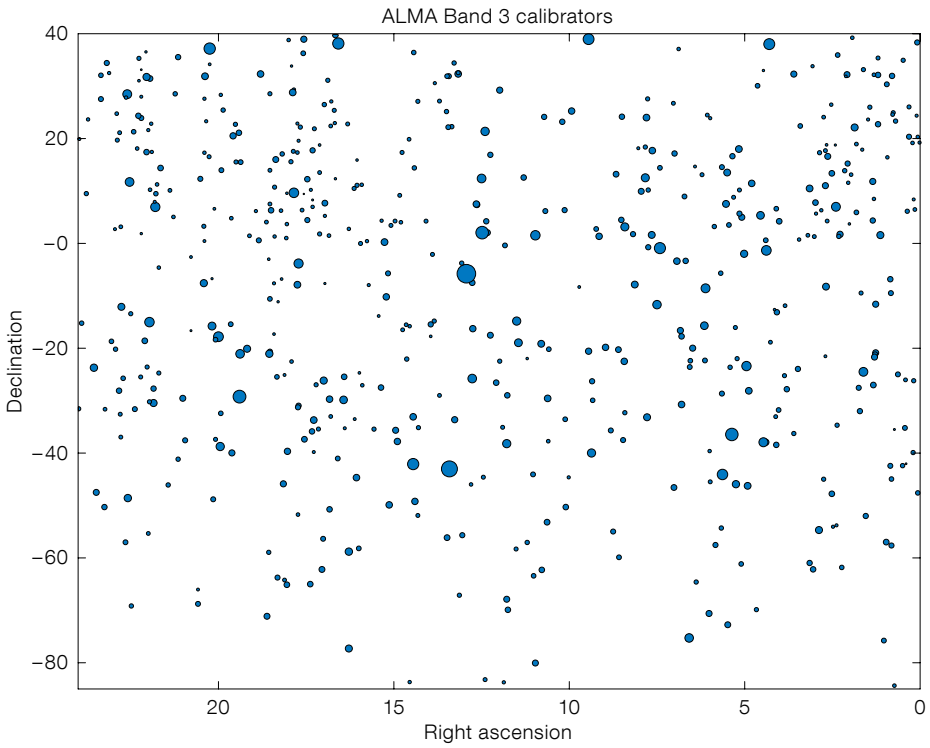

Figure 2. The distribution of ALMA Band 3 (100 GHz) calibrators are shown. Each circle represents a quasar with an ALMA-measured flux density at Band 3. The largest points are in the 10–20 Jy range; the smallest are near 0.1 Jy.

order to find quasars that are sufficiently strong for use as phase calibrators. At present there are 600 sources that are satisfactory calibrators, but several thousand are needed for future ALMA observations at baselines > 10 km, when target–calibrator separations of two degrees are needed to remove the large delay changes.

The ALMA quasar calibration methods

The observing schedule for an ALMA project is produced dynamically in order to accommodate optimally the requirements of the project with the variable conditions. Thus, the choice of calibrators is often made at run time. The relevant parameters of the scientific target are its position in the sky, the desired resolution (required size of the ALMA array) and the range of frequencies at which to observe. The latter depends on the molecule(s) the astronomer wishes to study. The amount of observing time requested depends on the image sensitivity that must be reached in order to achieve the proposed scientific results.

To accommodate the above scheme, just before the start of an observation a software-based calibrator query algorithm searches the ALMA Quasar Catalogue in order to find suitable quasar test sources that are needed to produce good quality images of the target. There are generally three kinds of test sources (calibrators) needed. If available, one of the Solar System objects is observed for about ten minutes in order to determine the flux density scale of the observation. Next, in order to determine the path length and gain changes across the range of frequencies relevant to the astronomical observations, one of the bright grid sources is observed for up to 15 minutes when narrowband channels are used. Both of the above test observations need only be done once per project execution and that can last up to several hours. If the grid source flux density has recently been measured and a Solar System object is not available, the grid source can be used for the flux density scale.

The final calibration type, called the phase referencing, removes path length variations that occur in the atmosphere above each of the antennas in the switching time between the calibrator and target, generally from 20 seconds to 5 minutes. The calibrator query for the most optimum phase calibrator has several criteria that must be balanced. First, the closer the quasar is to the science target in the sky, the more accurately it will remove the path length fluctuations in the target source. On the other hand, the calibrator must have sufficient signal in order to measure these fluctuations precisely and this depends on the intensity of the calibrator and its scan length. As shown in Figure 1, quasars often vary in flux density by more than a factor of two over a year. Since most of these fainter quasar calibrators have limited observations, it is possible that one or more may be too weak for use. Thus, a quick check of the flux density of such quasar candidates before the selection is recommended, especially for those quasars that are just above the sensitivity limit needed for sufficiently accurate measurements.

The switching time between calibrator and target also depends on the wind speed, the water vapour content, the observing frequency and the size of the array. Typically, a phase calibrator is observed for a scan length 10 to 120 seconds with a repetition rate that is about five times the scan length. Thus, the additional observations of calibrator sources can use up to 30 % of the total project observing time.

The distribution of the nearly 600 quasars measured with ALMA at Band 3 is given in Figure 2. The probability of finding one of these calibrators within a specified distance from a random target location is given in Figure 3. At the higher frequencies, the number of available calibrators decreases because of the poorer ALMA sensitivity and the lower flux density of most quasars. Although still at the experimental stage, it may be possible to observe a quasar calibrator at, for example, 100 GHz, to calibrate a science target at 350 or 650 GHz. This band-to-band calibration scheme will be successful if: (1) the phase change measured by

the quasar at 100 GHz can be scaled with frequency precisely (i.e., it represents a true path length change); and (2) the instrumental phase differences between the low and high frequencies are smoothly changing over several hours and can be measured by occasionally grid calibrator observations, not necessarily close to the target.

Even though the ALMA site is extremely dry, delay variations of 0.1 mm on time scales as short as a few seconds are produced by small "clouds" of water vapour moving across the beam of each antenna. Such changes on timescales of between about one second to twenty seconds cannot be removed by phase referencing with quasars near the target. However, a group at the University of Cambridge has developed a 183 GHz water vapour radiometer (WVR) system that has been placed on the ALMA antennas in order to measure the water vapour emission along the line of sight to the radio source (Nikolic et al., 2008; 2013). The amount of emission is well-correlated with the path length changes toward the source, and the application of these corrections often decreases the short-term phase variations by more than 50%.

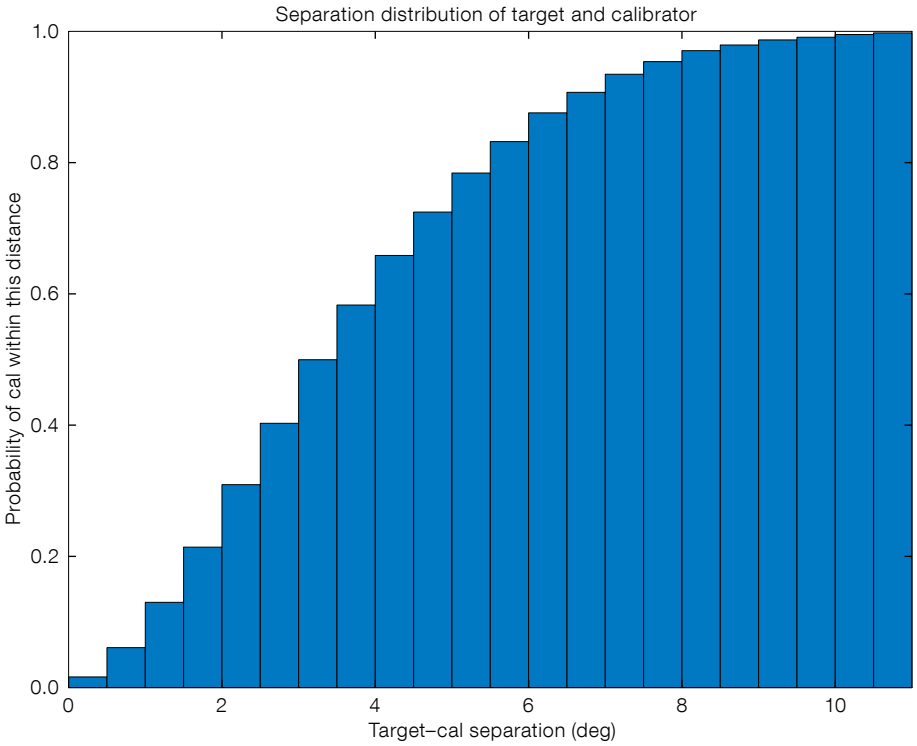

Figure 3. The histogram of the target–calibrator separation from the ALMA catalogue on 1 January 2014. The probability distribution for the minimum separation of a random position in the sky from the nearest Band 3 calibrator is shown. The median separation is 3.5° and there is a 90% probability of finding a calibrator within 7° of a random target.

Future ALMA calibrator developments

ALMA observation and development will continue over at least the next five years to improve the quasar calibration methods, at the level of about 5% of the total observing time. The detailed monitoring of the brightest 50 quasars at several frequencies will continue since these sources are secondary flux density calibrators for many ALMA observations. The need to have closer quasar and target pairs will increase for higher resolution, longer baseline projects, and will require the finding of more than one thousand additional calibrators. It is probably more efficient to search in a small area around likely targets for suitable quasars, rather than perform more global searches around the sky. Techniques to remove the dry-air component of the path delay changes (the WVR system only aids in the delay estimate from the wet component) will become more important for the longer baselines. Many ground weather and sounding devices would be needed, and multi-quasar calibrations can remove some of the longer temporal and angular changes. Finally, the experimental development of band-to-band phase quasar calibration is now in progress.

The uniqueness of the observing conditions in the high Atacama Desert, the quality of the ALMA antennas, the sensitivity of the receivers and electronics, and the infrastructure developed for array operation, have provided an array that can produce high quality images of a wide variety of astronomical objects at millimetre and submillimetre wavelengths. This image fidelity is significantly increased by interleaving relevant observations of a quasar calibrator with the target source, in order to remove the fast changing delay in the troposphere.

References

Antonucci, R. 1993, ARA&A, 31, 473
Nikolic, B. et al. 2008, The Messenger, 131, 14
Nikolic, B. et al. 2013, A&A, 552, A104

Links

[1] CRATES Flat-spectrum Catalogue: http://heasarc.gsfc.nasa.gov/W3Browse/all/crates.html
[2] AT20G 20 GHz catalogue: http://heasarc.gsfc.nasa.gov/W3Browse/all/at20g.html
[3] VLA Calibrator Manual: http://www.vla.nrao.edu/astro/calib/manual/csource.html
[4] SMA calibrator list: http://sma1.sma.hawaii.edu/callist/callist.html
[5] WMAP catalogue: http://lambda.gsfc.nasa.gov/product/map/dr3/ptsrc_catalog_get.cfm
[6] Planck compact source catalogue: http://www.sciops.esa.int/wikiSI/planckpla/index.php?title=Compact_Source_catalogues&instance=Planck_Public
[7] VLBA Sched Catalogue: http://www.aoc.nrao.edu/software/sched/Source_Catalog.html
[8] Petrov VLBI catalogue: http://astrogeo.org/vlbi/solutions/rfc_2013d/rfc_2013d_cat.txt
[9] ICRF2 catalogue: http://hpiers.obspm.fr/webiers/icrf2/icrf2.html 10 T van Kempen et al. 2014 in prep., ALMA Memo on Data-base filling

The Multi-Unit Spectroscopic Explorer, MUSE, instrument underwent its first commissioning run in Februrary 2014. Here MUSE is shown at the Nasmyth B focus of VLT Unit Telescope 4 (Yepun) during one of the commissioning nights.

ESO/Ghaouti Hansali/Fernando Selman

Eric Le Roux/University Claude Bernard Lyon 1/CNRS/ESO

MUSE shown in daylight on UT4. An image of the galaxy NGC 4650A from the commissioning run can be seen on p. 11. See Release eso1407 for more details.

VISTA Variables in the *Vía Láctea* (VVV): Halfway Status and Results

Maren Hempel[1,2]
Dante Minniti[1,3]
István Dékány[1]
Roberto K. Saito[1,4]
Philip W. Lucas[5]
Jim P. Emerson[6]
Andrea V. Ahumada[7,8,9]
Suzanne Aigrain[10]
Maria Victoria Alonso[7]
Javier Alonso-García[1]
Eduardo B. Amôres[11]
Rodolfo Angeloni[1]
Julia Arias[12]
Reba Bandyopadhyay[13]
Rodolfo H. Barbá[12]
Beatriz Barbuy[14]
Gustavo Baume[15]
Juan Carlos Beamin[1]
Luigi Bedin[16]
Eduardo Bica[17]
Jordanka Borissova[18]
Leonardo Bronfman[19]
Giovanni Carraro[8]
Márcio Catelan[1]
Juan J. Clariá[7]
Carlos Contreras[1]
Nicholas Cross[20]
Christopher Davis[21]
Richard de Grijs[22]
Janet E. Drew[5,23]
Cecilia Fariña[15]
Carlos Feinstein[15]
Eduardo Fernández Lajús[15]
Stuart Folkes[5,18]
Roberto C. Gamen[15]
Douglas Geisler[24]
Wolfgang Gieren[24]
Bertrand Goldman[25]
Oscar González[8]
Andrew Gosling[26]
Guillermo Gunthardt[12]
Sebastian Gurovich[7]
Nigel C. Hambly[20]
Margaret Hanson[27]
Melvin Hoare[28]
Mike J. Irwin[29]
Valentin D. Ivanov[8]
Andrés Jordán[1]
Eamonn Kerins[30]
Karen Kinemuchi[31]
Radostin Kurtev[18]
Andy Longmore[20]
Martin López-Corredoira[32]
Tom Maccarone[33]
Eduardo Martín[32]
Nicola Masetti[34]
Ronald E. Mennickent[24]
David Merlo[7]
Maria Messineo[35]
I. Félix Mirabel[36,37]
Lorenzo Monaco[8]
Christian Moni-Bidin[38]
Lorenzo Morelli[39]
Nelson Padilla[1]
Tali Palma[7]
Maria Celeste Parisi[7]
Quentin Parker[40,41]
Daniela Pavani[17]
Pawel Pietrukowicz[42]
Grzegorz Pietrzynski[24,43]
Giuliano Pignata[44]
Marina Rejkuba[8]
Alejandra Rojas[1]
Alexandre Roman-Lopes[12]
Maria Teresa Ruiz[19]
Stuart E. Sale[1,18,45]
Ivo Saviane[8]
Matthias R. Schreiber[18]
Anja C. Schröder[46,47]
Saurabh Sharma[18]
Michael Smith[48]
Laerte Sodré Jr.[14]
Mario Soto[12]
Andrew W. Stephens[49]
Motohide Tamura[50]
Claus Tappert[18]
Mark A. Thompson[5]
Ignacio Toledo[51]
Elena Valenti[8]
Leonardo Vanzi[52]
Walter Weidmann[7]
Manuela Zoccali[1]

[1] Instituto de Astrofísica, Pontificia Universidad Católica de Chile, Chile
[2] The Milky Way Millennium Nucleus, Santiago, Chile
[3] Vatican Observatory, Italy
[4] Universidade Federal de Sergipe, Departamento de Física, Cristóvão, Brazil
[5] Centre for Astrophysics Research, Science and Technology Research Institute, University of Hertfordshire, Hatfield, UK
[6] Astronomy Unit, School of Physics and Astronomy, Queen Mary University of London, UK
[7] Observatorio Astronómico de Córdoba, Argentina
[8] ESO
[9] Consejo Nacional de Investigaciones Científicas y Técnicas, Buenos Aires, Argentina
[10] School of Physics, University of Exeter, UK
[11] SIM, Faculdade de Ciências da Universidade de Lisboa, Portugal
[12] Departamento de Física, Universidad de La Serena, Chile
[13] Department of Astronomy, University of Florida, Gainesville, USA
[14] Universidade de São Paulo, Brazil
[15] Facultad de Ciencias Astronómicas y Geofísicas, Universidad Nacional de La Plata, Argentina
[16] Space Telescope Science Institute, Baltimore, USA
[17] Universidade Federal do Rio Grande do Sul, Porto Alegre, Brazil
[18] Departamento de Física y Astronomía, Facultad de Ciencias, Universidad de Valparaíso, Chile
[19] Departamento de Astronomía, Universidad de Chile, Santiago, Chile
[20] Institute for Astronomy, The University of Edinburgh, UK
[21] Joint Astronomy Centre, Hilo, USA
[22] Kavli Institute for Astronomy and Astrophysics, Peking University, China
[23] Astrophysics Group, Imperial College London, UK
[24] Departmento de Astronomía, Universidad de Concepción, Chile
[25] Max Planck Institute for Astronomy, Heidelberg, Germany
[26] Department of Astrophysics, University of Oxford, UK
[27] Department of Physics, University of Cincinnati, USA
[28] School of Physics & Astronomy, University of Leeds, UK
[29] Institute of Astronomy, University of Cambridge, UK
[30] Jodrell Bank Centre for Astrophysics, The University of Manchester, UK
[31] NASA-Ames Research Center, Moffett Field, USA
[32] Instituto de Astrofísica de Canarias, La Laguna, Tenerife, Spain
[33] Department of Physics, Texas Tech University, Lubbock, USA
[34] Istituto di Astrofisica Spaziale e Fisica Cosmica di Bologna, Italy
[35] Rochester Institute of Technology, Rochester, USA
[36] Service d'Astrophysique – IRFU, CEA-Saclay, Gif sur Yvette, France
[37] Instituto de Astronomía y Física del Espacio, Buenos Aires, Argentina
[38] Instituto de Astronomía, Universidad Católica del Norte, Antofagasta, Chile
[39] Dipartimento di Astronomia, Universitá di Padova, Italy
[40] Department of Physics, Macquarie University, Sydney, Australia

[41] Australian Astronomical Observatory, Epping, Australia
[42] Nicolaus Copernicus Astronomical Center, Warsaw, Poland
[43] Warsaw University Observatory, Warsaw, Poland
[44] Departamento de Ciencias Físicas, Universidad Andres Bello, Santiago, Chile
[45] Rudolf Peierls Centre for Theoretical Physics, Oxford, UK
[46] SKA/KAT, Cape Town, South Africa
[47] Hartebeesthoek Radio Astronomy Observatory, Krugersdorp, South Africa
[48] The University of Kent, Canterbury, UK
[49] Division of Optical and Infrared Astronomy, National Astronomical Observatory of Japan, Tokyo, Japan
[50] Gemini Observatory, Hawaii, USA
[51] ALMA Observatory, Santiago Chile
[52] Departamento de Ingeniería Eléctrica, Pontificia Universidad Católica de Chile, Santiago, Chile

The VISTA Variables in the *Vía Láctea* (VVV) survey is one of six near-infrared ESO public surveys, and is now in its fourth year of observing. Although far from being complete, the VVV survey has already delivered many results, some directly connected to the intended science goals (detection of variable stars, microlensing events, new star clusters), others concerning more exotic objects, e.g., novae. Now, at the end of the fourth observing period, and comprising roughly 50 % of the proposed observations, the status of the survey, as well some of results based on the VVV data, are presented.

Introduction

The Visible and Infrared Survey Telescope for Astronomy (VISTA, Emerson & Sutherland, 2010) has been operated by ESO for four years. Observations began with Science Verification in September 2009, and this was followed by the six public surveys, one of which is VISTA Variables in the *Via Láctea* (see Minniti et al., 2010; Saito et al., 2010; Catelan et al., 2011). The only science instrument currently available at VISTA is the wide-field camera VIRCAM (Dalton et al., 2006; Emerson & Sutherland, 2010), offering a 1.1 by 1.5 degree field of view, ideal for surveys covering many hundreds of square degrees. The large field of view in combination with the spatial resolution of 0.339 arcseconds per pixel make VISTA/VIRCAM an ideal instrument to observe the most crowded and extincted regions of the Milky Way, i.e. the central regions of the Bulge and the mid-plane regions of the Galactic Disc. The feasible observing period for the VVV survey is limited to six months, between February and October, requiring careful scheduling of the individual observing periods.

The first main phase of the survey, consisting of the *YZJHKs* multi-colour observations, was assigned to the first semester of the survey (Period 85, 2010) to obtain a first overview of the survey area (described in Section 2). The vast majority of the observations however form the variability campaign, which started in parallel with the multi-colour observations in Period 85, but then occupied all the following observing periods. For the variability campaign, VVV was allotted 300 hours in 2010 (including multi-colour observations), 292 hours in 2011, 275 hours in 2012 and 702 hours in 2013 (split between Periods 90 and 91). The remaining 360 hours of the survey will be used not only to gather additional data for the variability survey (see below), but also to aid the ongoing proper motion study on the Solar Neighbourhood and in searching for microlensing events in a selected Bulge area. The long-term status of the VVV survey, especially in combination with other data (e.g., 2MASS and WISE) make it very suitable to conduct proper motion studies, which are the subject of a later section.

The following observations were scheduled for each period (Minniti et al., 2010):
– P85 (April–October 2010): *YZJHKs* and additional *Ks*-band observations for the whole survey area;
– P87 (April–October 2011): *Ks*-band observations of the complete survey area;
– P89 (April–October 2012): main variability campaign on the Bulge area;
– P90 (November 2012 – March 2013): variability campaign on the outer Disc area;
– P91: (April–October 2013): variability campaign of the inner Disc region and the Bulge.

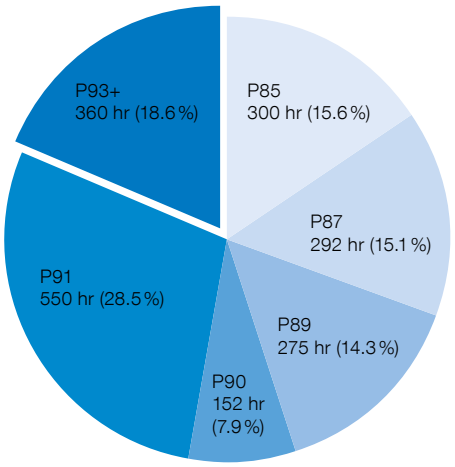

Figure 1. Observing schedule for the VVV survey in comparison with the total allotted observing time of 1929 hours. Note, that *ca.* 50 % of the P91 observations were delayed due to poor weather. The remaining 360 hours will be distributed over Period 93 (2014) and the following years.

Already, after the first two observing periods, despite the modest amount of data (see Figure 1) it has become obvious that the data reduction, analysis and even data storage/transfer are daunting tasks. These considerations affected not only the survey team, conducting a wide range of science projects, final quality control, preparation of observations and the public data release, but also the Cambridge Astronomical Survey Unit (CASU), in charge of the pipeline reduction of all data, as well as ESO, performing the observations, the first level of quality control and the final data release.

Multi-colour photometry

The multi-colour observations in the five broadband filters *Y*, *Z*, *J*, *H* and *Ks* commenced in March 2010 and were concluded by September 2011. Starting with the *J*-, *H*- and *Ks*-band data only, an unprecedented first multi-colour view on the inner region of the Milky Way Bulge composed of 84 million stellar sources was presented by Saito et al. (2012a; see also the ESO Release 1242[1]), followed by the study of Soto et al. (2013) of 88 million stellar sources in the southern Galactic Disc.

Multi-colour observations with high spatial resolution and photometric depth, like the VVV datasets, are not only valuable

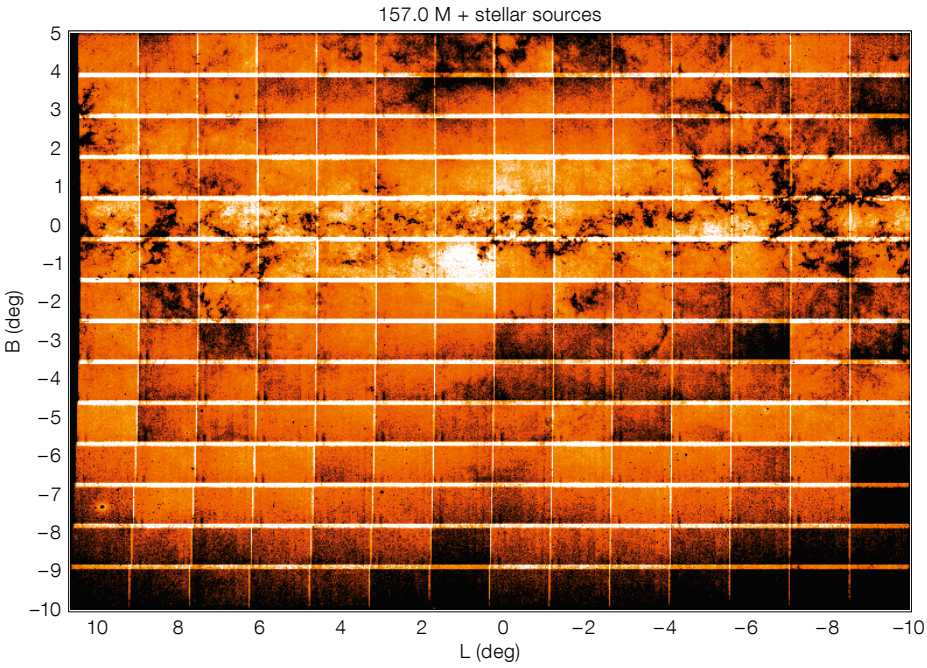

Figure 2. The source density in the Bulge region of the VVV survey is shown. Only point sources which were detected in all five bands are included in this plot. Empty fields represent data that did not fulfill the stringent quality criteria and are not part of the public data release. The latter observations will be repeated in due course.

probes of the Galactic structure, but also extremely important to tackle one of the large problems in Galactic studies, the effect of reddening. Line of sight reddening hampers all photometric methods, such as for age and metallicity determination. Detailed reddening maps, such as the ones provided by Schlegel et al. (1998) are widely used to correct for Galactic reddening, but were known to be less reliable for the most reddened regions near the Galactic Plane, where an extinction in the V magnitude (A_V) of 30 mag can be reached. Including the single epoch observations in the *Y*- and *Z*-bands reveals the distribution of the dust obscuring the inner regions of the Bulge, and enables the high stellar density to become clearly visible (see Figure 2).

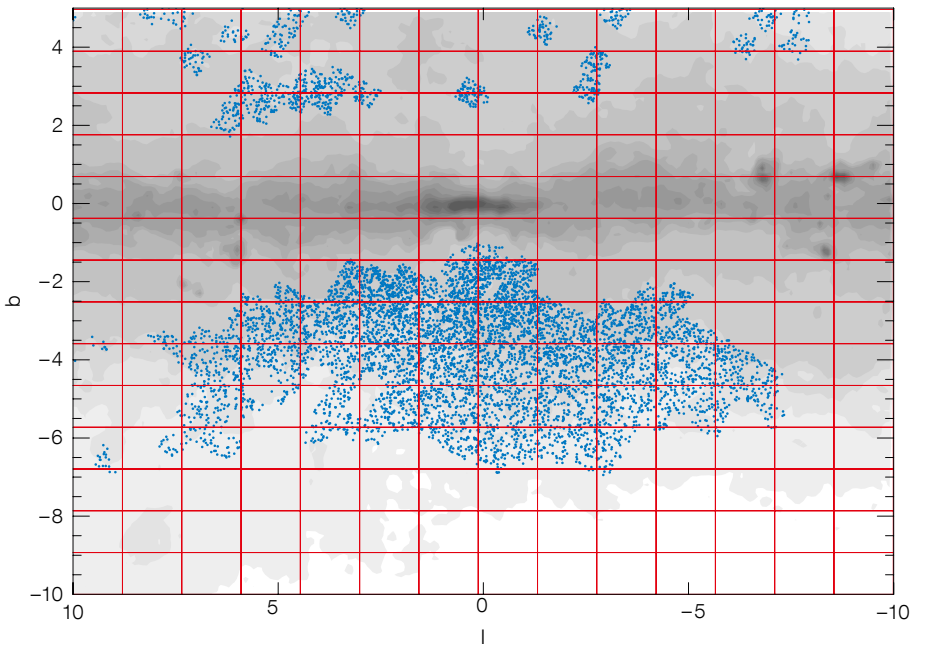

Red Clump (RC) stars are an ideal tracer of the reddening effect, since their colour and luminosity are well defined and the dependence on age and metallicity well understood. Gonzales et al. (2013) used the distribution of the RC stars within the VVV Bulge area to derive a reddening map covering the Galactic Bulge (see Figure 3 of Gonzalez et al. [2013]) within 4 degrees of the Galactic Plane with a spatial resolution of 2 arcminutes. At larger Galactic latitudes, where the reddening varies on a larger scale, the resolution is slightly lower, but still ≤ 6 arcminutes. Such a high spatial resolution is, for instance, essential when studying stellar populations in Milky Way star clusters, which, depending on their position, are affected by differential reddening.

Using the RC stars as *bona fide* distance indicators of the innermost region of the Bulge along various lines of sight, Gonzalez et al. (2011) could also study the inner Galactic Bar, and provide additional evidence for the existence of a secondary bar structure, as suggested by Nishiyama et al. (2005). In a similar way, Saito et al. (2011), based on 2MASS data, mapped the X-shaped structure of the Bulge, showing extension far beyond the spatial extent of the inner Bar structure.

Variability in the near-infrared

In addition to the multi-colour observations (see above) the first observing period of the survey also included five *Ks*-band observations for each of the 348 tiles. Although the main variability campaign for the two independent survey areas, i.e. the Bulge and Disc sections, were scheduled for the third and fourth year of VVV, the search for long-term variables required that at least a few epochs for each tile were obtained in each year/

Figure 3. The Bulge region of the VVV survey (196 tiles, red boxes). The blue dots mark the position of known RR Lyrae stars (> 13 000) based on the OGLE database.

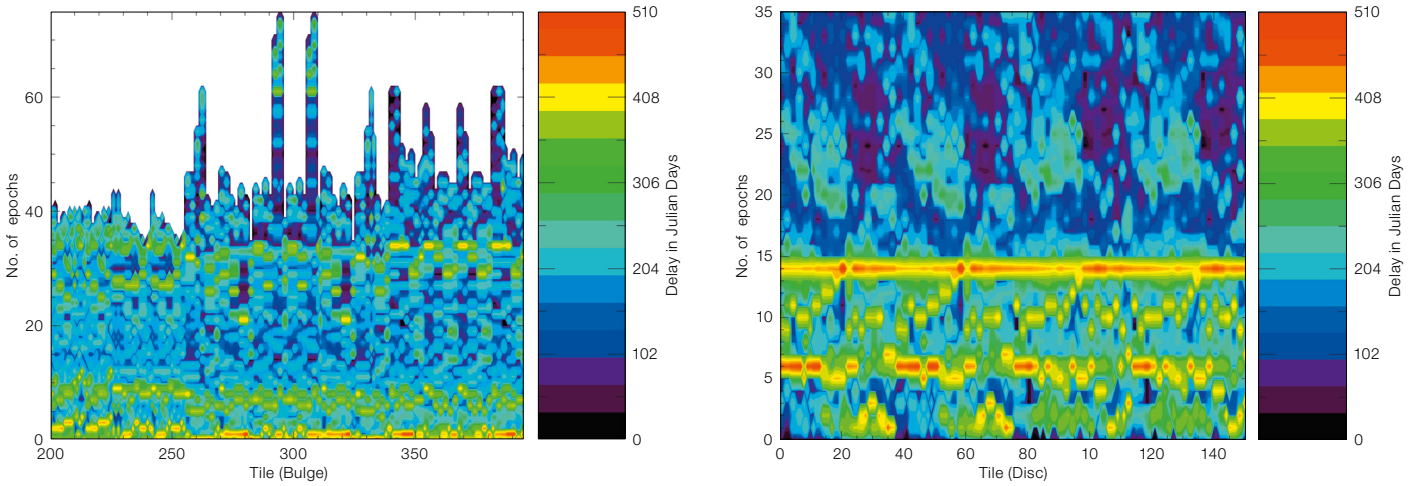

Figure 4. Distribution of delays between two consecutive epochs of the individual *Ks*-band observations for the Bulge (left panel) and the Disc region (right panel) of the VVV survey. The timeline covered by the Disk observations is February 2010 to October 2013.

semester. At the time of this article, the Disc area had been observed in the *Ks*-band 36 times, whereas the Bulge tiles, subject of the observing campaign in P91, had up to 75 epochs available.

In addition, the observations during Science Verification (e.g., Saito et al., 2010) included additional data for tiles b293 and b294 (a total of 71 epochs), coinciding with Baade's Window, which due to its low Galactic reddening had been studied extensively by the Optical Gravitational Lensing Experiment (OGLE) project in the optical, and for which a large number of RR Lyrae stars, the survey's primary targets, are known (see Figure 3).

The backbone of the light curve analysis is the frequency with which the observations were executed. This becomes even more important, when we have to combine data which were not simultaneously observed, as is the case for the individual VVV tiles. In order to be able to compare the derived stellar distances used to create the final 3D model of the inner Milky Way, we have to ensure that the individual light curves are indeed of comparable quality, i.e., that the light curves for the variable stars are populated in a similar fashion. As for any other observing campaign, this not only depends on the original schedule (e.g., Minniti et al., 2010; Saito et al., 2012b), but is also affected by the observing conditions, e.g., presence of clouds, high humidity, etc. As a result, the VVV observations vary significantly in their cadence, as shown in Figure 4.

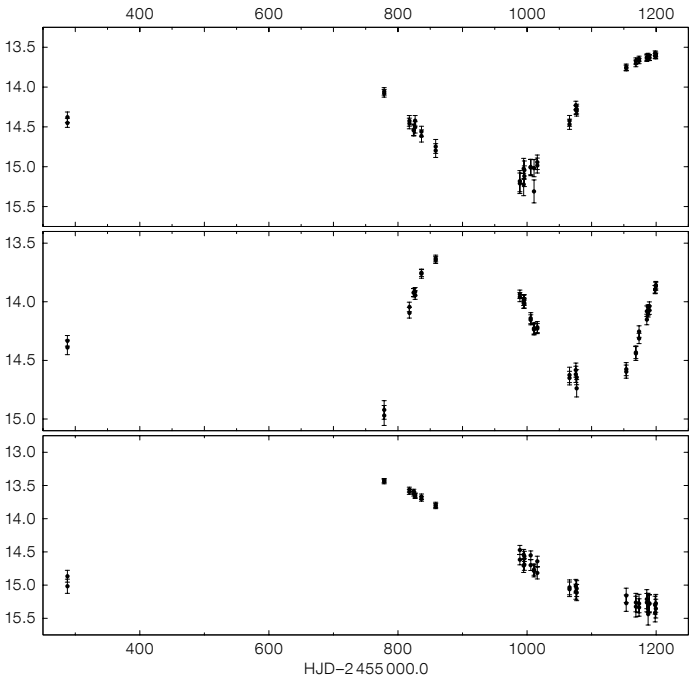

Figure 5. Examples of *Ks*-band light curves of long term variables. The light curves are based on the aperture photometry provided by the CASU VIRCAM pipeline, and use the individual pawprints (Emerson et al., 2004).

Although the observations are still ongoing and will require an additional 2–3 years, the analysis of the light curves has already begun; they show the excellent quality of the data. As shown in Figures 5 and 6, even at this early stage of the survey, and based on a limited number of observing epochs, long-term variables with periods of several hundreds of days (Figure 5) can be detected as unambiguously as well as the objects with a period of only a few days or even hours (Figure 6). Only surveys with an anticipated duration period of many years are suitable to study long-term variables such as the ones shown in Figure 5.

Although the VVV survey is targeted at various types of variable stars, of special importance are those classes of variable stars that show a well-defined luminosity–period correlation, because they will allow us to derive distances and eventually build a three-dimensional model of the observed Milky Way region. In addition the frequent observations, in

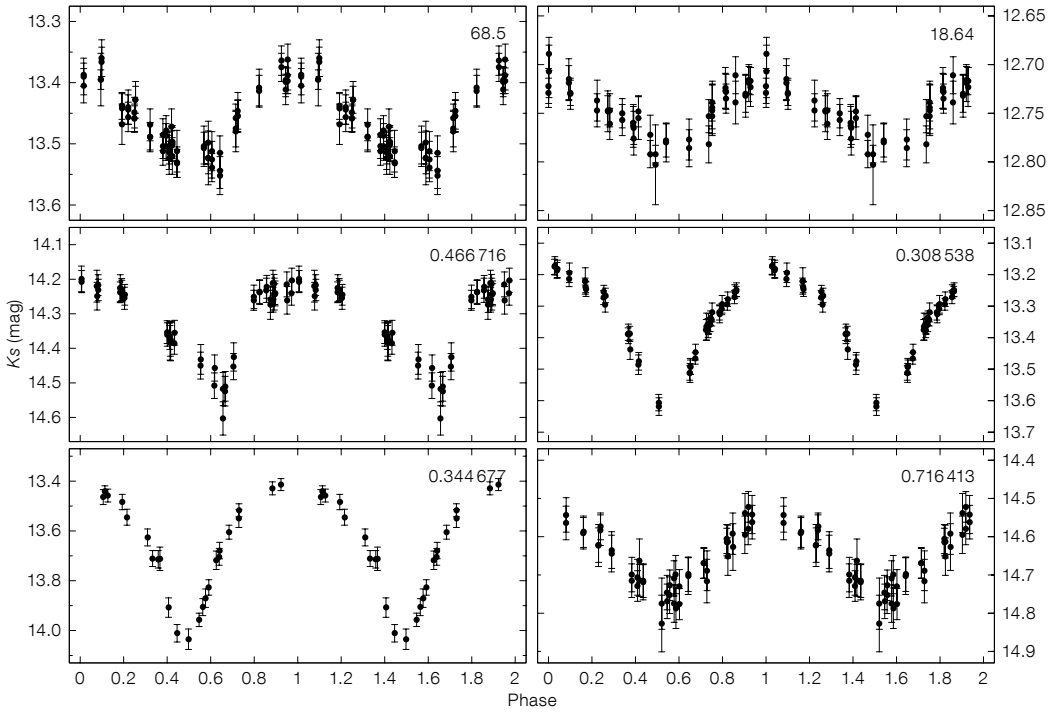

Figure 6. Examples of six *Ks*-band light curves of variable stars with periods ranging from a few hours up to several weeks are displayed. As in Figure 6 the aperture photometry of the CASU source catalogues was used.

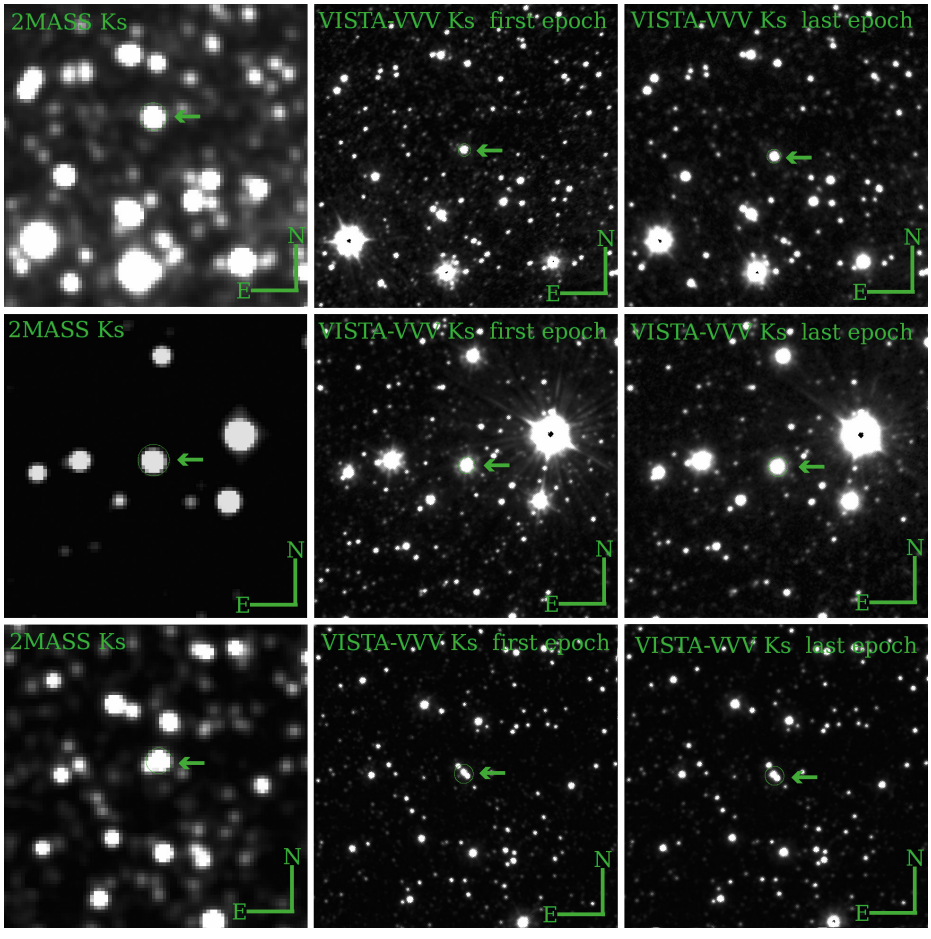

combination with a limiting *Ks* magnitude of ~18.0 for a single epoch, allows us to search for and follow up more exotic objects, like novae (Beamin et al., 2013; Saito et al. 2013).

Proper motions

The above-mentioned delays in the observing schedule, which are anything but helpful for the general progress of the survey, can be considered as a blessing in disguise for the proper motion studies, another essential part of the survey (Minniti et al., 2010). Proper motions are the most widely used method to search for close Solar neighbours and thus to complete the census of stars within a few tens of parsecs from the Sun. In particular, in the direction towards the Milky Way Bulge, severe crowding and extinction hamper the detection of faint, albeit nearby stars. (e.g., Lépine et al., 2008);

Figure 7. Selected sample of HPM objects, detected by Gromadzki et al. (2013, see also their Figure 1). The left column shows the 2MASS images, whereas the middle and right columns show the first and last VVV image taken of the object, used to derive the proper motions. Shown from top to bottom are: an HPM M dwarf; an M dwarf + white dwarf common proper motion binary; and a close common proper motion binary.

these drawbacks can however be overcome by the VVV observations. The 0.339-arcsecond pixels, the much-reduced dust extinction (in comparison with optical observations) and the long time-line of (eventually) up to seven years (i.e., the full duration of the VVV survey) make this survey an ideal tool with which to find those missing nearby stars. Already at this early stage of the survey, Gromadzki et al. (2013) have found several hundreds of those elusive objects (Figure 7) and, even more importantly, while searching only about 31 % of the survey area, which corresponds to ~1 % of the sky.

The VVV catalogue of high proper motion (HPM) objects includes M dwarfs towards the Galactic Bulge, common proper motion binaries (see also Ivanov et al., 2013), close common proper motion M dwarfs + white dwarf binaries and brown dwarfs towards the Galactic Bulge. At this point of the survey proper motions of ~1 arcseconds/yr are studied. Once the late phase of the survey is added, and also the earlier observations with 2MASS (Skrutskie et al., 2006) are included for the brighter (*Ks* < 14 mag) objects, an accuracy in the proper motion measurement that almost rivals the one of the Gaia mission (i.e. proper motion error: ~10 microarcseconds/yr) will be achievable. Further, near-infrared observations as provided by VVV, 2MASS and DENIS (e.g., Epchtein et al., 1994) allow us to carry out these studies in an area inaccessible for optical missions, such as Gaia.

The future

In recent years, 2MASS has become a veritable treasure trove for Milky Way studies, and the VVV survey will undoubtedly be its worthy successor for the innermost regions of the Milky Way. Extending the source lists by applying more sophisticated detection algorithms, such as point spread function photometry, will allow fainter sources to be detected and hence allow distant objects at the far side of the Galaxy to be probed. The distances derived for the variable stars within the VVV survey area, together with the proper motions, will allow us to build a model of the mostly unexplored inner regions of the Galaxy. By approximately 2016, the observations for the VVV survey will be complete and provide the data required to build a detailed model of the Milky Way Bulge and the southern Galactic Disc. From there we can take a large step closer to understanding the structure and dynamics of the Galaxy.

Acknowledgements

The VVV Survey is supported by ESO, the BASAL Center for Astrophysics and Associated Technologies PFB-06, the FONDAP Center for Astrophysics 15010003 and the MIDEPLAN Milky Way Millennium Nucleus P07-021-F. We would like to thank the staff of CASU and WFAU, who provide us with the pipeline processing, data calibration and archive. Some VVV tiles were made using the Aladin sky atlas, SExtractor software and products from TERAPIX pipeline. This publication makes use of data products from the Two Micron All Sky Survey, a joint project of the University of Massachusetts and IPAC/CALTECH, funded by NASA and the NSF.

References

Beamin, J. C. et al. 2013, ATel, 5215
Catelan, M. et al. 2011, Carnegie Observatories Astrophysics Series, Vol. 5
Dalton, G. B. et al. 2006, Proc. SPIE, 6269
Emerson, J. & Sutherland, W. 2010, The Messenger, 139, 2
Epchtein, N. 1994, A&SS, 217, 3
Gonzalez, O. A. et al. 2011, A&A, 543, L14
Gonzales, O. A. et al. 2013, The Messenger, 152, 23
Gromadzki, M. et al. 2013, Mem. S. A. It., 75, 282
Ivanov, V. D. et al. 2013, A&A, accepted, arXiv:1309.4301v1
Lépine, S. 2008, AJ, 135, 1247
Minniti, D. et al. 2010, New Astronomy, 15, 433
Minniti, D. et al. 2012, ATel, 4041
Nishiyama, S. et al. 2005, ApJ, 621, L105
Saito, R. K. et al. 2010, The Messenger, 141, 24
Saito, R. K. et al. 2012a, A&A, 544, 147
Saito, R. K. et al. 2012b, A&A, 537, 107
Saito, R. K. et al. 2013, A&A, 554, 123
Schlegel, D. et al. 1998, ApJ, 500, 525
Skrutski, M. F. et al. 2006, AJ, 131, 1163
Soto, M. et al. 2013, A&A, 552, 101

Links

[1] VVV stellar density map of the Galactic Bulge: http://www.eso.org/public/news/eso1242

B. Fugate (FASORtronics)/ESO

Stunning view of the plane of the Milky Way above the Paranal Observatory. At the lower right, the dome of the Residencia reflects the light from the sky and the Large Magellanic Cloud is discernible above.

Search for Supernovae in Starburst Galaxies with HAWK-I

Matteo Miluzio[1]

[1] INAF–Osservatorio Astronomico di Padova, Italy

With the aim of testing the relation between supernova (SN) rate and star formation rate, we conducted a SN search in a sample of local starburst galaxies (SBs) where both star formation rates and extinction are extremely high. The search was performed in the near-infrared, where the bias due to extinction is reduced using HAWK-I on the VLT. We discovered six SNe, in excellent agreement with expectations, when considering that, even in our search, about 60 % of events remain hidden in the nuclear regions due to a combination of reduced search efficiency and very high extinction.

Why supernova rates?

The determination of the star formation history (SFH) of the Universe is one of the main goals of modern cosmology, as it is crucial to our understanding of how structures in the Universe form and evolve. The estimate of the star formation rate mainly relies on measurements of integrated galaxy luminosity, most often in the infrared or for specific emission lines, e.g., Hα. The luminosity measurements are converted to total luminosity assuming an initial mass function (IMF) for the stellar population and including a number of corrections to account for the presence of multiple stellar populations, non-thermal source contributions and extinction.

In principle a direct test of the star formation rate (SFR) estimate can be achieved by directly counting the number of dying massive stars, namely core collapse supernovae (CC SNe). Indeed, because of their short-lived progenitors, CC SNe trace the current SFR. On the other hand, for an adopted SFR, measurements of the CC SN rates give information on the mass range of their progenitors and on the slope of the IMF at the high-mass end. Type Ia SNe, however, are the results of thermonuclear explosions of white dwarfs in binary systems, and they trace the whole history of star formation, due to the wide range in the delay times of their progenitors. Recently, it was claimed that a significant fraction of SN Ia have a short delay time of about 10^7 years (Mannucci et al, 2006). As with CC SN, the rate of such prompt SNe Ia events is proportional to the current SFR.

Motivations: The SN rate problem

During the last decade significant effort has been devoted to the measurement of the cosmic SFR, using a combination of many different probes (e.g., Hopkins & Beacom, 2006). Also, as a result of a number of dedicated surveys, new estimates of the SN rate have become available. Although the focus was on type Ia SN, a few estimates of the CC SN rates have been published (e.g., Melinder et al., 2012). In particular, the evolution of SN rates with redshift was found to track the SFR evolution very well, considering the large uncertainties in the extinction corrections. Botticella et al. (2008) obtained a good match between the observed SN and star formation rates assuming a lower limit for CC SN progenitors of 10 $M_{\odot}$.

However, recent study of the core collapse SN progenitors, based on direct detection on pre-explosion archival images, set a lower limit of 8 $M_{\odot}$ (Smartt et al., 2009). It was claimed that if this value is adopted, the observed SN rates would be a factor of two lower than those expected from the observed SFR, sometimes called the SN rate problem (e.g., Horiuchi et al., 2011). While we should keep in mind the uncertainties in SFR calibrations, there are also possible important biases in the SN rate estimates. The two most severe are the possible existence of a large population of very faint CC SNe and/or underestimates of the correction for extinction. In particular, several authors (e.g., Mattila et al., 2012) argue that up to 70–90 % of CC SNe remain hidden in the highly dusty nuclear regions of starburst galaxies. If a correction for the hidden SN population is included in the rate calculation, the discrepancy between SN and star formation rates at high redshifts seems to disappear. It is unclear whether this effect is large enough to also explain the discrepancy observed in the local Universe.

An infrared search in starburst galaxies: Why?

Starburst galaxies have very high SFRs, in the range of 10–100 $M_{\odot}$/year, compared to the few solar masses per year of normal star-forming galaxies. Many starburst galaxies are in close pairs or have disturbed morphology, which is a sign that merging is enhancing their SFR. Since the ultraviolet radiation from young and massive stars heats the surrounding dust and is re-emitted in the far-infrared, the most luminous starbursts are Luminous Infrared Galaxies (LIRGS) with $10^{11} < L_{IR} < 10^{12}$ $L_{\odot}$ and UltraLuminous Infrared Galaxies (ULIRGs) with $L_{IR} > 10^{12}$ $L_{\odot}$.

The first attempts to measure SN rates in starburst galaxies in the optical band date back to 1999 (Richmond et al., 1998) with only a handful of events detected. The first results of a systematic search in starburst galaxies in the infrared (IR) domain were reported by Maiolino et al. (2002) and Mannucci et al. (2003). The main conclusion was that the observed SN rate in starburst galaxies is one order of magnitude higher than that expected from the blue luminosity of the galaxies, but still three to ten times lower than would be expected from the far-IR luminosity. They suggested that the most plausible explanation for this discrepancy was the extreme extinction in the galaxy nuclear regions ($A_V > 25$ mag) that hides SNe even in the IR. Recently, Mattila et al. (2007) conducted an IR search in starburst galaxies using ground-based telescopes with adaptive optics, a technique that allows the nuclear regions to be observed with high spatial resolution. This approach led to the discovery of a handful of SNe, but not yet an estimate of the CC SN rate. About a dozen SNe have been discovered by IR searches so far. Therefore the statistics are still based on very low numbers, and many of the original questions are still unanswered. Entering into this debate, we started a new search to measure the SN rate using the High Acuity Wide-field *K*-band Imager (HAWK-I), the infrared camera mounted at the ESO Very Large Telescope (VLT).

The search strategy

We conducted the HAWK-I search in *K*-band, monitoring a sample of local

starburst galaxies retrieved from the IRAS Revised Bright Galaxy Sample. We selected galaxies with $z < 0.07$ and total infrared luminosity of $L_{TIR} > 10^{11}\ L_{\odot}$. We collected a sample of 30 starburst galaxies for Paranal observation, considering seasonal observability. Given that the SN IR light curves evolve relatively slowly, remaining within one or two magnitudes of maximum for two or three months, an IR SN search did not require frequent monitoring. We planned on average three visits per galaxy per semester, which implies a total of about 100 observing blocks per semester.

The programme was allocated three observing periods and the fraction of useful observing time was 100% of the allocated time in the first season and 70% in the second and third semesters. In total, we obtained 210 *K*-band exposures (with a single exposure time of 15 minutes). Spectroscopic confirmation of the SN candidates was obtained with ISAAC and X-shooter at the VLT (and in one case at the Gran Telescopio Canarias [GTC]). The average image quality was excellent: for about 90% of the exposures the seeing was less than 1.0 arcseconds, with an average value across the whole programme of 0.6 arcseconds. Data reduction was performed by integrating EsoRex (the ESO Recipe EXecution tool) with custom programs. Figure 1 shows the high quality of an image of the galaxy NGC 6926 (one galaxy of our sample) after reduction. SN detection was performed by subtracting images taken at different epochs with the technique of point spread function (PSF) matching. In many cases, the difference images showed significant spurious residuals that correspond to the galaxy nuclear regions, in particular when seeing was poor (full width at half maximum [FWHM] > 1 arcsecond; see Miluzio et al., 2013).

Figure 1. *K*-band HAWK-I image of the spiral galaxy NGC 6926 recorded with seeing of 0.4 arcseconds (from Miluzio et al., 2013).

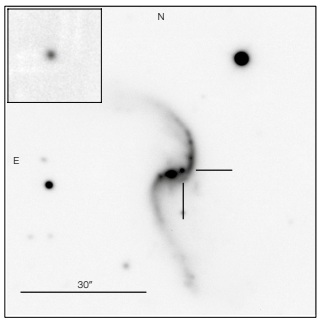

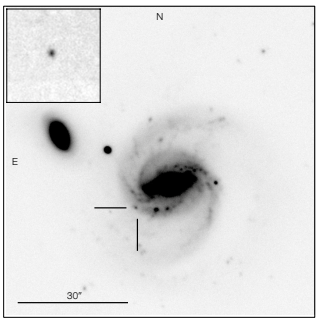

Figure 2. *K*-band finding charts for two SNe discovered in our search (left: SN 2012hp; right: SN 2011ee). The insets show the transients as they appeared in the difference images.

Supernova discoveries and characterisation

During our monitoring campaign six transients were detected in at least two consecutive epochs separated by around one month. We obtained spectroscopic confirmation for four of them: three as CC SN (SN2010bt; SN2012hp, see CBET2446; and SN2011ee, see CBET 2773) and one as a type Ia SN (SN 2010gp). Two candidates were too faint for spectroscopy and the transient classification was based on analysis of multicolour photometry. We argued that they are also likely CC SN. SN e2010bt and 2010gp were discovered by optical searches before our detection, but we rediscovered them independently (Miluzio et al., 2013). Figure 2 shows the *K*-band HAWK-I discovery images of SN 2010hp and SN 2011ee found in MCG-02-01-52 and NGC 7674, respectively. The inset box is a zoom of the difference image where we detected the SN.

Search detection limit

In order to derive the SN rate from the number of detected events, it is crucial to obtain an accurate estimate of the detection efficiency of the search. Through artificial star experiments, we estimated the magnitude detection limit for each of the search images and for different locations in the images. The detection efficiency is influenced by the sky conditions at the time of observations (namely seeing and transparency) and by the location of the transient inside the host galaxy. Indeed, the magnitude limit is brighter in the nuclear regions for a typical galaxy of our sample, corresponding to the inner 1.5–2.0 kpc. While the detection limit in the galaxy outskirts is largely independent of the seeing of the images (typically K ~ 19 mag), this is not true in the nuclear region, where the magnitude limit is significantly brighter when the seeing is poor (in the worst case even 5–6 mag brighter than in the galaxy outskirts; see Miluzio et al., 2013).

SN search simulation

To evaluate the significance of the detected events, we developed a simulation tool that computes the number and properties of the expected events based on specific assumptions and features of our SN search. The basic ingredients of the simulation are:

- the properties of the starburst galaxies of our sample;
- the expected SN properties;
- the details of the search campaign;
- the number of SNe expected from the stellar population after a star formation episode;
- the depth and distribution of dust extinction inside the parent galaxies;
- the star formation location in the parent galaxies.

The tool uses a Monte Carlo approach that simulates the stochastic nature of SN explosions. Based on the analysis of several Monte Carlo experiments with the same input parameters, we can test whether the observed events are within the expected distribution. On the other hand, to test the influence of specific assumptions, we varied some of the input parameters in the Monte Carlo experiments.

Observed *vs.* expected SN discoveries

Outcomes of the simulations are the expected number of SN discoveries, their types, magnitudes, extinctions and positions inside the host galaxies. In Figure 3 we show the histogram of the number of expected SNe compared to the number of observed events (dashed vertical line). Each bin represents the predicted probability of observing the specific number of actual SNe discovered and the shaded areas shows its 1σ Poissonian uncertainty range.

We found that, with the consolidated simulation scenario and input parameters, we could predict the discovery of 5.3 ± 2.3 SNe on average, of which 5.1 are CC SNe and 0.2 are type Ia SNe (Miluzio et al., 2013). This is in excellent agreement with the observed number of six events, one of which is a type Ia SN. If we had computed the expected number of SNe in our survey based on the cosmic average of the SN rate per unit *B*-band luminosity or mass, we would predict the discovery of only 0.5 events. The observed number is one order of magnitude higher, which is consistent with the fact that the thermal IR emission of starburst galaxies is about ten times higher than for average galaxies with the same *B*-band luminosity (Miluzio et al., 2013).

As a consistency check, we verified that the distribution of the expected and observed apparent magnitudes at discovery and the simulated *vs.* observed extinction distributions are in good agreement. This agreement confirms the consistency of our estimates of the magnitude detection limit and the assumption that the extinction is very high in the nucleus and rapidly decreases with the galaxy radius, following the same trend as the SFR.

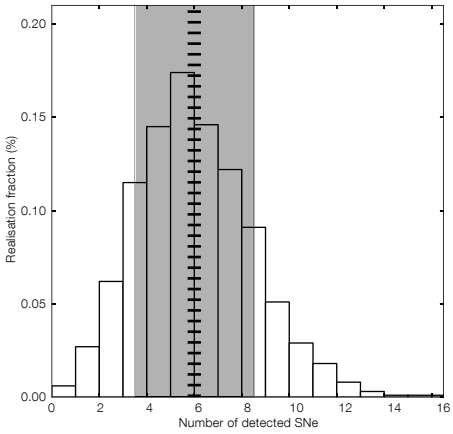

Figure 3. Histogram showing the number of expected SNe from our Monte Carlo simulations. The dashed vertical line indicates the number of observed events and the grey area its 1σ Poissonian uncertainty (from Miluzio et al., 2013).

We also analysed the distribution of the locations of the expected events for an ideal case, where the magnitude detection limit in the nuclear regions is as deep as in the outskirts, and extinction is negligible. The experiment shows that the fraction of events that remain hidden to our search in the galaxy nuclear regions, due to the combined effect of reduced search efficiency and extinction, is very high, about 60 %. The number of CC SNe found in starburst galaxies is consistent with what is predicted from the high SFR (and the canonical mass range for the progenitors) when we recognise that a major fraction of the events remain hidden in the inaccessible starburst regions. This has important consequences for the use of CC SN as a probe of the cosmic SFR, because the fraction of SBs is expected to increase with redshift (Miluzio et al., 2013). This conclusion appears to agree with that of previous, similar searches (e.g., Mannucci et al., 2003; Mattila et al., 2012).

Finally, to understand how a different choice of the test parameters can influence the expected rate, we varied each of them and computed the rate, repeating the Monte Carlo simulation. One of the main sources of uncertainty is related to the estimate of the magnitude detection limit, which can vary the predicted number of SNe by about 15 %. The other source of uncertainty is the assumption of the CC SN progenitor mass range: in particular considering that a different upper limit (10 $M_{\odot}$ instead of 8 $M_{\odot}$) results in an expected number of SNe about 30 % lower than the reference case (5.3 SNe). Moreover, while the uncertainty on the extinction does not significantly affect the simulation (because where the extinction is high our search is limited by the bright magnitude detection limit), the most uncertain input of the galaxy characterisation is the spatial distribution of the star formation; uncertainty in the adopted distribution propagates with an error of about 50 % on the expected SN number (Miluzio et al., 2013).

The future of IR SN searches

While continuing to search for SNe in starburst galaxies in the optical and infrared can certainly help to improve the still poor statistics, one may argue at this point for a change in strategy. In this respect, it is worth mentioning the attempt to reveal the hidden CC SNe through infrared SN searches that exploit adaptive optics at large telescopes, e.g., Gemini or the VLT. The early results are encouraging, with the discovery of two SNe with very high extinction (SN 2004ip with A_V between 5 and 40 mag, and SN 2008cs with A_V of 16 mag) and another two SNe discovered very close to the galaxy nucleus, although in these cases with low extinction. On account of the need to monitor one galaxy at a time and to access heavily subscribed large telescopes, this approach cannot promise a large statistical sample, although even a few events would be valuable, mostly for exploring the innermost nuclear regions. On the other hand, a new opportunity that should be exploited is to piggyback on wide-field extragalactic surveys by the next generation of infrared facilities, in particular the Euclid mission. This would allow, for the first time, IR SN searches to be performed on a large sample of galaxies, exploring a range of star formation activity and, by monitoring galaxies at different redshifts, probing the cosmic evolution of SN rates.

References

Botticella, M. T. et al. 2008, A&A, 479, 49
Horiuchi, S. et al. 2011, ApJ, 738, 154
Hopkins, A. M. & Beacom, J. F. 2006, ApJ, 651, 142
Maiolino, R. et al. 2002, A&A, 389, 84
Mannucci, F. et al. 2003, A&A, 401, 519
Mannucci, F., Della Valle, M. & Panagia, N. 2006, MNRAS, 370, 773
Mattila, S. et al. 2007b, ApJ, 659, L9
Mattila, S. et al. 2012, ApJ, 756, 111
Melinder, J. et al. 2012, A&A, 545, A96
Miluzio, M. & Cappellaro, E. 2010, Central Bureau Electronic Telegrams, 2446, 1
Miluzio, M. et al. 2011, Central Bureau Electronic Telegrams, 2773, 1
Miluzio, M. et al. 2013, A&A, 554, A127
Richmond, M. W., Filippenko, A. V. & Galisky, J. 1998, PASP, 110, 553
Smartt, S. J. 2009, ARA&A, 47, 63

The VIMOS VLT Deep Survey: Final Public Release of ~ 35 000 Galaxies and Active Galactic Nuclei Covering 13 Billion Years of Evolution

Olivier Le Fèvre[1] (PI)
Christophe Adami[1]
Stéphane Arnouts[1]
Sandro Bardelli[2]
Micol Bolzonella[2]
Marco Bondi[3]
Angela Bongiorno[4]
Dario Bottini[5]
Alberto Cappi[2]
Paolo Cassata[1]
Stéphane Charlot[6]
Paolo Ciliegi[2]
Thierry Contini[7]
Olga Cucciati[2]
Sylvain de la Torre[1]
Sebastien Foucaud[8]
Paolo Franzetti[5]
Bianca Garilli[5]
Isabelle Gavignaud[9]
Luigi Guzzo[10]
Olivier Ilbert[1]
Angela Iovino[10]
Vincent Le Brun[1]
Brian Lemaux[1]
Carlos López-Sanjuan[11]
Dario Maccagni[3]
Henry J. McCracken[6]
Bruno Marano[12]
Christian Marinoni[13]
Alain Mazure†[1]
Yannick Mellier[6]
Roberto Merighi[2]
Paolo Merluzzi[3]
Chrystel Moreau[1]
Stephane Paltani[14,15]
Roser Pellò[7]
Agnieszka Pollo[16,17]
Lucia Pozzetti[2]
Roberto Scaramella[4]
Marco Scodeggio[5]
Lidia Tasca[1]
Laurence Tresse[1]
Daniela Vergani[2]
Giampaolo Vettolani[3]
Giovanni Zamorani[2]
Alessandra Zanichelli[3]
Elena Zucca[2]

[1] Aix–Marseille Université, CNRS, LAM–Laboratoire d'Astrophysique de Marseille, Marseille, France
[2] INAF–Osservatorio Astronomico di Bologna, Bologna, Italy
[3] INAF–IRA, Bologna, Italy
[4] INAF–Osservatorio Astronomico di Roma, Monte Porzio Catone, Italy
[5] INAF–IASF, Milano, Italy
[6] Institut d'Astrophysique de Paris, UMR7095 CNRS, Université Pierre et Marie Curie, Paris, France
[7] Institut de Recherche en Astrophysique et Planétologie, Toulouse, France
[8] Department of Physics & Astronomy, Shanghai JiaoTong University, Shanghai, China
[9] Departamento de CienciasFisicas, Universidad Andres Bello, Santiago, Chile
[10] INAF–OsservatorioAstronomico di Brera, Milano, Italy
[11] Centro de Estudios de Físicadel Cosmos de Aragón, Teruel, Spain
[12] Università di Bologna, Dipartimento di Astronomia, Bologna, Italy
[13] Aix-Marseille Université, CNRS, Centre de Physique Théorique, Marseille, France
[14] Integral Science Data Centre, Genève, Switzerland
[15] Geneva Observatory, Genève, Switzerland
[16] Astronomical Observatory of the Jagiellonian University, Kraków, Poland
[17] National Centre for Nuclear Research, Warszawa, Poland

The VIMOS VLT Deep Survey (VVDS) final and public data release offers an excellent opportunity to revisit galaxy evolution with a sample of 35 016 galaxies and active galactic nuclei covering the redshift range $0 < z < 6.7$. The VVDS includes three tiered surveys, the wide, deep and ultra-deep surveys, covering up to 8.7 square degrees, and each magnitude-selected with limits $i_{AB} = 22.5$, 24 and 24.75 respectively. The VVDS redshifts, spectra, and all associated multi-wavelength data are available at http://cesam.lam.fr/vvds. The highlights and scientific legacy of the VVDS are summarised.

Galaxy evolution is the result of a complex interplay between several fundamental physical processes. The underlying picture is that of hierarchical clustering, in which dark matter halos build up in mass along cosmic time with small halos merging to produce larger halos. Galaxies form with strong bursts of star formation, and appear as baryonic matter collapses in those halos, starting stellar lives that endure for millions to several billions of years. In galaxies, the stars evolve along their respective evolutionary tracks, the gas reservoir, possibly replenished by gas accretion, is gradually transformed into new stars, the environment leaves its imprint and spectacular galaxy mergers modify the morphology and content of galaxies. Simulations, which are becoming more and more sophisticated, seem (always!) to agree with observations. From a distance one would then say that most is understood, but we are still faced with major unknowns, particularly concerning which processes dominate in driving evolution for different galaxy types, and on which timescales.

Deep galaxy surveys are the key elements that enable progress in this understanding of galaxy evolution. A fundamental parameter is the knowledge of the redshift, linked to the distance and look-back time via the cosmological world model. With the redshift, we are able to probe back in cosmic time and compare galaxies at different times in their history. The advent of efficient multi-object spectrographs in the 1990s allowed, for the first time, truly representative samples of the high-redshift Universe to be assembled (e.g., the Canada France Redshift Survey [CFRS]; Le Fèvre et al., 1995), and demonstrated the rapid evolution of galaxy properties since $z \sim 1$, or about half the current age of the Universe. The statistical weight of large samples has become a major driver in all surveys, as one aims to know the average multivariate properties of a certain galaxy population as accurately as possible.

The VIMOS VLT Deep Survey

The VVDS was conceived with these considerations in mind. Originally based on guaranteed time to our consortium for the building of the Visible MultiObject Spectrograph (VIMOS) for the VLT under contract with ESO (Le Fèvre et al., 2003), the 50 guaranteed nights allocated to programme 070.A-9007, of which only 33 were under clear weather, were complemented by a 150-hour Large Programme (177.A-0837) for the ultra-deep part. The powerful VIMOS instrument and the observing strategy led to a competitive sample (Le Fèvre et al., 2004a; 2005a), comparable to the best programmes conducted at other facilities,

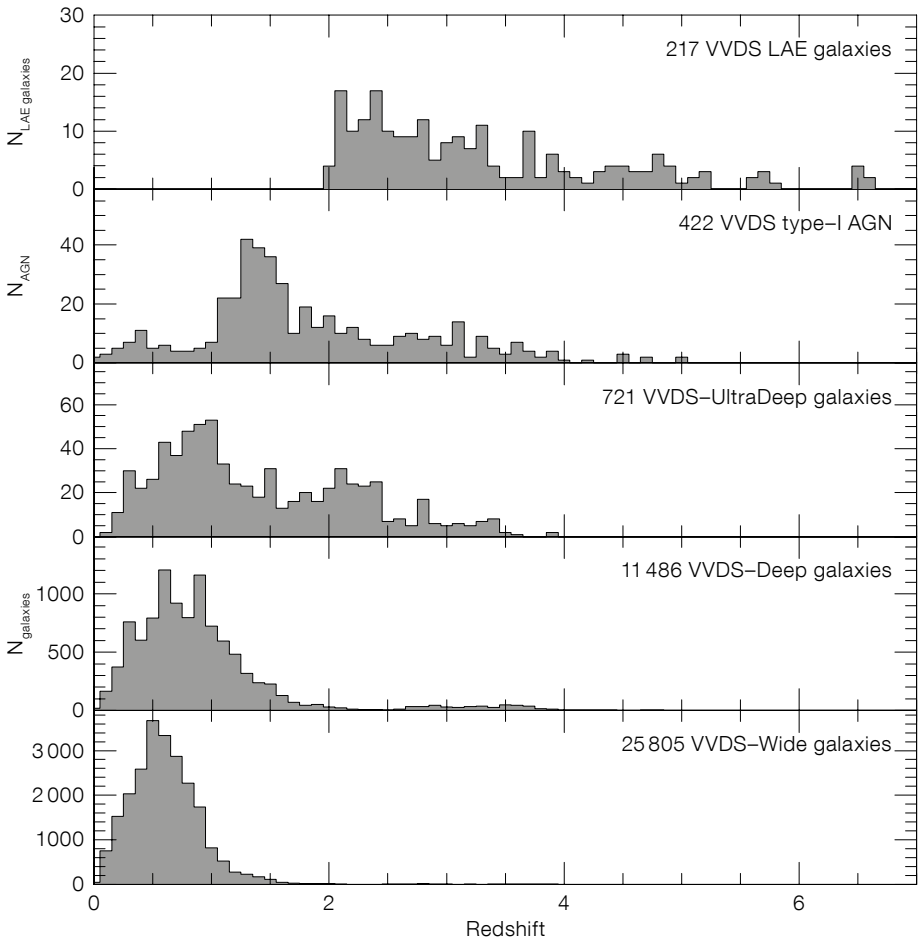

Figure 1. The redshift distribution and sample numbers for the VVDS wide ($i_{AB} \leq 22.5$), deep ($i_{AB} \leq 24$) and ultra-deep ($23 \leq i_{AB} \leq 24.75$) surveys, as well as for the AGN and Lyman-α emitter (LAE) populations are shown from bottom to top.

like the DEEP2 survey with the DEIMOS spectrograph on the Keck Telescope (Davis et al., 2003).

In total more than 58 000 targets have been observed. While the original goal of obtaining 100 000 redshifts in 16 square degrees could not be reached with this time allocation, more than 34 594 galaxies, 422 Type I active galactic nuclei (AGN) and 12 430 Galactic stars have been identified. Redshift measurements however failed for another ~ 10 000 objects; thus the spectroscopic incompleteness represents ~ 20 % of all sources. The Galactic stars mainly come from the VVDS-Wide, as no attempt was made to exclude stars from the photometric sample prior to selecting spectroscopic targets in order to keep all compact objects, in particular AGN, as possible targets.

The redshift distribution of the different VVDS surveys is presented in Figure 1. The median redshift increases from $z \sim 0.5$ to $z \sim 1.2$ from the wide to ultra-deep samples, and a high-redshift tail of bright galaxies extends to $z \sim 5$ for the magnitude-limited surveys and up to $z \sim 6.7$ for the Lyman-α emitter (LAE) serendipitous sample. From one single survey with a well-defined selection function, the VVDS therefore allows coverage of about 13 billion years of evolution and traces quantitatively the evolution of galaxy populations and large-scale structures. Another great strength of the VVDS is the wealth of ancillary data. First and foremost deep multi-band photometry was obtained with the Canada France Hawaii Telescope (CFHT), first with the CFH12K wide-field CCD mosaic camera (McCracken et al., 2003; Le Fèvre et al., 2004b), then with the 1-square-degree MegaCam, processed at Terapix in Paris (Cuillandre et al., 2012). Multi-wavelength data include near-infrared photometry (Bielby et al., 2012), Very Large Array (VLA; Ciliegi et al., 2005), Spitzer-SWIRE (Spitzer Space Telescope Wide-area Infrared Extragalactic Survey; Lonsdale et al., 2003), XMM (X-ray Multi-Mirror Mission; Pierre et al., 2004), GALEX (Galaxy Evolution Explorer; Arnouts et al., 2005) and Herschel (Lemaux et al., 2013) measurements. Due to the pressure on the Hubble Space Telescope (HST) to observe many of the extragalactic fields under study by different groups, we have not yet succeeded in getting HST high spatial resolution imaging on the VVDS-02h 0226-04 field, which is quite unfortunate given the immediate science return to be reaped from the more than 12 000 galaxies with spectroscopic redshifts. This opportunity remains open.

Science highlights

The science exploitation of the VVDS has led to numerous new results detailing the evolution of galaxies, such that it is hard to single out only a few highlights. The characterisation of the survey using classical statistical functions has been performed, describing the time evolution of luminosity functions, stellar mass functions and correlation functions. The complete census of star-forming galaxies, enabled by the magnitude selection, led to our claim that magnitude-selected surveys identify more galaxies at redshifts $z \sim 2$–3 than colour-selected surveys (Le Fèvre et al. 2005b); a claim confirmed with the full dataset (Le Fèvre et al., 2013b).

While the expected *N(z)* distributions down to $i_{AB} = 24$, based on mid-1990s basic knowledge of the high-*z* galaxy population, were predicting almost no detections at $z > 2$, the VVDS-Deep has unveiled an unexpectedly large galaxy population at $2 < z < 5$ (Le Fèvre et al., 2005b). With its three surveys, the VVDS provides a robust counting of galaxies with reference redshift distributions *N(z)* at increasing depth. Comparing the VVDS to state-of-the art simulations, we find that these under-predict the number of luminous high-redshift galaxies and

over-predict the number of lower luminosity galaxies at low redshifts (de la Torre et al., 2011; Le Fèvre et al., 2013b).

The luminosity function of different galaxy types from the VVDS showed that most of the luminosity evolution (Ilbert et al., 2005) comes from late-type irregular-like galaxies, while early-type elliptical-like galaxies were already mostly in place at $z \sim 1$ (Zucca et al., 2006). The stellar mass function showed that galaxies with elliptical-like evolved spectral types were already in place at $z \sim 1$ (Pozzetti et al., 2007). The stellar mass density showed a striking behaviour with the first evidence of the rapid build-up of elliptical–red galaxies at the epoch $1 < z < 2$ (Arnouts et al., 2007); the stellar mass density of these galaxies was increasing by a factor ~ 10 over this period, a trend which has been confirmed by several subsequent studies.

One surprising result is the evidence for a strong evolution of the colour (morphology)–density relation, which tells us that in the local Universe early-type galaxies reside preferentially in the densest environments, while late types are located in lower density neighbourhoods. Using a finely sampled galaxy density field enabled by the spectroscopic redshift coverage, we find that this relation is flattening and even tentatively inverting at redshifts beyond $z \sim 0.8$–1 (Cucciati et al., 2006); the implication is that at half the current age of the Universe galaxies of different types were equally distributed in different density environments.

The ultraviolet (UV) restframe luminosity functions from the VVDS data led to a remarkable account of the evolution of the star formation rate density (SFRD) derived from the integrated luminosity density over 12 billion years of evolution. First reported in Tresse et al. (2007), the SFRD, corrected for dust, is well established from $z \sim 4$ to $z \sim 0.2$ with unsurpassed robustness (Cucciati et al., 2012). We find that the SFRD rose mildly from early times to a peak or plateau at $z \sim 2$, before decreasing strongly to the present time by about one order of magnitude. The contribution of galaxies of different types to the SFRD history showed a downsizing pattern, with the most luminous galaxies contributing mostly at high-z, while less luminous galaxies dominate the SFRD at lower redshifts. We derived for the first time the evolution of the mean dust attenuation A_{FUV} of the observed galaxy population: it rises up to $z \sim 1$ followed by a plateau to $z \sim 2$ and a fast decrease to $z \sim 4$. The VVDS revealed the first evidence for a delayed dust attenuation peak, appearing ~ 2 Gyr after the SFRD peak (Cucciati et al., 2012); a result later confirmed with Herschel data.

The volumes of 0.5×10^6 to 2×10^7 h^{-3} cubic Mpc probed by the VVDS enabled the distribution of galaxies in large-scale structures to be quantified, and this was employed to infer some useful constraints on cosmology. The apparent evolution of the clustering length r_0 is relatively mild, which translates into an important intrinsic evolution since $z \sim 1$ (Le Fèvre et al., 2005c). We demonstrated that "red" galaxies are already more clustered at $z \sim 1$ than "blue" galaxies (Meneux et al., 2006), a classical property in local surveys never before observed at a time when the Universe was half of its present age. At these redshifts more luminous galaxies are more clustered than fainter galaxies (Pollo et al., 2006) and the dependence of clustering on galaxy mass (Meneux et al., 2008) has been established. The evolution of the galaxy to dark matter halo bias (Marinoni et al., 2005) and the growth of dark matter halos (Abbas et al., 2010) were also reported.

The usefulness of high-redshift surveys to constrain the origin of the apparent accelerated expansion of the Universe was demonstrated using the redshift space distortions (RSD) measured in the clustering of VVDS galaxies (Guzzo et al., 2008). The RSD is one of the only cosmological probes capable of identifying whether our current understanding of gravity in the framework of general relativity is accurate or needs further refinement in modified gravity models that might eliminate the need for dark energy. Since the VVDS proof of concept, RSD at high redshift is much in focus, as exemplified by the recent VIPERS measurements with VIMOS (Guzzo et al., 2013a,b; de la Torre et al., 2013), and is at the heart of large experiments like the Euclid European Space Agency mission (Laureijs et al., 2011).

Thanks to the VVDS sample size and observing strategy, several interesting populations could be studied in detail, including Lyman-α emitters, He II 1640 Å emitters and Type 1 AGN. A large spectroscopic sample of LAEs with $2 < z < 6.7$ was identified, found serendipitously in the observed VIMOS slit masks of the main survey targets — a nice bonus. The total sample of 217 LAEs, still the largest to date, was used to identify that the LAE luminosity function at these redshifts has a steep slope $\alpha = -1.7$, and to show that the ratio of the luminosity density (LD) from LAE to the LD of the general population is increasing with redshift, becoming more than half of the total LD by $z \sim 6$ (Cassata et al., 2011). A peculiar population of He II 1640 Å emitters was identified, with half of these showing properties compatible with residual Population III star formation in pockets of leftover pristine gas from the original reservoir, or from recently accreted gas, down to redshifts $z \sim 3$ (Cassata et al., 2013).The VVDS sample of Type 1 AGN (Gavignaud et al., 2006) was used to measure the faint end of their luminosity function and to better constrain their cosmological evolution (Bongiorno et al., 2007), finding, for the first time in an optically-selected AGN sample, clear evidence of AGN cosmic downsizing.

In the hot debate about galaxy assembly, the VVDS accurately quantified the amount of mass assembled by galaxies in merger events. From the fraction of pairs identified from their concordant spectroscopic redshifts, we have established that 40–50% of the mass of a galaxy today went through a merger event since $z \sim 3$, either from major mergers (de Ravel et al., 2009) or minor mergers (Lopez-Sanjuan et al., 2011). Contrary to what is often assumed from the current cold accretion picture, having a large fraction of the mass of galaxies assembled in mergers is not in contradiction with cold accretion driving star formation, and the two processes are likely to act together in building up galaxies. Mergers are a powerful means to accumulate stellar mass, with major mergers producing galaxies with as much as twice the mass of the progenitors, while often producing only a small and temporary increase in star formation. The VVDS established that merging is a most

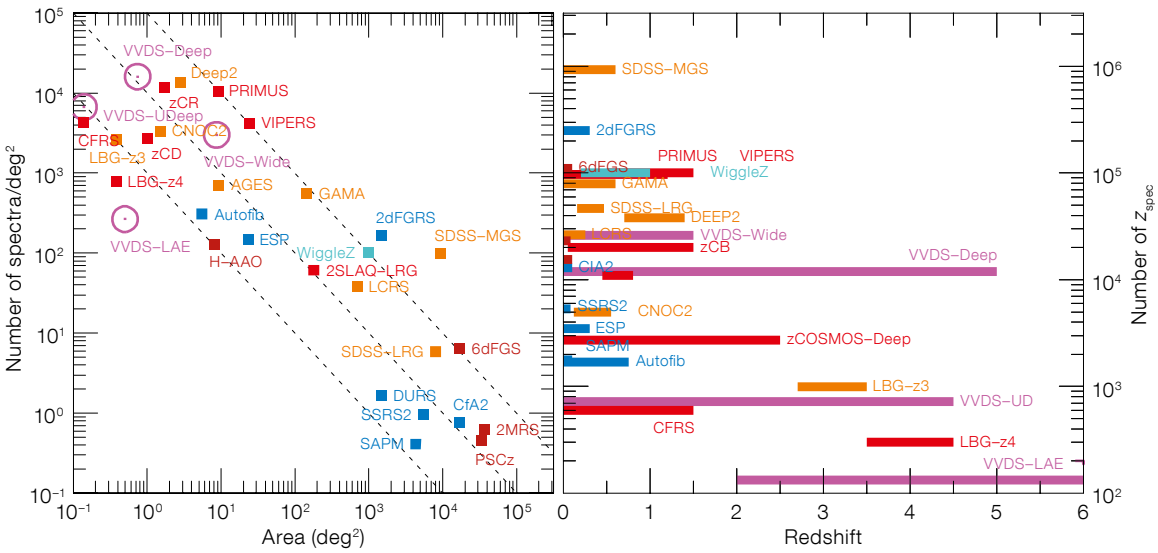

Figure 2. Comparison of VVDS surveys to other spectroscopic redshift surveys. Left: The density of spectra by number per square degree (inspired by Baldry et al., 2010). Right: The number of spectroscopic redshifts measured as a function of redshift (see Le Fèvre et al. 2013a). The important contribution of VVDS among these surveys both in terms of number of spectra and redshift coverage is evident.

important physical process driving galaxy evolution, perhaps not too surprisingly if the picture of hierarchical structure assembly is valid.

It is important to recognise the role of spectroscopic surveys, like the VVDS, in the emergence of the widely used photometric redshift technique. Photometric redshift methods need to be calibrated on reliable spectroscopic redshifts, so that they can then be applied in computing photometric redshifts for hundreds of thousands of sources. This was done for the CFHT Legacy Survey, which was calibrated using the VVDS (Ilbert et al., 2006). Photometric redshifts can in turn provide pre-selected targets for the new generation of spectroscopic surveys (e.g., the VIMOS Ultra Deep Survey [VUDS], Le Fèvre et al., p. 37). Photometric and spectroscopic redshift surveys are therefore highly complementary.

VVDS legacy

More than 50 refereed papers were published from the VVDS collaboration, the latest in 2013, and more than 50 other papers published by other teams making use of previous VVDS data releases. The possibility for young scientists to be involved in a large international project is an important aspect of the VVDS, which has been an excellent training ground for young scientists. More than 15 PhD theses have been defended based on the VVDS and an equivalent number of postdocs have made the VVDS their main project. In all, the VVDS has helped to develop key expertise on deep spectroscopic surveys in Europe, which have motivated and supported other VIMOS surveys at the VLT (e.g., zCOSMOS, Lilly et al., 2007; VIMOS Public Extragalactic Redshift Survey [VIPERS], Guzzo et al., 2013a,b; VUDS, Le Fèvre et al., p. 37), or enabled a large target base for specific and unbiased follow-up surveys, like 3D spectroscopy (e.g., Mass Assembly Survey with SINFONI in VVDS [MASSIV], Contini et al., 2012a,b).

The VVDS contributes to maintaining a strong European presence in the rich field of deep galaxy redshift surveys, as identified in Figure 2, where the return of the VVDS is compared to other surveys in this field. The legacy of this survey rests on the publicly available data[1] and on the invaluable expertise developed all along, with a broad base of scientists now planning for the next generation surveys with the VLT and the European Extremely Large Telescope.

References

Abbas, U. et al. 2010, MNRAS, 406, 1306
Arnouts, S. et al. 2005, ApJ, 619, 43
Arnouts, S. et al. 2007, A&A, 476, 137
Baldry, I. K. et al. 2010, MNRAS, 404, 86
Bielby, R. et al. 2012, A&A, 545, 23
Bongiorno, A. et al. 2007, A&A, 472, 433
Cassata, P. et al. 2011, A&A, 525, 143
Cassata, P. et al. 2013, A&A, 556, 68
Ciliegi, P. et al. 2005, A&A, 441, 879
Contini, T. et al. 2012a, A&A, 539, 91
Contini, T. et al. 2012b, The Messenger, 147, 32
Cucciati, O. et al. 2006, A&A, 458, 39
Cucciati, O. et al. 2012, A&A, 539, 31
Cuillandre, J. C. et al. 2012, SPIE, 8448
Davis, M. et al. 2003, SPIE, 4834, 161
De la Torre, S. et al. 2011, A&A, 525, 125
De Ravel, L. et al. 2009, A&A, 498, 379
Gavignaud, I. et al. 2006, A&A, 457, 79
Guzzo, L. et al. 2008, Nature, 451, 541
Guzzo, L. 2013a, The Messenger, 151, 41
Guzzo, L. et al. 2013b, A&A, in press, arXiv:1303.2623
Ilbert, O. et al. 2005, A&A, 439, 863
Ilbert, O. et al. 2006, A&A, 457, 841
Laureijs, R. et al. 2011, arXiv:1110.3193
Le Fèvre, O. et al. 1995, ApJ, 455, 60
Le Fèvre, O. et al. 2003, SPIE, 4841, 1670
Le Fèvre, O. et al. 2004a, A&A, 428, 1043
Le Fèvre, O. et al. 2004b, A&A, 417, 839
Le Fèvre, O. et al. 2005a, A&A, 439, 845
Le Fèvre, O. et al. 2005b, Nature, 437, 519
Le Fèvre, O. et al. 2005c, A&A, 439, 877
Le Fèvre, O. et al. 2013a, A&A, 559, 14
Le Fèvre, O. et al. 2013b, A&A, submitted, arXiv:1307.6518
Lilly, S. J. et al. 2007, ApJS, 172, 70
Lemaux, B. et al. 2013, A&A, submitted, arXiv:1311.5228
Lonsdale, C. et al. 2003, PASP, 115, 897
Lopez-Sanjuan, C. et al. 2011, A&A, 530, 20
Marinoni, C. et al. 2005, A&A, 442, 801
McCracken, H. J. et al. 2003, A&A, 410, 17
Meneux, B. et al. 2006, A&A, 452, 387
Meneux, B. et al. 2008, A&A, 478, 299
Pollò, A. et al. 2006, A&A, 451, 409
Pozzetti, L. et al. 2007, A&A, 474, 443
Tresse, L. et al. 2007, A&A, 472, 403
Zucca, E. et al. 2006, A&A, 455, 879

Links

[1] Access to all VVDS data: http://cesam.lam.fr/vvds

The VIMOS Ultra Deep Survey: 10 000 Galaxies to Study the Early Phases of Galaxy Assembly at $2 < z < 6+$

Olivier Le Fèvre[1] (PI)
Ricardo Amorin[2]
Sandro Bardelli[3]
Peter Capak[4]
Laetizia Cassara[5]
Paolo Cassata[1]
Marco Castellano[2]
Stéphane Charlot[6]
Andrea Cimatti[7]
Thierry Contini[8]
Jean-Gabriel Cuby[1]
Olga Cucciati[7]
Ania Durkalec[1]
Sylvain de la Torre[1]
Adriano Fontana[2]
Sotira Fotopoulou[9,10]
Bianca Garilli[5]
Mauro Giavalisco[11]
Andrea Grazian[2]
Nimish Hathi[1]
Olivier Ilbert[1]
Vincent Le Brun[1]
Brian Lemaux[1]
Carlos Lopez-Sanjuan[12]
Dario Maccagni[5]
Yannick Mellier[6,13]
Chrystel Moreau[1]
Stéphane Paltani[9,10]
Laura Pentericci[2]
Bruno Ribeiro[1]
Mara Salvato[14]
Daniel Schaerer[10]
Marco Scodeggio[5]
Nick Scoville[15]
Veronica Sommariva[2]
Margherita Talia[3]
Yoshi Taniguchi[16]
Lidia Tasca[1]
Romain Thomas[1]
Laurence Tresse[1]
Eros Vanzella[7]
Daniela Vergani[17]
Pin-Wei Wang[1]
Gianni Zamorani[3]
Elena Zucca[3]

[1] Aix–Marseille Université, CNRS, LAM – Laboratoire d'Astrophysique de Marseille, France
[2] INAF–Osservatorio Astronomico di Roma, Monte Porzio Catone, Italy
[3] INAF–Osservatorio Astronomico di Bologna, Italy
[4] Spitzer Science Center, California Institute of Technology, Pasadena, USA
[5] INAF–IASF, Milano, Italy
[6] Institut d'Astrophysique de Paris, UMR7095 CNRS, Université Pierre et Marie Curie, Paris, France
[7] Dipartimento di Astronomia, Università di Bologna, Italy
[8] Institut de Recherche en Astrophysique et Planétologie, Toulouse, France
[9] ISDC Data Centre for Astrophysics, University of Geneva, Versoix, Switzerland
[10] Department of Astronomy, University of Geneva, Versoix, Switzerland
[11] Department of Astronomy, University of Massachusetts, Amherst, USA
[12] Centro de Estudios de Físicadel Cosmos de Aragón, Teruel, Spain
[13] CEA/Irfu/SAp Saclay, Laboratoire AIM, Gif-sur-Yvette, France
[14] Max Planck Institut für extraterrestrische Physik, Garching, Germany
[15] California Institute of Technology, Pasadena, USA
[16] Research Institute for Space and Cosmic Evolution, Ehime University, Matsuyama, Japan
[17] INAF–IASFBO, Bologna, Italy

The VIMOS Ultra Deep Survey (VUDS) aims to study the early phases of galaxy assembly from a large, well-defined sample of ~ 10 000 galaxies with spectra obtained from very deep VIMOS observations. This sample is by far the largest to date, with spectroscopic redshifts covering a redshift range $2 < z < \sim 6$ and it enables a range of fundamental studies to better understand the first major steps in galaxy evolution. The first results from the VUDS survey are summarised, including the discovery of a galaxy protocluster at $z = 3.3$.

Over the past 20 years our view of galaxy formation and evolution has dramatically improved. Observational cosmology has reached an unprecedented level of precision, and we have in hand a plausible scenario to explain the time evolution of galaxies over more than 13 billion years, resting on the hierarchical assembly of dark matter halos in a Lambda Cold Dark Matter (ΛCDM) cosmology, and supported by detailed numerical simulations.

However, the observational evidence sustaining a robust picture of galaxy formation and evolution is still limited at redshifts beyond $z \sim 1$–3, and much remains to be learned about the critical time when the progenitors of today's galaxies were assembling. Our current observational knowledge rests solely on the ability to find all distant galaxies, as this provides the basic input to derive volume-averaged quantities of cosmological value. A primary key question arises, and is one of the basic quests throughout the history of extragalactic astronomy: are we properly counting galaxies of all types in order to be able to derive a complete census of stars, gas and black holes at any epoch?

The peak of the star formation rate in the Universe seems to have happened at a redshift $z \sim 1.5$; but do we understand what the star formation history was at earlier times? Evolved passive/quiescent galaxies are already observed at $z \sim 2$, some of them very compact; but when they were formed, what their progenitors were, and what the history of mass build-up at earlier times was, are largely unexplored questions. When did the progenitors of the massive clusters of galaxies identified at redshifts $z \sim 1$–2 assemble? How were galaxies distributed in space, and what was the impact of the local environment during the first phases of galaxy assembly? Are galaxies building up their mass with time from cold gas accretion or through mergers, or both? What are the consequences of the co-evolution of supermassive black holes and galaxies? At which epochs are these different processes playing a dominant role?

The importance of large statistically representative surveys

Large statistically representative surveys of the Universe at different epochs constitute a fundamental tool in this quest. To measure a quantity (e.g., volume density) at better than 5σ, one needs at least 25 independent measurements (assuming Poisson statistics). For a multivariate quantity, the required sample size multiplies by each variable. Taking a classical example, measuring the luminosity function in the ten luminosity bins necessary to constrain the three parameters of a Schechter function (ϕ^*,

L*, α) takes about 250 galaxies at each redshift. To study the multivariate dependence for five different galaxy types and over a range of three different environments, one therefore needs 3750 galaxies, or about 10 000 galaxies to cover three redshift ranges. Another key element is the need to mitigate the effects of cosmic variance by observing large (and possibly unconnected) volumes. It is only on field sizes of order of one square degree that cosmic variance can be reduced to below 10% for galaxies with a typical mass M^* at $z \sim 3$ (Moster et al., 2011).

In addition to these simple statistical arguments, the selection function of a survey is of paramount importance: the pre-selection of galaxies in any survey will preset which questions can be investigated by a particular survey. The ultimate goal is for representative surveys. This requires that we make a census of all galaxy types at a given epoch, imposing as few as possible of our priors when exploring the high-redshift Universe. This is obviously a difficult concept, as we do not know *a priori* what we are attempting to measure. With all this in mind, exploratory investigations with a few tens, or even a few hundreds of objects, in small fields must be followed up by systematic surveys strictly guided by the above principles.

VUDS: The VIMOS Ultra-Deep Survey

The high-redshift galaxy population has been extensively studied with spectroscopic surveys, reaching ~ 10^5 redshifts at $z \sim 1$. Such surveys at the VLT include: the VIMOS Very Deep Survey (VVDS; Le Fèvre et al., 2005; 2013); zCOSMOS (Lilly et al., 2007); and VIPERS (Guzzo et al., 2013; 2014). However, at redshifts $z > 2$ spectroscopic samples are much more limited: a few thousand Lyman-break galaxies (LBGs) at $z \sim 3$ (Steidel et al., 2003; Bielby et al., 2011), about 800 galaxies selected for their *i*-band luminosity or Lyman-α flux (VVDS; Le Fèvre et al., 2013; and the article on p. 33), Lyman-α emitters in narrow redshift ranges (e.g., Ouchi et al., 2008), and other targeted populations (e.g., Stark et al. 2010; Vanzella et al., 2009). It is worth noting that the majority of today's most referenced studies at redshifts $z > \sim 3.5$ are conducted on the basis of colour-selected samples and photometric redshifts, but on samples containing relatively few objects (e.g., Bouwens et al., 2007) and with significant uncertainties associated to their exact redshifts and the catastrophic failure rate. Further, the spectroscopic samples at these redshifts reach only a few hundred galaxies altogether.

To improve our understanding of the population at $z > 2$, we are conducting the VIMOS Ultra-Deep Survey, based on ESO Large Programme 185.A-0791 with 640 hours awarded. The key features of VUDS are: (i) the large sample, with about 10 000 galaxies observed with multi-slit spectroscopy; (ii) the 1 square degree field coverage in three separate fields (COSMOS, Extended Chandra Deep Field-South [ECDFS], VVDS-02h), currently unprecedented at this depth; (iii) the large wavelength coverage 3650 Å ≤ λ ≤ 9350 Å; and (iv) the long exposure times of 14 hours. All these aspects make for a unique survey, the largest at these redshifts to date.

The primary target selection criterion for VUDS is photometric redshifts of $z \geq 2.4$, computed from the multi-wavelength data using Le Phare (e.g., Ilbert et al. 2013). This is definitely using more information than basic colour–colour selection (such as *BzK* or LBG-like *ugr* or *gri* selection), and is therefore expected to be more complete and more robust against photometric errors. However, photometric redshifts have associated degeneracies and catastrophic failure modes, so we have elected to be inclusive rather than exclusive by selecting galaxies for which either of the primary or secondary peaks of the photometric redshift probability distribution function is at $z \geq 2.4$. To be as inclusive as possible in our target selection strategy, we have supplemented this primary selection by targets satisfying various other photometric criteria if not selected by the primary selection, including those galaxies in the right location of the LBG *ugr*, *gri* and *riz* colour–colour diagrams, as well as galaxies showing a continuum break at any wavelength redder than the *r*-band with bluer colours compatible with intergalactic medium (IGM) extinction at high redshift.

VUDS observations and data processing are quite challenging. Never before had anyone assembled such a large sample of very faint galaxies for these redshifts. The first important input was to assemble reference multi-wavelength catalogues covering at least from the *u*-band to the *K*-band, and the spectroscopic redshifts needed to calibrate the photometric redshifts. We have selected three of the best fields where these conditions are met: the COSMOS field with extensive deep multi-band data including Hubble Space Telescope (HST) imaging (Scoville et al., 2007) and the recent addition of the UltraVista photometry (see, e.g., Ilbert et al., 2013), as well as extensive spectroscopy (with VIMOS on the VLT and the Keck Telescope); the ECDFS (see Cardamone et al. [2010] for the photometry and Le Fèvre et al. [2013] and references therein for the spectroscopy); and the VVDS 0226-04 field with deep Canada-France-Hawaii Telescope Legacy Survey [CFHTLS] and WIRcam Deep Survey [WIRDS] photometry and extensive spectroscopy from the VVDS Deep and Ultra Deep surveys (Le Fèvre et al., 2005; 2013; and references therein).

VIMOS slit masks have been designed implementing several levels of target priority using the VIMOS Mask Preparation Software (VMMPS) software. In particular shorter slits, as discussed in Scodeggio et al. (2009), were employed, which enable about 600 objects to be observed simultaneously. A total of 16 VIMOS pointings have been observed, each with 14 hours of integration in both of the LRBLUE and LRRED gratings, with a spectral resolution $R \sim 230$. The large wavelength range 3650 Å < λ < 9350 Å is a key factor in minimising any redshift desert (Le Fèvre et al., 2014a). Observations for each pointing consist of 13 different observing blocks and a total of 40 individual ~ 20-minute exposures, executed in service mode by the Paranal staff. The data processing is performed within the VIMOS Interactive Pipeline and Graphical Interface environment (VIPGI; Scodeggio et al., 2005), optimised to take into account the large number of individual exposures to be combined, and for joining the blue and red spectra.

Spectra and redshift measurements

The next critical step is to measure redshifts. We follow the methodology initiated with the Canada France Redshift Survey (CFRS) and further iterated with the VVDS: independent measurements are performed by two team members using the EZ software (Garilli et al., 2010), who then compare their measurements to assign a final redshift. As part of this process a reliability flag is assigned to each redshift, giving the probability that a redshift is correct. The team expertise has grown steadily as more spectra have been measured, but we realised that some measurements needed to be revised because the measurers were assigning wrong redshifts to spectra with which they were previously unfamiliar, the most common being M-stars *vs*. redshift $z \sim 5$ galaxies, or Lyman-α vs. [O II] 3727 Å emission. We therefore decided to setup a "Tiger team" in charge of reviewing all redshifts, again with two reviewers (and independent of the first two). As a result about 10% of the measurements or flags were changed through this process. In the end about 80% of the target sample received a redshift measurement, an impressive result given that observations reach beyond i_{AB} = 25–25.5 mag. A paper presenting a complete survey description has been submitted (Le Fèvre et al., 2014b).

First results

We present examples of the VUDS spectra in Figure 1, and average spectra in several redshift ranges in Figure 2. The average signal-to-noise (S/N) of the spectra is about five in the continuum in the magnitude bin i_{AB} = 24–25 mag. It is very illustrative and striking to display all VUDS spectra between redshift 2 and redshift ~ 6 in a single image, as shown in Figure 3. The most prominent feature is the hydrogen Lyman-α line at 1215 Å, which enters the VIMOS spectral domain at 3650 Å for z = 2 and is redshifted to 8500 Å at z = 6; it is observed in emission or in absorption (or both). On the red side of Lyman-α a wealth of photospheric and interstellar medium (ISM) lines are readily seen at all redshifts, including Si II, Si IV, O I, C II, C III], C IV, He II, Al II, Al III and Fe II. On the blue side, one can iden-

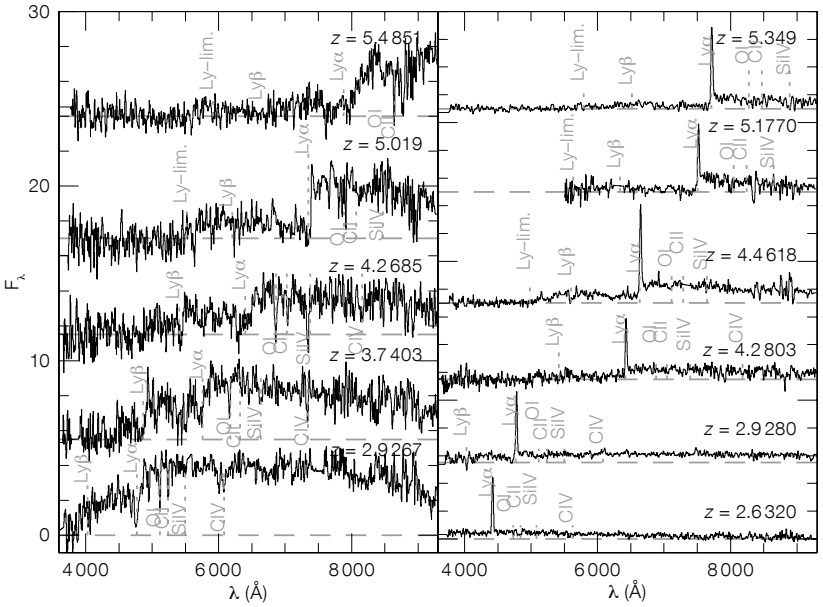

Figure 1. (Above) Examples of VUDS spectra obtained with VIMOS are displayed, covering the redshift range 2.6 to 5. Galaxies with Lyα in absorption are shown in the left panels, those with Lyα in emission in the right panels.

Figure 2. (Below) Average spectra of VUDS galaxies in five redshift ranges from $z \sim 2$ to $z \sim 6$ are shown.

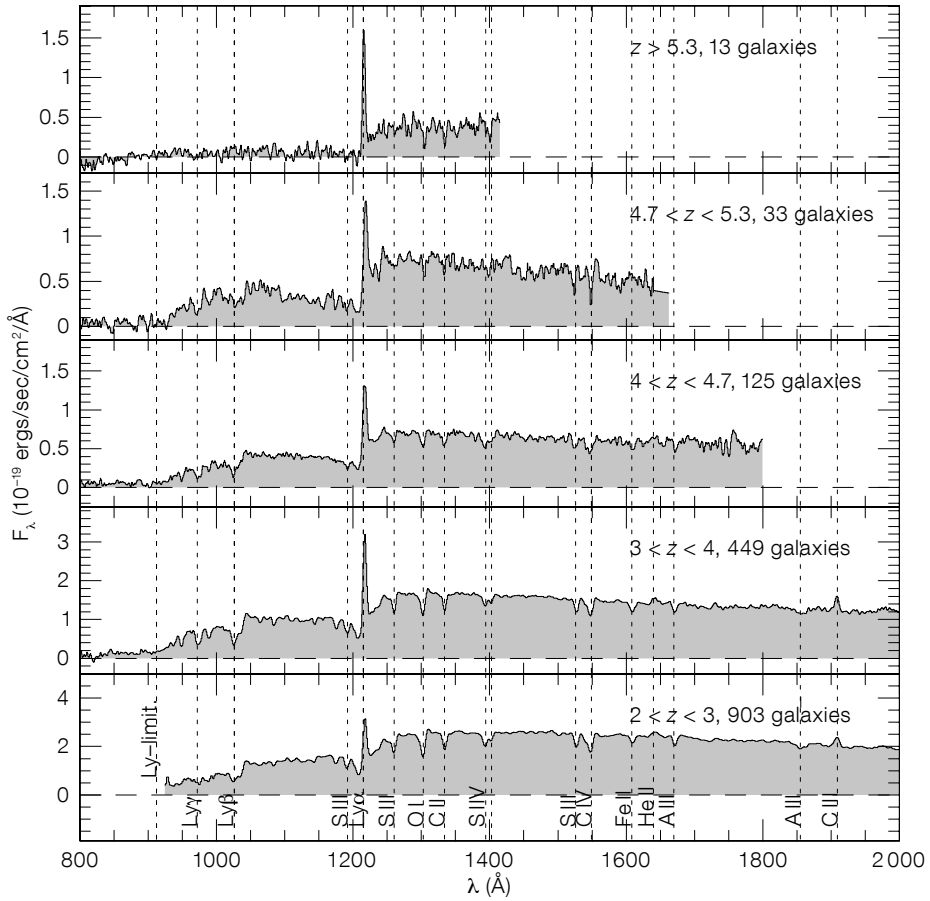

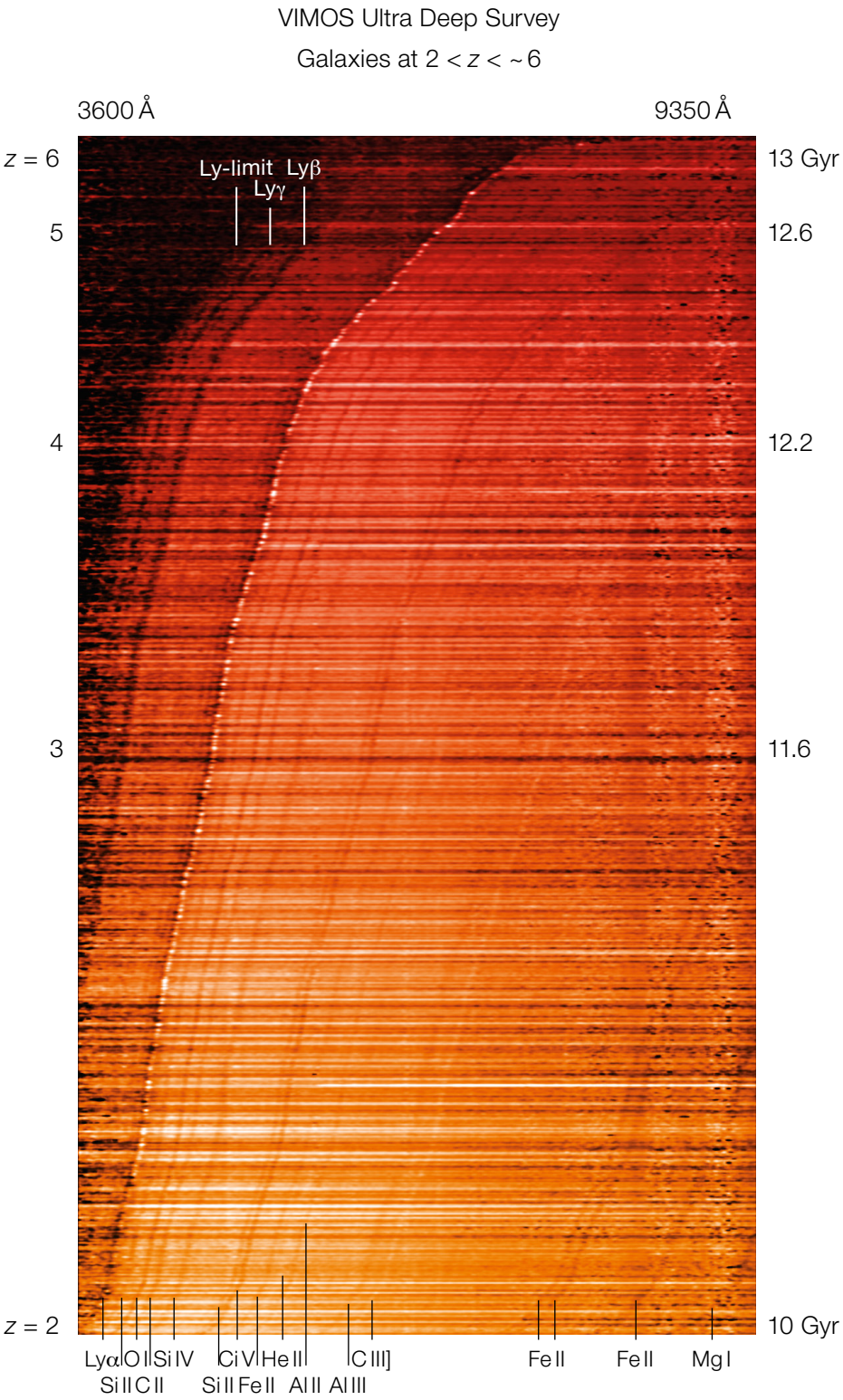

Figure 3. Stacked display of VUDS spectra between redshift 2 and ~ 6 (left-hand axis), covering between ~ 10 and 13 billion years back into the history of the Universe (right-hand axis). Prominent absorption and emission lines and the Lyman limit are indicated.

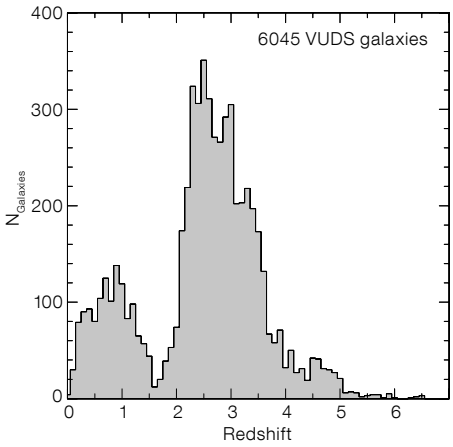

Figure 4. The redshift distribution of the current VUDS sample of 6045 galaxies is shown.

tify at the higher redshifts the hydrogen Lyman-β and Lyman-γ absorptions, and the Lyman limit at 912 Å.

The current redshift distribution of the VUDS sample is presented in Figure 4. The main sample is at $z > 2$, peaks at $z \sim 3$–4, and extends beyond $z = 6$, providing an unprecedented continuous redshift coverage at these early epochs (10–13 Gyr lookback time). Targets at $z < 2$ originate either from galaxies for which the photo-z pre-selection was ambiguous (e.g., through the degeneracy between the 4000 Å and 1215 Å continuum breaks when computing photometric redshifts, leading to a secondary peak at high redshift), and from a random sample selected down to $i_{AB} \leq 25$ mag added to the slit masks when space was available after the primary target selection. It quickly appeared that galaxies at $z \sim 3$ are quite often involved in major merging events. As reported in Tasca et al. (2014), the major pair fraction is about 20% at these redshifts, and these pairs should have merged into a more massive galaxy with approximately twice the mass by the peak of star formation rate at $z \sim 1.5$, indicating that merging is an important contributor to stellar mass assembly.

Several large overdensities have been unambiguously identified, particularly at redshifts 2.9 and 3.3 and could be proto-structures, the high-redshift analogues to the rich clusters found at $z \sim 1$ and below (Cucciati et al., 2014; Lemaux et al., 2014). The properties of galaxies in

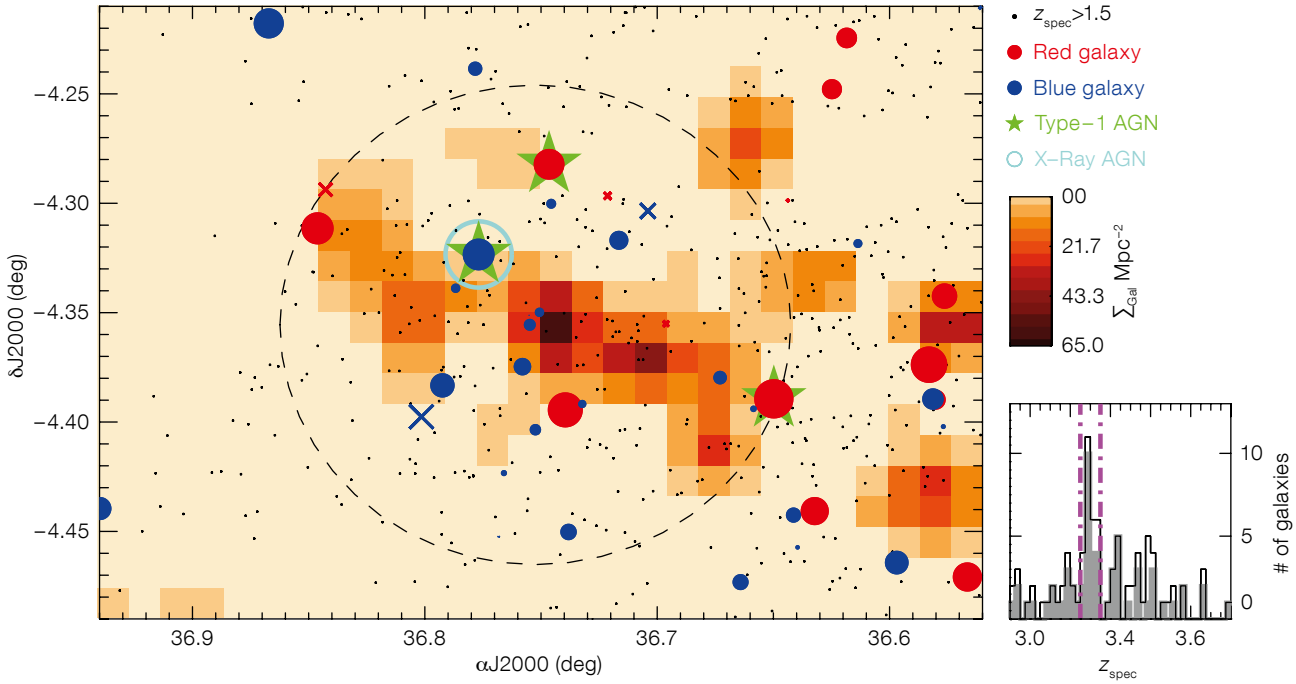

Figure 5. A rich z = 3.3 proto-cluster identified from the VUDS survey in the VVDS-02h/CFHTLS-D1 field is shown. The redshift distribution of the cluster members is shown in the lower right. The most reliable spectroscopic redshifts are represented as filled circles, the others as crosses. Red symbols indicate galaxies which appear at the expected location of the colour–magnitude red sequence observed in clusters at z ~ 1, assuming passive evolution from z ~ 3.3; blue symbols represent active star-forming galaxies. Three Type-I active galactic nuclei (AGN) are identified from broad emission lines in their spectra and are shown as stars; one of them is an X-ray source identified by XMM (circled blue). Other galaxies with spectroscopic redshifts z > 1.5 from VVDS and VUDS are indicated as small black dots. The surface density of all galaxies with photometric redshifts consistent with being in the structure is indicated by the colour-coded pixel map, and the dashed circle has a 3 h^{-1} Mpc radius.

these structures have been compared to field galaxies to try and identify signatures of the environment. In Figure 5 we show the strong overdensity in redshift and projected distribution for the z = 3.3 proto-cluster identified in the VVDS-02h/CFHTLS-D1 field. We found 27 cluster members identified with spectroscopic redshifts between 3.27 and 3.35. This proto-cluster is the richest identified so far at these redshifts.

The brightest and more massive galaxies at z ~ 4 show a diversity of properties, and we single out the more compact ones as the possible progenitors of the compact passive galaxies identified at z ~ 2 (Tasca et al., in prep). We follow the evolution of the fraction of strong Lyman-α emitters and find that it is increasing by a factor two from z ~ 2 to z ~ 6, providing an important reference on the post-reionisation era, necessary to understand what the main ionising sources in the early Universe are (Cassata et al., 2014). The knowledge of the redshift, combined with very deep *U*-band imaging data enables an accurate estimate of the Lyman escape fraction (Grazian et al., in prep.). Interestingly this survey turns up some of the faintest low-mass galaxies at z ~ 1 (Amorin et al., 2010). Several other investigations on the VUDS dataset are ongoing.

Next steps

With the observations recently completed, we are now processing the last data to assemble the final VUDS sample. Analyses requiring the full sample will then be carried out.

The VUDS survey provides an unprecedented sample of ~ 10 000 galaxies with spectra in one square degree to study early galaxy formation and evolution in the key redshift range 2 < z ~ 6+. Analysis of the current data demonstrates that this sample is ideally suited to establish the volume-averaged properties of a complete sample of star-forming galaxies, which are the progenitors of the galaxy populations observed at later epochs. As a legacy, we will produce staged public releases of this survey.

References

Amorin, R. et al. 2014, submitted, arXiv:1403.3692
Bielby, R. et al. 2011, MNRAS, 414, 2
Bouwens, R. et al. 2007, ApJ, 670, 928
Cardamone, C. et al. 2010, ApJS, 189, 270
Cassata, P. et al. 2014, submitted, arXiv:1403.3693
Cucciati, O. et al. 2014, submitted, arXiv:1403.3691
Garilli, B. et al. 2010, PASP, 122, 827
Guzzo, L. et al. 2013, The Messenger, 151, 41
Guzzo, L. et al. 2014, A&A, in press, arXiv:1303.2623
Ilbert, O. et al. 2013, A&A, 556, 55
Le Fèvre, O. et al. 2005, A&A, 439, 845
Le Fèvre, O. et al. 2013, A&A, 559, 14
Le Fèvre, O. et al. 2014a, A&A, submitted, arXiv:1307.6518
Le Fèvre, O. et al. 2014b, A&A, submitted, arXiv:1403.3938
Lemaux, B. et al. 2014, submitted, arXiv:1403.4230
Lilly, S. J. et al. 2007, ApJS, 172, 70
Moster, B. P. et al. 2011, ApJ, 731, 113
Ouchi, M. et al. 2008, ApJS, 176, 301
Scodeggio, M. et al. 2005, PASP, 117, 1284
Scodeggio, M. et al. 2009, The Messenger, 135, 13
Scoville, N. et al. 2007, ApJS, 172, 1
Stark, D. et al. 2010, MNRAS, 408, 1628
Steidel, C. C. et al. 2003, ApJ, 592, 728
Tasca, L. et al. 2014, A&A, in press, arXiv:1303.4400
Vanzella, E. et al. 2009, ApJ, 695, 1163

When VLT Meets HST: The HUGS Survey

Adriano Fontana[1]
Jim S. Dunlop[2]
Diego Paris[1]
Thomas Targett[2,3]
Konstantina Boutsia[1]
Marco Castellano[1]
Audrey Galametz[1]
Andrea Grazian[1]
Ross McLure[2]
Emiliano Merlin[1]
Laura Pentericci[1]
Styin Wuyts[4]
Omar Almaini[5]
Karina Caputi[6]
Ranga-Ram Chary[7]
Michele Cirasuolo[2]
Chris Conselice[5]
Ashanta Cooray[8]
Emanuele Daddi[9]
Mark Dickinson[10]
Sandra M. Faber[11]
Giovanni Fazio[12]
Henry Ferguson[13]
Emanuele Giallongo[1]
Mauro Giavalisco[14]
Norman Grogin[13]
Nimish Hathi[15]
Anton Koekemoer[13]
David C. Koo[11]
Ray Lucas[13]
Mario Nonino[16]
Hans-Walter Rix[17]
Alvio Renzini[18]
David Rosario[4]
Paola Santini[1]
Claudia Scarlata[19]
Veronica Sommariva[1,20]
Daniel P. Stark[21]
Arjien van der Wel[17]
Eros Vanzella[20]
Vivienne Wild[22,2]
Haojing Yan[23]
Stefano Zibetti[24]

[1] INAF–Osservatorio Astronomico di Roma, Monte Porzio Catone, Italy
[2] Institute for Astronomy, University of Edinburgh, Royal Observatory, Edinburgh, UK
[3] Department of Physics and Astronomy, Sonoma State University, Rohnert Park, USA
[4] Max-Planck-Institut fur extraterrestrische Physik, Garching, Germany
[5] The School of Physics and Astronomy, University of Nottingham, UK
[6] Kapteyn Astronomical Institute, University of Groningen, the Netherlands
[7] Spitzer Science Center, California Institute of Technology, Pasadena, USA
[8] Department of Physics and Astronomy, University of California, Irvine, USA
[9] CEA-Saclay/DSM/DAPNIA/Service d'Astrophysique, Gif-sur-Yvette, France
[10] National Optical Astronomy Observatories, Tucson, USA
[11] UCO/Lick Observatory, Department of Astronomy and Astrophysics, University of California, Santa Cruz, USA
[12] Harvard–Smithsonian Center for Astrophysics, Cambridge, USA
[13] Space Telescope Science Institute, Baltimore, USA
[14] Department of Astronomy, University of Massachusetts, Amherst, USA
[15] Aix–Marseille Université, CNRS, Laboratoire d'Astrophysique de Marseille UMR 7326, Marseille, France
[16] INAF–Osservatorio Astronomico di Trieste, Italy
[17] Max Planck Institute for Astronomy, Heidelberg, Germany
[18] INAF–Osservatorio Astronomico di Padova, Italy
[19] Minnesota Institute of Astrophysics and School of Physics and Astronomy, University of Minnesota, Minneapolis, USA
[20] INAF–Osservatorio Astronomico di Bologna, Italy
[21] Department of Astronomy, Steward Observatory, University of Arizona, Tucson, USA
[22] School of Physics and Astronomy, University of St. Andrews, United Kingdom
[23] Department of Physics and Astronomy, University of Missouri, Columbia, USA
[24] INAF–Osservatorio Astrofisico di Arcetri, Firenze, Italy

A new ultra-deep near-infrared imaging survey has been completed using the HAWK-I imager at the VLT. It is named HUGS (HAWK-I Ultra Deep Survey and GOODS Survey) and delivers the deepest, highest quality images ever collected in the *K*-band. HUGS complements the data delivered by the HST CANDELS survey over two well-studied extragalactic fields, and promises to open up exciting new opportunities to explore the highest redshift Universe. The survey is outlined and faint galaxy number counts and the search for passive galaxies in the early Universe are highlighted. The HUGS data have been completely analysed and are being made public to the worldwide community.

Why HUGS: The general context

Ultra-deep imaging surveys are of fundamental importance for advancing our knowledge of the early phases of galaxy formation and evolution. In general, each technological advance in telescopes and/or detectors has been swiftly applied to obtain ever deeper images of the extragalactic sky over a range of wavelengths. An obvious example of this technology-driven progress is the early Hubble Deep Field (HDF) campaigns (in the north, HDFN, and the south, HDFS) which have paved the way for the subsequent exploration of the high-redshift Universe. Building on the experience of these surveys, the concepts of colour-selection criteria and photometric redshifts have become commonly used tools in the exploration of galaxies at high redshifts. ESO has been major player in this field, as witnessed by various surveys like the New Technology Telescope (NTT) Deep Field (Fontana et al., 2000), the Very Large Telescope (VLT) FORS Deep Field (Heidt et al., 2003), the VLT-HDFS campaign (Fontana et al., 1999) and the near-infrared (NIR) coverage of the GOODS-South field (Retzlaff et al., 2010).

In recent years, the emphasis has started to shift progressively towards undertaking deep imaging surveys in the NIR, motivated by the need to sample the restframe optical (and even ultraviolet [UV]) emission in highly-redshifted galaxies in the young Universe. The most recent and spectacular case is the long series of Hubble Ultra Deep Field (HUDF) campaigns (Illingworth et al., 2013 and references therein), obtained with the infrared channel of the Wide Field Camera 3 (WFC3/IR), the latest and most efficient instrument on board the Hubble Space Telescope (HST).

The CANDELS survey (PI: S. Faber, Co-PI: H. Ferguson) is the latest, and most ambitious enterprise of this kind. CANDELS is a 900-orbit HST Multi-Cycle Treasury (MCT) programme delivering 0.18-arcsecond J_{F125W} and H_{F160W} images reaching ≈ 27.2 (AB mag; 5σ) over

0.25 square degrees, with even deeper (≈ 28 AB mag; 5σ) three-band (*Y*, *J*, *H*) images over ≈ 120 square arcminutes (within GOODS-South and GOODS-North). It also delivers the necessary deep optical HST Advanced Camera for Surveys (ACS) parallels to complement the deep WFC3/IR imaging.

The major scientific goals of the CANDELS MCT programme are: the assembly of statistically useful samples of galaxies at $6 < z < 9$; the measurement of the morphology and internal colour structure of galaxies at $z = 2–3$; the detection and follow-up of supernovae at $z > 2$ for validating their use as cosmological distance indicators; and the study of the growth of black holes in the centres of high-redshift galaxies.

As soon as CANDELS was approved, it was immediately realised that the addition of an adequately deep *K*-band coverage of the CANDELS fields might significantly expand the scientific exploitation of this wonderful dataset. It is worth remembering that, at $z = 6$, the wavelength gap between *H*-band and 3.6 μm is comparable to the gap between the observed *Z*- and *K*-bands at $z = 3$. Thus, bridging this large spectral range with deep *K*-band photometry is crucial for an accurate determination of the restframe physical quantities (e.g., stellar age, stellar mass and dust content) of galaxies at very high redshifts.

The scientific goals of HUGS

To fill this gap, we decided to undertake an ambitious programme designed to make optimum use of the most advanced NIR imager available at any current ground-based telescope: HAWK-I (the High Acuity Wide field *K*-band Imager; Kissler-Patig et al., 2008) at the VLT. On account of its unprecedented combination of depth and area coverage, HAWK-I is the ideal choice to deliver the ultra-deep and wide *K*-band images that are needed over the CANDELS field.

Although HUGS is designed to complement the WFC3 CANDELS observations, it is a free-standing survey that will enable independent scientific investigations, thanks to the depth of the *K*-band images.

The *K*-band is indeed considered an excellent proxy for the selection of mass-selected samples of galaxies at high redshift (Fontana et al., 2006). A primary goal of HUGS is hence the measurement of the evolution of the galaxy mass function at high redshift, especially at the faint end where *K*-band selected samples are required to be as complete in mass as possible. As another example, the wavelength shift from the H_{F160W} band (the longest accessible with HST) to the *K*-band enables us to extend the redshift coverage of the restframe *B*-band from $z \approx 2.6$ to $z \approx 4$. This will allow analysis of the restframe optical morphology and spectral energy distribution of $z \approx 4$ galaxies.

The data

The HUGS survey has been executed over the last three years as an ESO Large Programme (186.A-0898, PI: A. Fontana). It consisted of 208 hours of observations with HAWK-I, mostly in the *K*-band. The final HUGS dataset includes also all the previous imaging programmes that have been executed with HAWK-I in recent years over the GOODS-South field, both in the *Y*-band and *K*-band. These are an earlier Large Programme designed to select $z \approx 7$ galaxies (181.A0717, P.I. Fontana; see Castellano et al., 2010) as well as early HAWK-I Science Verification data (60.A-9284). Our survey targets two of the three CANDELS fields accessible from Paranal, namely GOODS-South and the UKIRT Infrared Red Deep Sky Survey (UKIDSS) Ultra-Deep Survey (UDS), since the ongoing UltraVISTA survey is already delivering ultra-deep *Y*-, *J*-, *H*- and *K*-band imaging within the COSMOS CANDELS field.

The depth of the images in the *K*-band has been tuned in order to match the depth of the WFC3/IR images produced in the J_{F125W} and H_{F160W} filters. In practice, the target depth was chosen to be 0.5 mag shallower than obtained with WFC3/IR in H_{F160W}, as appropriate to match the average (*H* - *K*) colour of faint galaxies.

The pointing strategy is also designed to best cover the CANDELS fields. In the UDS field, three different pointings are able to cover 85 % of the field, with a small overlap that has been used to cross-check photometric calibration. The coverage of the GOODS-South field with CANDELS is more complex, and forced us to adopt a more complicated pattern for the HUGS observations. The WFC3 observations are deeper in a rectangular region at the centre, where the HUDF is also located, and shallower in the upper

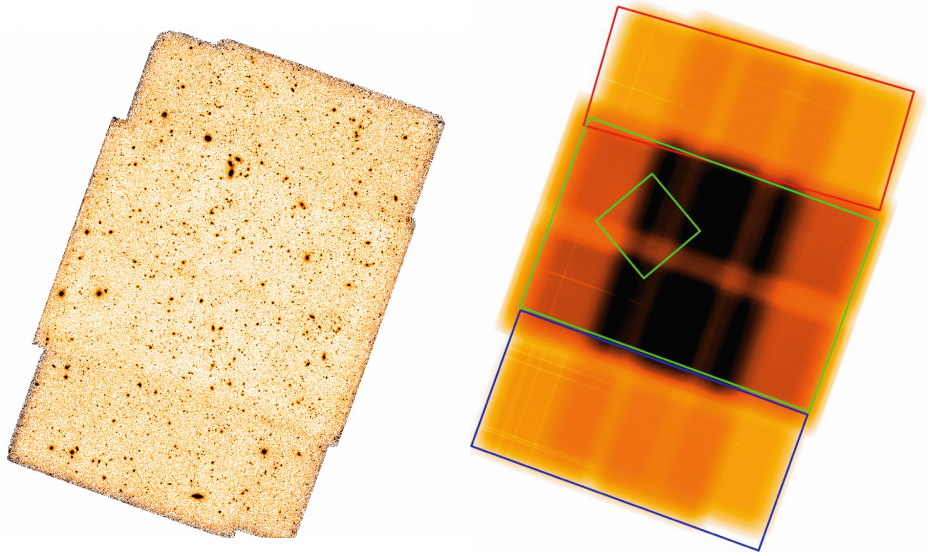

Figure 1. The final HUGS image of the GOODS-South field, in the *K*-band is shown (left image). On the right, the exposure map is shown: darker regions correspond to longer exposure. Overlaid are also the main WFC3 regions: CANDELS-deep (large green rectangle), CANDELS-wide (blue rectangle), Early Release Science (ERS as red rectangle) and HUDF (smaller green box).

and lower part of the field. We have therefore adopted a 2 × 3 grid of pointings, with significant overlaps. The resulting image is shown in Figure 1, including the position of the six individual pointings overlaid upon the WFC3 exposure map (that also includes the position of the HUDF and the other parallel deep fields) as well as the final exposure map.

It is immediately appreciated that the coverage of the GOODS-Deep area is not uniform, because of the combined effects of the pointing locations and the HAWK-I gaps. It reaches about 85 hours of net exposure time in the most central area that covers most of the HUDF, and still reaches more than 40 hours of exposure time over the remaining part of the GOODS-Deep area.

All the data have been collected and analysed. We initially used two pipelines (one developed in Rome and one in Edinburgh) to independently reduce the images acquired in the first year of observations. We then compared the two pipelines and the resulting reduced images: the two results agreed very well and this comparison was utilised to help yield a final, optimised version of the Rome pipeline that has been used in the final processing of all the data. We eventually cross-checked the relative calibration, not only internally (in the regions where the different pointings overlap), but also against wider area but shallower surveys (obtained with UKIDSS or the SOFI instrument), finding that images are calibrated at the 1–2 % level.

Final images and catalogues

The final quality of the output data is simply spectacular, and shows that HAWK-I on the VLT is capable of approaching HST's performance, even in the case of NIR deep imaging where HST is unrivalled. In the *K*-band the seeing is exceptional and homogeneous across the various pointings, confined to the range 0.38–0.43 arcseconds, the former value holding in particular in the ultra-deep area with 85 hours of exposure. In this deepest region (which includes most of the HUDF) we reach a 1σ magnitude limit per square arcsecond of ≈ 28.0 AB mag. In the UDS field the survey is about one magnitude shallower (to match the correspondingly shallower depth of the CANDELS images), but also includes *Y*-band imaging, which also has an excellent seeing between 0.45 and 0.5 arcseconds. A summary of the final quality of the data is presented in Table 1.

A visual comparison of the WFC3/IR and HAWK-I data is offered in Figure 2, where we compare the deepest region from HUGS and CANDELS. It can be immediately appreciated that the depth and quality of the HUGS images is comparable in all aspects to the WFC3 data.

In addition to final images, we have also obtained high-quality photometric catalogues in both areas. These have been obtained using the WFC3 *H*-band image from CANDELS as the detection image, and HUGS magnitudes have been obtained using a point spread function (PSF) matched photometry technique that takes into account the morphology of each object during the deblending process. The photometry was accomplished using the TFIT package (Laidler et al., 2007).

It may be of some interest to use these catalogues to show how effective the HUGS images are in providing us with useful information on the CANDELS-detected objects, since that is one of the main aims of the HUGS survey. In the case of GOODS-S, it is seen that as much as 90 % of the *H*-band detected galaxies have some flux measured at signal-to-noise (S/N) > 1 in the *K*-band, down to the faintest limits of the *H*-band catalogue, and that nearly 50 % of the $H \approx 26$ galaxies (and 15 % of the $H \approx 27$ galaxies) have a solid *K*-band detection with S/N > 5. As a practical example, we show in Figure 3 the spectral energy dis-

Table 1. Summary of HUGS observations for the various pointings.

Field	Band	Exposure time	Seeing (arcsec)	Lim. mag (AB, 1σ arcsec^{-2})
GOODS-DEEP1,2	*K* (2.2 μm)	31.5 hours	0.38–0.39	27.8
GOODS-WIDE1,2,3,4	*K* (2.2 μm)	11.3–13 hours	0.38–0.42	27.3–27.4
UDS1,2,3	*K* (2.2 μm)	12.5–13.5 hours	0.37–0.43	27.3–27.4
UDS1,2,3	*Y* (0.98 μm)	8 hours	0.45–0.5	28.2–28.4

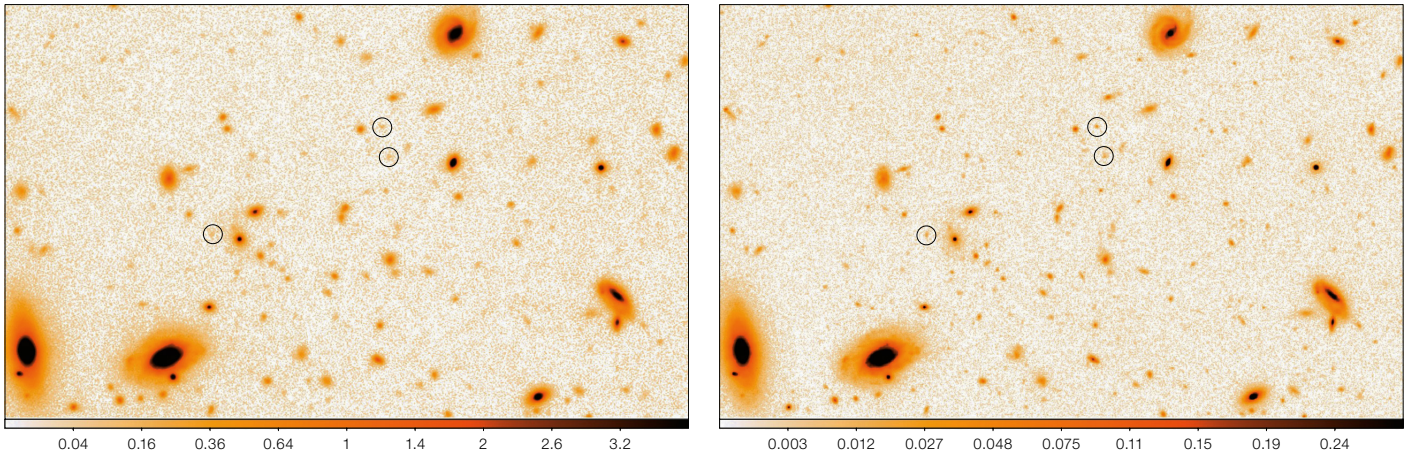

Figure 2. The centre of the deepest GOODS-S field as observed with HAWK-I is shown in the *K*-band (left) and with WFC3/IR in the *H*-band (right). The displayed area is 1 arcminute wide. Objects encircled have $H \approx 26$ mag and a colour $(H - K) \approx 0.5$, typical of faint galaxies.

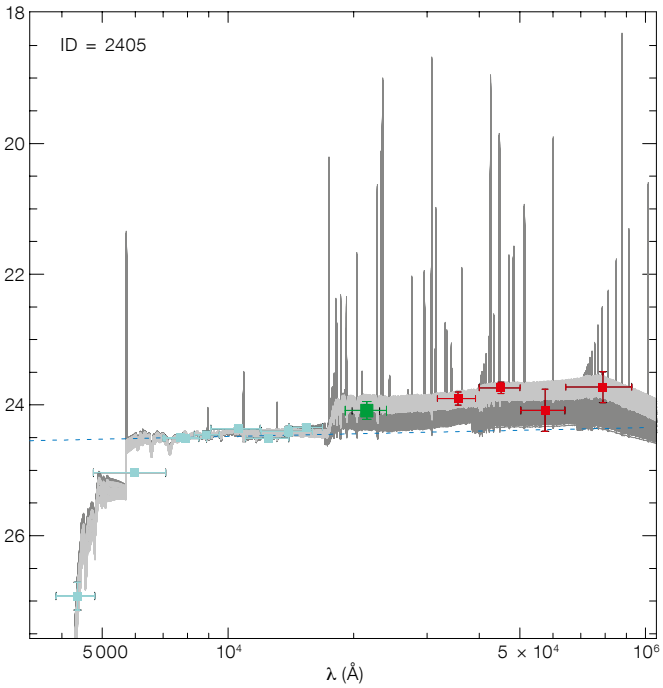

Figure 3. Spectral energy distribution of a galaxy at spectroscopic redshift $z \approx 3.7$, among the highest-redshift galaxies with measured metallicity (Castellano et al., 2014). The magnitudes (in the AB system) are $H \approx 24.3$ and $K \approx 24$. Cyan points represent photometric measures from HST; the green point from the HUGS *K*-band; red points are Spitzer data. Spectral fits in light grey are best fitting Bruzual and Charlot (2003) models with no nebular emission lines; fits in dark grey are Bruzual and Charlot models with nebular emission included.

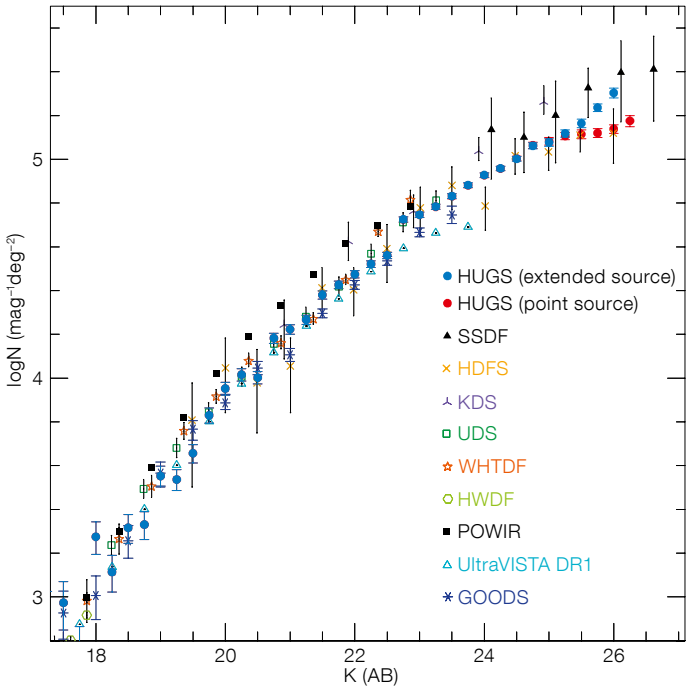

Figure 4. The *K*-band galaxy number counts derived from the HUGS survey, corrected for incompleteness and other systematic effects as described in the text. HUGS points in blue have been corrected for incompleteness with point sources; those in red by extended sources. Data from other deep surveys are also included.

tribution of a galaxy at spectroscopic redshift $z \approx 3.7$ in the GOODS-South field (adapted from Castellano et al., 2014). It is clearly seen that the HAWK-I band data is crucial to sample, at high S/N, the region immediately long-ward of the Balmer break. A full analysis of this and other $z \approx 3$ galaxies can be found in Castellano et al. (2014).

The faintest galaxies as observed in the *K*-band

An immediate glimpse of the scientific merit of a deep field is the derivation of the number counts. In the *K*-band, these are scientifically important since it has been claimed that the total extragalactic background light (EBL), as measured by satellite observations, exceeds the integrated contribution of observed galaxies, if the number counts are as shallow as those obtained by the deepest available observations so far (Subaru Super Deep Field [SSDF]: Minowa et al., 2005). These galaxy number counts have been computed from adaptive-optics-assisted Subaru observations on quite a small field (1 × 1 arcminute). If confirmed, this would imply the existence of some exotic population of primeval galaxies that appear at very faint fluxes.

The HUGS observations reach the same depth as the Subaru observations, but over a much larger area, and are hence perfectly suited to address this issue. Number counts have been derived independently from each pointing on both UDS and GOODS-S images, and a weighted average of these has then been used to obtain the final number counts. After trimming the outer regions of the images, the final area over which we compute the number counts is 340.58 square arcminutes, i.e. about 1/10th of a square degree. However, the deepest number counts (i.e., those determined at $K > 25$) are in practice determined from a sub-area of 50.17 square arcminutes within the GOODS-S field.

Central to a robust determination of the number counts is a thorough and reliable estimate of the incompleteness and other systematics, which must be obtained through the use of simulations. The estimate of the size and magnitude dependence of the correction depends on a critical assumption, namely the distribution of galaxy sizes. At the exquisite resolution of the HUGS images the difference between compact and point-like sources is indeed measurable. We therefore computed the correction for incompleteness in two cases: i) assuming point-like sources; and ii) assuming a distribution in size between 0.1 and 0.3 arcseconds, the typical size that we measure in the *H*-band HST images. The derived number counts are shown in Figure 4, for both assumptions about galaxy size (blue symbols for point sources, red for extended), compared with a number of recent results from the literature. As expected, the number counts agree very well with previous results from the literature. It is immediately appreciated that the HUGS number counts exceed in depth and statistical accuracy of all previous estimates at faint magnitudes, the only exception being the very faintest bin from the SSDF (Minowa et al., 2005).

At the faint limit, it is immediately clear how dramatic is the impact of the assumptions on galaxy size. Assuming point-like sources we confirm the flattening of the number counts at $K \approx 24$–26 reported by Minowa et al. (2005), in our case with a much larger statistical accuracy (due to the 50 times larger field of view of our images). However, assuming instead a more realistic, typical galaxy size in the range 0.1–0.3 arcseconds, we find that the slope of the number counts remains essentially unchanged up to $K \approx 26$, with a slope of about ≈ 0.18 (see Figure 4). If we assume that the steep slope that we find for resolved galaxies holds to even fainter limits, the consequence is that most of the diffuse EBL observed from space can be ascribed to ordinary galaxies, without the need to invoke more exotic populations.

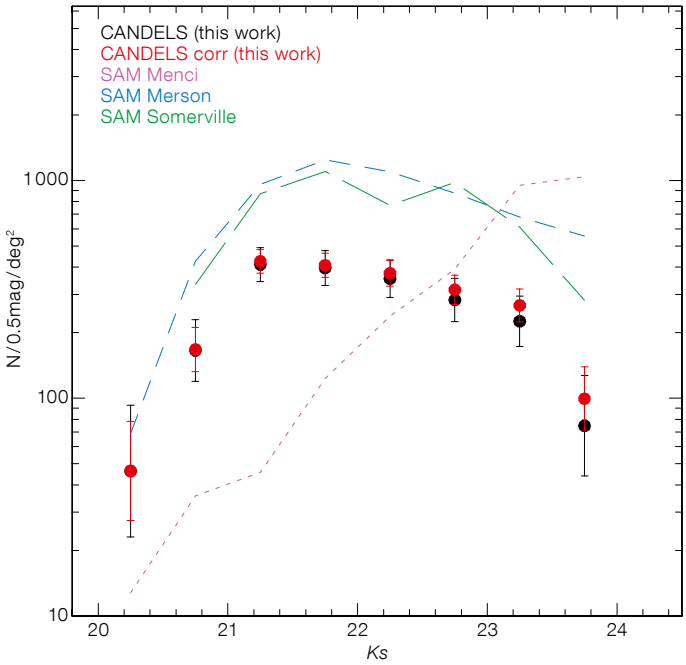

Figure 5. Number counts of passively evolving galaxies at $z \approx 2$ (black: raw counts, red: corrected for incompleteness), from the HUGS survey is illustrated. Comparison of the observed points to three different semi-analytic galaxy models (SAM) are shown.

Passive galaxies in the early Universe

Another early scientific result that we have obtained from these data, in conjunction with the other CANDELS data, is related to the study of passively evolving galaxies at $z \approx 2$. Adopting the *pBzK* criterion proposed by Daddi et al. (2004) to identify such objects, and thanks to the unprecedented depth of our observations, we have now extended the selection of these objects at magnitudes ($K \approx 25$), fainter than was possible in any previous analysis. We have demonstrated for the first time through simulations that we can select passive galaxies down to $K \approx 24$ without being significantly affected by incompleteness, and that the latter is still treatable down to $K \approx 25$.

Our central result (shown in Figure 5) is that the *pBzK* number counts show a flattening at $K \approx 21$, and a turn-over at $K \geq 22$, equivalent to restframe absolute *I*-band magnitudes of $M_I = -23$ and -22 respectively. Converted into stellar mass, our result corresponds to a decrease in the number density of passive-evolving galaxies at stellar masses below $10^{10.8}\ M_\odot$ for a Salpeter initial mass function. As judged against the still steeply rising number counts of the overall galaxy population at these redshifts, this turnover is fairly abrupt, indicating that at high redshift the mechanism that quenches star formation activity is much less efficient below this mass limit.

Comparing our observed number counts with a population of quiescent galaxies extracted from three different theoretical models of galaxy formation, we find that only two of these models reproduce even qualitatively the observed trend in the number counts, and that none of the models provides a statistically acceptable description of the number density of quiescent galaxies at these redshifts. This result clearly shows that the mass and luminosity distribution of quiescent galaxies at high redshift continues to present a key and demanding challenge for proposed models of galaxy formation and evolution. Full details are given in a dedicated paper (Sommariva et al., 2014).

A wealth of data made public

We are fully aware that the data described here may have a much larger impact if the whole astronomical community is allowed access to them. The survey strategy and all the details of data reduction and the number counts are presented in Fontana et al. (2014). All the data from the HUGS survey are available in various forms — as images for individual pointings, as images of full mosaics, as well as multi-wavelength catalogues. Data are available from the ASTRODEEP website[1] as well as from the ESO archive as Phase 3 data products[2]. We look forward to the science that will be possible with this wonderful dataset.

References

Bruzual, G. & Charlot, S. 2003, MNRAS, 344, 1000
Castellano, M. et al. 2010, A&A, 511, A20
Castellano, M. et al. 2014, A&A, in press, arXiv:1403.0743
Daddi, E. et al. 2004, ApJ, 617, 746
Fontana, A. et al. 1999, A&A, 343, 19
Fontana, A. et al. 2000, AJ, 120, 2206
Fontana, A. et al. 2006, A&A, 459, 745
Fontana, A. et al. 2014, A&A, in press
Heidt, J. et al. 2003, A&A, 398, 49
Kissler-Patig, M. et al. 2008, A&A, 491, 941
Illingworth, G. D. et al. 2013, ApJS, 209, 6
Laidler, V. G. et al. 2007, PASP, 119, 1325
Menci, N. et al. 2005, ApJ, 632, 49
Merson, A. I. et al. 2012, arXiv:1206.4049
Retzlaff, J. et al. 2010, A&A, 511, A50
Somerville, R. S. et al. 2012, MNRAS, 423, 1992
Sommariva, V. et al. 2014, A&A, submitted

Links

[1] ASTRODEEP website: www.astrodeep.eu
[2] ESO Phase 3 products: https://www.eso.org/sci/observing/phase3.html

The ESO Director General, Tim de Zeeuw, addresses the participants at the celebration of 50 years of ESO in Chile held at the ESO offices in Vitacura, Santiago, on 30 October 2013.

ESA astronaut Pedro Duque (centre) visited Paranal on 27 October 2013 and is shown with the Director General Tim de Zeeuw (left) and the ESO Representative in Chile Fernando Comerón (right).

Celebrating Fifty Years of ESO in Chile

Fernando Comerón[1]
Tim de Zeeuw[1]

[1] ESO

The fiftieth anniversary of the signing of the agreement between the Government of Chile and ESO to set up a new observatory occurred on 6 November 2013. The anniversary was marked by a formal occasion in Santiago, more informal celebrations at all the ESO sites in Chile and by visits from two European astronauts. A round-up of the anniversary events is presented.

Figure 1. Many staff and their families attended the 50th anniversary celebration event at the ESO premises in Vitacura in Santiago.

Figure 2. Both present and former staff celebrated the 50th anniversary during the event at Vitacura. From left to right: Erich Schumann, Jean-Michel Bonneau at back, Domingo Durán, Albert Triat, Rolando Medina, Albert Bosker at back, Wolfgang Eckert, Daniel Hofstadt and his wife Sonia Hofstadt, the current ESO Director General Tim de Zeeuw, Óscar Orrego and Jorge Moreno.

The 6th of November 2013 marked the 50th anniversary of the signing of the initial agreement between the Government of Chile and the European Southern Observatory (ESO), which enabled ESO to site its astronomical observatory in northern Chile beneath its exceptionally clear skies. This was a significant milestone in the scientific, technical and cultural cooperation between Chile and Europe, and the beginning of an international success story that started very shortly after the establishment of ESO itself.

It is remarkable that this celebration happened just one year after the one held in Germany in October 2012, which marked the 50 years since the signature of the ESO convention on 5 October 1962 (see *The Messenger* 150 and Sirey [2012]). The process by which ESO came into existence, with the goal of achieving together that which individual countries could not achieve separately, took more than ten years from conception to reality, and was set against the difficult backdrop of post-war Europe (see Blaauw, 1991). Taking into account the long preparation time, and the fact that when ESO was established it was still undecided where its telescopes were to be located (South Africa was the primary candidate at the time; Blaauw [1991]), the speed with which the decision was made to go to Chile is striking. Intense site-testing activity of the deserts in northern Chile, carried out by both North American and European astronomers in the earlier 1960s, resulted in the establishment of fully fledged observatories by ESO, by the Association of Universities for Research in Astronomy (AURA) on behalf of the US National Science Foundation and by the Carnegie Institution of Washington. This was the beginning of an endeavour that has resulted in the association of Chile with some of the best and most productive telescopes. The list continues with the current world-leading facilities, among which the Very Large Telescope and the Atacama Large Millimeter/submillimeter Array (ALMA) are foremost (Madsen, 2012).

The signature of the agreement between ESO and the Government of Chile was a recognition of the combination of the unique conditions that nature provides in the northern part of the country with a political appreciation that these conditions offer outstanding advantages for the country, but also yield obligations — on behalf of humanity — to enable scientific research that can only be conducted efficiently from a limited number of geographical locations. The recognition of these aspects by the Chilean government 50 years ago was far-sighted in every sense of the word. It is equally important that this vision has permeated all other levels of the administration, including the collaboration with the regional and local governments. What began in 1963 has evolved into a remarkable success story and a long-term relationship.

Development of ESO in Chile

In 1969, the observatory at La Silla was inaugurated. In 1976, the 3.6-metre telescope, the largest of the telescopes there, saw first light. La Silla grew over the years, but in 1990, ESO decided to place its next-generation flagship facil-

Figure 3. The 50th anniversary party at Paranal was held on 26 November 2013.

Figure 4. Alfonso Silva Navarro, the State Secretary of Foreign Affairs (centre), Xavier Barcons, the President of the ESO Council (left) and Tim de Zeeuw, the ESO Director General (right) pictured at the reception held at the Club de La Unión de Santiago, formally celebrating 50 years of ESO's collaboration with Chile.

ity, the Very Large Telescope, on Cerro Paranal. In the wake of this decision, the original agreement between the Government of Chile and ESO was amended, recognising that, in the years that had passed, both Chile and ESO had undergone great changes. The new agreement foresaw much closer and wider cooperation, with ESO actively supporting the development of Chilean astronomy and related technologies and, through its public outreach activities, also supporting efforts to strengthen the awareness and interest of the public at large in science and technology.

Yet, this was only the beginning. Paranal is now recognised as the most advanced optical and near-infrared astronomical observatory in the world. The ALMA radio telescope has been built in a global partnership with the US National Science Foundation (NSF) and the Japanese National Institutes of Natural Sciences (NINS) and is operational at Chajnantor, taking advantage of the superb conditions that this unique high site offers for millimetre and submillimetre astronomy. Soon, on Cerro Armazones, near to Paranal, construction will start on the 39.2-metre European Extremely Large Telescope (E-ELT), which will be the largest optical telescope ever built. The E-ELT will ensure that the Paranal Observatory will continue to have a privileged place in astronomy for many decades to come.

Celebrations in Chile

ESO celebrated its first 50 years in Chile with a number of activities. The celebrations started on 30 October 2013 with an open-air party at the ESO offices in Vitacura (Santiago), with the participation of staff and their families (see Figure 1 and the upper image on p. 47). On this special occasion ESO was honoured by the presence of the many former employees invited to participate in the event, who could meet long-time colleagues and friends, and shared memories that often went back over many decades of history of ESO (see Figure 2). A series of activities, carefully arranged by a dedicated organising committee, included an open-air exhibition of retrospective material composed of both observatory hardware and pictures, the projection of movies depicting some of ESO's activities, and astronomy-related hands-on activities for the youngest family members. Site celebrations of the 50 years of ESO in Chile took place also at the La Silla and Paranal Observatory sites on 29 and 26 November 2013 respectively (e.g., Figure 3), with the presence of some local and regional authorities.

The 50th anniversary celebrations culminated in a formal ceremony on 8 November 2013 at the imposing Club de la Unión in Santiago, with the attendance of the President of the ESO Council Xavier Barcons, the Director General of ESO and many members of the ESO Finance Committee and senior management. The President of the Republic of Chile was represented by the Secretary of State of Foreign Affairs, Mr. Alfonso Silva Navarro (Figure 4), who was accompanied by other government authorities. Senior representatives from Chilean academia and leading figures of the Chilean astronomical community attended the celebration, as well as the ambassadors of several ESO Member States. Speeches by the ESO Director General, the Secretary of State of Foreign Affairs and the President of the ESO Council highlighted the significance and rich outcome of these 50 years of cooperation between ESO and Chile and the promise for the future. The history of Chilean astronomy from its pioneering beginnings onwards was reviewed by the renowned Chilean astronomer José Maza. Finally, Óscar González, a young Chilean astronomer who was an ESO student in Garching and is now an ESO Fellow in Chile, offered some perspectives on his career as an example of how the cooperation between ESO and Chile has benefitted generations of astronomers.

The ceremony on 8 November 2013 included the gift by ESO to the Government of Chile of the first atomic clock belonging to ESO, which started working at the La Silla Observatory in 1976. Besides its historical value, this clock also has strong symbolic resonance with the cooperation between ESO and Chile, since the official time in Chile was obtained for many years by synchronising with the La Silla atomic clock. This gift was clearly appreciated by the Government of Chile, which arranged for a private ceremony at the Presidential palace on 14 November 2013, where the ESO Director General delivered the clock personally to the President of the Republic of Chile, His Excellency Sebastián Piñera (see Announcement ann13092 for details).

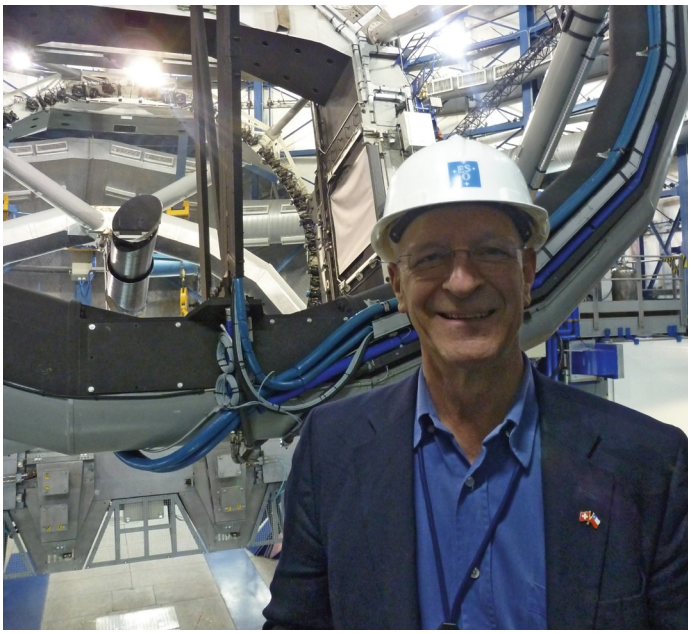

Figure 5. ESA astronaut and former ESO visiting astronomer Claude Nicollier seen inside a VLT dome during his visit to Paranal on 3–4 December 2013.

Anniversary visitors and events

The fiftieth anniversary celebrations also presented an opportunity for special guests to visit the observatories. Among these visitors, ESO was honoured by the presence of two ESA astronauts: Pedro Duque, who has orbited the Earth on board both the Space Shuttle and the International Space Station (see lower image on the Astronomical News section page); and Claude Nicollier, an astronomer by training who had observed at La Silla in the early 1970s, before becoming a veteran of five Space Shuttle missions, including two repair expeditions to the Hubble Space Telescope (see Announcement ann13088 and Figure 5). In addition to his visit to Paranal, Pedro Duque participated in a public colloquium on science and art organised by the Cultural Centre of Spain in Santiago de Chile and gave talks on his experiences in space to ESO staff both on Paranal and in Santiago. Claude Nicollier also gave public talks organised by the Swiss embassy in Chile, which hosted his visit, and by the University of Santiago de Chile. By a fortunate coincidence, astronaut Pedro Duque arrived on Paranal almost at the same time that President Piñera was landing at the observatory premises to deliver the decrees of donation of the Cerro Armazones land to ESO, on 27 October 2013 (see Release eso1345), thus allowing the President and the astronaut to meet and warmly greet each other on Paranal.

In addition to these visits, which were actively supported by the Spanish and the Swiss embassies, other embassies of the ESO Member States also contributed, with a variety of events in Santiago to highlight the significance of the first 50 years of ESO in Chile as a cultural link between Europe and Chile, extending beyond the strict domains of science and technology. Coordinated by the Delegation of the European Union in Chile, activities were organised by the embassies of France, Germany and Italy, as well as by the delegation in Chile of the region of Wallonie-Brussels. The celebrations extended even beyond the current ESO Member States, as the embassies of Greece and Poland also organised astronomy-related events under the umbrella of the 50th anniversary of ESO in Chile.

Towards the next 50 years in Chile

To highlight the history and achievements of these 50 years of collaboration, the brochure *ESO y Chile: Un puente científico y cultural* was produced (in Spanish) and widely distributed in Chile. Its purpose is to promote knowledge about ESO and its activities in the host state among the general public. The brochure briefly describes the current facilities of ESO in Chile, the history of the past 50 years, the existing collaborations between ESO and Chile and the expectations for the future represented by the E-ELT.

In these past 50 years, Chile has become the world centre for ground-based astronomy. This owes much to the determination of the Government of Chile and all the levels of the Chilean administration to protect the extraordinary but fragile treasure of its clear and dark skies. This achievement is also attributable to its equally determined support of science and technology in the country, to the active promotion of international cooperation and to the public appreciation of the night sky as a part of its cultural heritage. ESO is proud to be associated with such an impressive growth of capabilities and looks forward toward an even closer collaboration in the future, enabling astronomy in its Member States and in Chile to continue growing together in this example of international cooperation at its best.

References

Blaauw, A. 1991, *ESO's Early History – The European Southern Observatory from Concept to Reality*, (Garching: ESO)

Madsen, C. 2012, *The Jewel on the Mountaintop – The European Southern Observatory through Fifty Years*, (Weinheim: Wiley-VCH)

Sirey, R. 2012, The Messenger, 150, 7

Report on the Workshop

Deconstructing Galaxies: Structure and Morphology in the Era of Large Surveys

held at ESO Vitacura, Chile, 18–22 November 2013

Dimitri A. Gadotti[1]
Rubén Sánchez-Janssen[2]

[1] ESO
[2] NRC Herzberg Institute of Astrophysics, Canada

Over 120 researchers — observers and theoreticians — gathered to present new results and discuss ongoing investigations on the structure of galaxies. The study of the structure and morphology of galaxies is one of the major tools that astronomers have to address how galaxies form and evolve. Recent progress in the field has enabled a boost in our understanding of the properties of the different structural components in nearby galaxies, as well as in galaxies at intermediate redshifts (z ~ 1–2).

Two main topics motivated this workshop. Firstly, there is the connection between galaxy structure and the physics of galaxy formation and evolution. After decades of fitting galaxy light profiles or images with mathematical functions to describe the various components (e.g., bulge and disc), it is imperative to advance from a stamp-collecting approach and connect the results to the physics. The link between structural properties, kinematics, stellar population content and the complex physics involved in the formation and evolution of galaxies is a much more challenging step. One of the main goals of the workshop was to address this connection, by questioning, for instance, what the structure of galaxies tells us about their formation and evolution, and how observations can help constrain models.

The second consideration was the tools that are used to measure the structural parameters in galaxies. The complexity of these tools has grown considerably in recent years. It is thus extremely important to address the strengths and limitations of the different techniques, particularly with the expectation that automated procedures designed to handle large surveys may prevail in the future.

Our first announcement ended with a bold statement: "This ESO Workshop should set the basis for the study of galaxy structure and morphology in the next decade." It was with deep satisfaction that we concluded the meeting with the realisation that this might indeed have been achieved. The conference website[1] contains the slides for all oral presentations, as well as for most posters; audio/video recordings are also available for the talks. Highlights of the meeting, necessarily biased by our own perspective and limitations of space, are subsequently presented.

Day 1: Structure, morphology and the underlying physics

The first day (Monday) began with results from GalaxyZoo, presented by Karen Masters, and the Millennium and the Galaxy And Mass Assembly (GAMA) surveys, by Simon Driver. Karen convincingly showed the power of citizen science, something that many in the community may have looked at with scepticism initially. By using statistical methods it is possible to not only separate early-types and disc galaxies, but also to assess bar fractions and sizes and even galaxy morphology at higher redshifts. Simon described the logical filter used to evaluate the quality of automated decompositions, and showed results that lead him and his collaborators to conclude that processes that form discs are more efficient than processes that form spheroids. He also questioned what a spheroid looks like when it is forming, noting that at high redshifts nothing resembles one, but possibilities include clumpy discs, thick turbulent discs and blue spheroids. Pat Côté followed, showing new results on the structure of galaxies at the core of the Virgo cluster (with the New Generation Virgo Survey [NGVS]), including the difficulties of dealing with background subtraction. He showed that nuclei are often bluer than the surrounding areas in low-mass galaxies. Lisa Fogarty showed the power of studying stellar kinematics with the Sydney Australian Astronomical Observatory Multi-object Integral Field Spectrograph (SAMI). She presented two surprising observations, namely the presence of slow rotators on the outskirts of clusters, and two brightest cluster galaxies (BCGs) that are fast rotators.

Next, the spectacular features revealed by deep imaging of galaxies, such as shell-like structures and streams, were shown by Pierre-Alain Duc and Yun-Kyeong Sheen. Duc discussed how these features provide clues to understanding galaxy formation mechanisms. For example, while gas-rich major mergers produce tidal tails lasting for about 2 Gyr — in contrast with gas-poor major mergers, which do not seem to produce lasting features — intermediate-mass mergers appear to induce shells with a lifetime of 3–4 Gyr. Chris Conselice described how more massive galaxies become Hubble types earlier than less massive galaxies and results indicating that the number of major mergers an average massive galaxy undergoes from z ~ 3 to zero is about two, roughly doubling its stellar mass. Minor mergers and gas accretion/*in situ* star formation would contribute equally to the stellar mass budget.

The properties of fast and slow rotators were reviewed by Michele Cappellari who discussed the mass–size relation and its evolution with redshift. A strong size increase with redshift is found only for galaxies more massive than 10^{11} $M_{\odot}$, perhaps indicating that growth via mergers is unimportant for galaxies below this mass threshold. Andi Burkert gave an inspired talk emphasising the strong role of the environment on galaxy formation via gas accretion and minor mergers. He also pointed out that we still do not know how to form the Milky Way, or how its progenitors appear at higher redshift. In addition, he showed simulations (by R. Teyssier) in which discs — contrary to common belief — are not destroyed in major mergers.

Day 2: Structure and morphology of early-type and spheroidal galaxies

Laura Ferrarese started the second day by reviewing the morphology and structure of massive early-type galaxies. She showed that early, *in situ* star formation builds high phase-space density cores, while minor mergers mostly contribute to the formation of extended envelopes — with the balance between both processes depending on mass and environment. Bililign Dullo subsequently showed

that the stellar mass deficits in core Sérsic lenticular galaxies favour a two-step inside-out scenario for their assembly: an early violent “dry” merger, followed by late accretion of gas and stars. Rhea-Silvia Remus presented evidence that the total mass density profile of elliptical galaxies is related to their merging history: at high redshift the density slopes are steep ($\gamma = -3$), and at each subsequent gas-poor merger event the slope evolves towards $\gamma = -2$. Pablo Pérez-González introduced the Survey for High-z Absorption Red and Dead Sources (SHARDS), a Gran Telescopio Canarias (GTC) narrow-band imaging survey. Through 25-point spectral energy distribution (SED) fitting, he showed that $z \sim 1$ red and dead galaxies have stellar population ages ~ 3 Gyr and formation timescales ~ 300 Myr.

Guillermo Barro followed, showing that the build-up of the red sequence occurs rapidly as star-forming galaxies at redshifts 2–3 first compactify, and then quench. Using Keck spectroscopy, Sirio Belli presented evidence for a significant evolution of quiescent galaxies in both mass and size since $z \sim 2$. However, their study suggests there is no evolution in their dynamical-to-stellar mass ratios. These results were challenged by Paolo Saracco, who argued that ellipticals have completed their mass growth by $z \sim 1.3$, with little to no subsequent structure evolution. Veronica Strazzulo presented a study of the structure of massive early-type galaxies in a cluster at $z \sim 2$. These galaxies seem to be larger than field early-types of similar masses, but larger cluster samples at high redshifts are needed to confirm these first results. Marc Huertas-Company showed that the mass–size relation of $z < 1$ early-type galaxies appears to be almost universal for all environments, and indicated that semi-analytic models of galaxy formation fail to reproduce this effect. Phil Hopkins summarised recent progress on the physics of feedback and how it regulates star formation. He pointed out that possibly the most pressing question in astrophysics today is why star formation is so inefficient.

The afternoon was devoted to the structure of dwarf galaxies. Thorsten Lisker showed that early-type dwarfs are continuously shaped by processes acting in groups and clusters. Joachim Janz showed that quiescent dwarfs are structurally complex, but the level of complexity decreases towards the faint end. It is however not yet clear what the physical nature of the “extra” structural components in these galaxies is. Rubén Sánchez-Janssen presented the first study on the intrinsic shape of dwarf spheroidal (dSph) galaxies using data from the NGVS survey. dSphs are oblate spheroids, and there appears to be no evidence for very elongated shapes in this population. On the other hand, Ricardo Muñoz showed that the ultra-faint Milky Way satellites tend to be elongated, possibly due to tidal effects. These extreme systems bridge the mass–size relation region between globular clusters and the classic satellite galaxies. Numerical simulations of the destructive effects of ram-pressure stripping on tidal dwarfs were presented by Rory Smith, who showed that 50–100 % of all stars become unbound as a result of the drag force created by the gas stripping.

Day 3: Structure and morphology of disc galaxies

Victor Debattista started the morning session by describing simulations of secular evolution in disc galaxies. He showed models in which the growth of a surrounding disc compresses a pre-existing (classical) bulge, raising its velocity dis-

Figure 1. Participants at the workshop in the Vitacura garden.

persion. This effect qualitatively accounts for the observed offset between elliptical galaxies and classical bulges in some scaling relations. Elena D'Onghia showed simulations where the formation of bars is suppressed and long-lived spiral arms form as a result of density perturbations in the disc. Then, impressive HI data were shown by Marc Verheijen, where tidal streams display no gas content and ram-pressure stripping can be seen in action. He also showed HI-derived rotation curves indicating that discs are submaximal.

Alister Graham then showed that the locus of high-redshift ellipticals in the mass–size relation is similar to that of low-redshift bulges, suggesting that the two systems may be connected. Jairo-Méndez-Abreu came next, showing that there is no clear kinematical difference among bulges spanning a range of structural properties in a small early-type galaxy sample from the Calar Alto Legacy Integral Field Area (CALIFA) survey. Ronald Läsker subsequently demonstrated that the black hole mass – galaxy luminosity relation appears to be very tight, and then Mauricio Cisternas showed that most active galactic nuclei (AGN) activity is in discs, with only a minority in mergers.

Day 4: Structure and morphology of disc galaxies (cont'd)

Thursday saw us continuing the discussion on disc galaxies, with Stéphane Courteau reviewing scaling relations. He pointed out that scale parameters, obtained through decompositions, are rarely derived with an accuracy better than 20%, and showed further evidence for submaximal discs. Nacho Trujillo next reviewed the outer structure of disc galaxies, concluding that down-bending breaks are associated with changes in the stellar population at the position of the break — possibly through radial migration and bar resonances. Truncations, on the other hand, are associated with real drops in the density of stars. Up-bending breaks and outer light excesses are related to the stellar halo and/or interactions with companion galaxies.

The effects of ignoring the variety in disc profile shapes in galaxy image decompositions was discussed by Taehyun Kim. Using data from the Spitzer Survey of Stellar Structure in Galaxies (S^4G) , she showed that bars almost exclusively have exponential profiles in bulgeless galaxies, whereas the presence of a bulge almost always results in bars with flat luminosity profiles. She further showed that in galaxies with prominent bulges, down-bending breaks in discs are at the bar outer Lindblad resonance.

Thick discs, their existence and formation mechanisms were reviewed by Peter Yoachim, who showed that early mergers create a population of old stars that later can radially migrate and thicken. David Streich presented results on thin and thick discs from the GHOSTS survey, and noted that thick disc heating seems to happen on time scales larger than ~ 500 Myr. By using numerical simulations, Ivan Minchev showed that radial migration is able to cool discs during mergers. In addition, he suggested that thick discs form from the flaring of the different age populations. Further impressive data from the GHOSTS survey were shown by Roelef de Jong with findings that inner stellar halos (< 25 kpc) have Sérsic indices around 4–6, and are very flattened (c/a ~ 0.3). These data show that the substructure in stellar halos is diverse.

The afternoon session was devoted to bars. Alfonso Aguerri reviewed studies on the fraction of barred galaxies in the local Universe. He showed that the bar fraction is strongly dependent on galaxy mass — this is likely the main cause of the disagreement among studies in the literature. He also presented results that indicate that a dense environment can heat up thin discs and destroy bars in low-mass galaxies, whereas it induces bar formation in more massive galaxies. Kartik Sheth pushed the topic to higher redshifts, showing the decline of bar fraction to $z \sim 1$. He argued that more massive discs form bars earlier than less massive ones, as they become dynamically mature earlier. Using data from the Near Infrared S0 Survey (NIRS0S) and the S^4G survey, Eija Laurikainen introduced barlenses, a stellar structure often seen in barred galaxies. These structures are probably box/peanuts seen at a different projection, and not inner discs or classical bulges.

Evidence for bar-induced secular evolution in massive disc galaxies was presented by Dimitri Gadotti. He showed that: (i) longer bars tend to be stronger; (ii) discs in barred galaxies show fainter central surface brightness and longer scale lengths than discs in unbarred galaxies; and (iii) that bars rejuvenate the stellar population of bulges. Juan Carlos Muñoz-Mateos followed, showing with S^4G data how bars and spiral arms can produce down-bending disc breaks through resonances and radial migration. With CO data, he also showed that molecular gas profiles are broken too, with sharper breaks than stellar profiles.

Lia Athanassoula showed the variety and complexity of the physical phenomena that influence bar formation and evolution. Dark matter halo triaxiality and mass, disc kinematics, gas fraction and the presence of a thick disc, all influence the speed with which bars form. These factors, plus the velocity distribution function in the halo, and the presence of a central mass concentration, also influence the angular momentum redistribution in the galaxy, and therefore how strongly the bar develops. Classical bulges and halos slow down bar formation, but help bars to grow stronger later. To close this important section, Francesca Iannuzzi showed her promising, ongoing work on the signatures box/peanuts imprint on 2D stellar kinematic maps. By using numerical simulations of edge-on systems, she showed that these maps can reveal hidden peanuts seen end-on, thus avoiding the likely confusion of an end-on bar with a classical bulge.

Day 5: Structure of the Milky Way, tools and analysis methods

The last day of the meeting was an atypical closing day, which led us to finish the meeting on a high point. Joss Bland-Hawthorn reviewed the properties of the Milky Way in the context of external galaxies. He also made the important remark that half of all stars in the Galaxy were in place by $z \sim 1$, and that its current star formation rate puts it in the green valley.

The session on tools and analysis methods began with Luc Simard discuss-

ing the pros and cons of automated bulge/disc decomposition applied to very large samples. Boris Häussler followed, describing MegaMorph and its multi-wavelength galaxy image fitting, showing that structural parameters are recovered with lower uncertainties if they are forced to vary smoothly with wavelength. Lee Kelvin showed how the stellar mass content is distributed among different structural components and morphological types, using data from the GAMA survey.

Imfit, a new, flexible and powerful image decomposition code was introduced by Peter Erwin, who also showed how using Cash statistics — as opposed to the familiar χ^2 statistics — leads to more accurate measures of galaxy structural parameters, particularly in low signal-to-noise regimes. Marina Vika discussed the tricky distinction between elliptical and lenticular galaxies when using two-component image decompositions. The last talk of the meeting was given by Steven Bamford, who showed how including a non-parametric component to account for difficult features, such as spiral arms, improves the determination of structural parameters through parametric fits.

The meeting closed with a lively general discussion that lasted for over an hour and consisted of three sections. The first dealt with practices that should be avoided. For observers, these include: (i) not using v/σ alone, without information on ellipticity, to separate fast and slow rotators; (ii) not fitting edge-on galaxies without taking into account the dependence of the luminosity on the vertical distance from the disc plane; and (iii) not ignoring the presence and harmful effects of bars on decompositions that contain only models for the bulge and disc. For modellers, it was pointed out that the term “morphology” has been often used to express concepts that are not equivalent from a physical perspective. A remark that applies to both modellers and observers is not to use catalogues of morphology or structural measures without paying attention to the biases and limitations of such catalogues.

The second section concerned practices that we, as a community, suggest for advancing the field. Two observed properties that were often discussed during the meeting are found to be robust, and modellers are encouraged to try and reproduce them. The first property is the offset in the mass–size relation observed at the high-mass end between elliptical galaxies and bulges at $z = 0$. The second property is the merger rate as a function of lookback time.

Finally, the third section was devoted to a wish list of facilities/concepts deemed necessary for further progress. These included obtaining data on resolved stellar populations out to the Virgo cluster (feasible with the European Extremely Large Telescope, but with some pioneering work using the MUSE narrow-field mode also possible), and making simulations/models publicly available in a style similar to the Virtual Observatory initiative. Gas distributions out to $z \sim 1$ (with the Square Kilometer Array), and an imaging survey providing a physical spatial resolution similar to that of the Sloan Digital Sky Survey at $z \sim 0.05$, but out to $z \sim 1$ (with the Euclid satellite), were also mentioned. Finally, we agreed that the future of studies like the ones presented during the workshop depends on the interest of the general public in astronomy in general and galaxies in particular. Initiatives like GalaxyZoo are widely viewed as fantastic ways to keep the general public engaged.

Links

[1] Workshop website: http://www.eso.org/sci/meetings/2013/morph2013.html

ESO/P. Grosbol

Gallery of six spiral galaxies in near-infrared images taken by HAWK-I on the VLT. They represent just a few examples for the enormous variety of spiral patterns in galaxies. From left to right the galaxies are NGC 5247, M100 (NGC 4321), NGC 1300 (upper row) and NGC 4030, NGC 2997 and NGC 1232 (lower row). See Release eso1042 for more details.

Report on the Workshop

400 Years of Stellar Rotation

held at Natal, Brazil, 21–26 November 2013

José Renan de Medeiros[1]
Claudio Melo[2]
Luca Pasquini[2]

[1] Departamento de Fisica, Universidad Federal do Rio Grande do Norte, Natal, Brazil
[2] ESO

The workshop marked the 400th anniversary of the observation of sunspots by Galileo and his deduction of the rotation of the Sun. The topics covered extensively both the theoretical and observational aspects of stellar rotation for stars of all types, from pre-main sequence to evolved stages, and including binary stars and stars hosting planets. A summary of the selected themes is presented.

Figure 1. The participants at the workshop "400 years of Stellar Rotation" by the beach at Tabatinga.

Motivation

Stellar rotation is both a very old topic, going back to the time of Galileo, and a very topical one, at the forefront of current research in stellar physics. As described on the webpage of the conference[1], Galileo Galilei reported in 1613 in his book the *"l'Istoria e dimostrazioni intorno alle macchie solari e loro accidenti"* evidence for sunspots and the interpretation of their motion as due to Solar rotation. A few centuries separated this first reported evidence of the rotation of the Sun from the first studies at the beginning of the 20th century, by Eddington, Milne, von Zeipel and others, addressing the impact of rotation on stars from a theoretical point of view. Thus, 400 years after the discovery of Galileo, the subject of the rotation of the Sun and of other stars is still a very active area of research, as testified by the 144 scientists from 21 countries who attended the conference held in the beautiful city of Natal, Brazil. The conference was co-sponsored by ESO, the University Federal of Rio Grande do Norte and the International Institute of Physics of Natal.

Conference themes

The conference occupied five full days, with more than 60 invited reviews, contributed talks and almost 50 posters. The topics were organised into nine sessions, including: pre-main sequence and low-mass stars; massive stars; evolved stars; modelling evolution with rotation; rotation, magnetic fields and binaries. A session on the Sun was followed by: rotation and chemical abundances; rotation, activity and planets; and the conference ended with sessions devoted to the legacy of space missions and to our understanding of stellar rotation.

The conference also featured two enlightening talks about Galileo and his cultural environment. In his opening review "Galileo, the man and the scientist", Alberto Righini summarised the entire scientific life of Galileo with emphasis on his discovery of sunspots and rotation. He was of the opinion that Galileo Galilei was close to a sort of Florentine Protestant movement and this motivated the strong reaction of the Catholic Church. He has described this thesis in full in his book on Galileo (Righini, 2008). In his talk "Galileo, the artist and the scientist", given on the final day of the conference (not at the conference venue, but in the exotic surroundings of Tabatinga Beach), Paolo Molaro emphasised that Galileo was not only the father of modern science, but also an innovative and inspirational mind in many fields, a real man of the *rinascimento*, dominating philosophy, music and painting. Paolo Molaro also presented the fascinating story of a mysterious portrait that might be of Galileo himself (Molaro, 2012).

To summarise the results of such a broad-ranging conference and select scientific highlights is a difficult task, which may lead to unfair omissions. Accepting this risk, we present a short summary of some, subjectively selected, scientific highlights covering many aspects of observations and theory, including rotational periods, magnetic fields, activity and abundances, dynamo theory and its relationship with stellar structure and differential rotation.

The many different talks presented recent results both from theoretical and observational standpoints. Experiments like SOHO have provided a detailed view of the internal and surface rotation of the Sun. The precise photometry obtained with the Kepler and CoRoT satellites has made rotation periods for thousands of stars available. In addition, projected rotational velocities ($V \sin i$) are provided for thousands of stars, thanks to ground-based high-resolution spectroscopy. These data offer the unique possibility of detailed studies of the behaviour of the rotation of the Sun in time, as well as the evolutionary behaviour of stellar rotation

all along the Hertzsprung–Russell (HR) diagram. Techniques like interferometry allow the shape of fast-rotating stars to be explored directly and spectropolarimetry provides information about the external magnetic field and, together with measures of rotation, gives indications on how these two properties interact. Asteroseismology also provides invaluable information on the internal rotation of stars and poses new challenges to stellar modellers.

Theory and models

From a theoretical point of view, rotation does appear to be an essential ingredient for understanding the evolution of single and close binary stars. Rotation has an impact not only in the area of stellar physics, but also on the evolutionary scenarios and lifetimes of different types of stars, leading to the modification of stellar populations, and thus the photometric evolution of galaxies. It may change the yields of some elements, especially at very low metallicity, providing new insights into the early chemical evolution of galaxies. Rotation has an impact on the nature of progenitors of core-collapse events and of long soft gamma ray bursts. The range of initial masses that give birth to white dwarfs, neutron stars and black holes will probably also depend to some extent on rotation. How the rotation of a star depends on the presence of planets, a question already addressed by Struve, was discussed during the conference, as well as what may happen when a planet is engulfed by its host star. As demonstrated by these few points, rotation is at the crossroads of many topical subjects in modern astrophysics, from planet and star formation to the evolution of galaxies passing through the first stellar generations in the Universe.

Stellar rotation studies discriminate between Solar-type stars and those, hotter than the Sun, without an external convective zone. It is no exaggeration to state that “the Universe without rotation would have been much less interesting”. Thus Georges Meynet concluded his vibrant review in which he explained that, for massive stars, rotation explains a number of observed phenomena, from unexpected surface chemical composition, to the interferometric measurements of flattening (presented by Antoine Merand and John Monnier) and departures from the Von Zeipel darkening law. A positive conclusion is that evolutionary models of massive stars incorporating stellar rotation seem to be able to reproduce many of the observations. Models are therefore an essential tool to predict the production of key elements produced by massive, very metal-poor stars, that are barely observable at present. The impact of satellite missions has also dramatically changed what we know about white dwarfs, revealing large discrepancies between observed rotation periods and spectroscopically determined $V \sin i$ values. In an equally energetic talk, Andre Maeder walked us through a number of the present puzzles (such as the abundance of nitrogen at low metallicity and the *s*-elements), where rotation of massive stars could play a role, concluding that the early Universe was controlled by stellar rotation.

Observations

Currently there are a striking number of stars for which the ages and stellar masses are quite well known. This favourable situation arises mostly from the results of the CoRoT and Kepler satellites, which were reviewed by Annie Baglin and Soeren Meibom respectively. However ground-based photometric surveys of thousands of stars with measured rotational periods all over the HR diagram, including stars in many open clusters, also contribute strongly. Jerome Bouvier reviewed how this wealth of data has allowed the modelling of the early angular momentum evolution taking place in stars from the pre-main sequence (PMS) up to Solar age. Although the main ingredients of early angular momentum evolution have been known for quite some time, the amount, and mainly the quality, of the data have now allowed a much more refined modelling of the physics involved. Luiza Rebull reviewed the legacy of the Spitzer Space Telescope for our understanding of stellar discs; more detailed studies of the young stellar disc–rotation interaction in the infrared have been enabled for a wider range of ages and masses than ever before.

As usual more information does not necessarily mean more answers, but rather more questions! For many of the stars studied with other techniques, the physical characteristics can also be derived by using asteroseismology. In contrast to main sequence stars, these data show that in evolved stars, the nucleus rotates about 13 times faster than the external atmosphere. This finding indicates that the cores rotate slower than expected if the star were a solid body, but faster than if a shellular rotation model (i.e., one where the rotation in the interior of the star mainly depends on the radius, so that each incremental shell rotates with the same angular velocity, but different from the nearby shells) is assumed. The presence of a certain amount of coupling between the core and the surface is deduced. This coupling is of course fundamental to understanding the internal mixing of the chemical elements, and may therefore help to explain some of the peculiar abundances observed in giants. What, however, is the missing angular momentum transport process: internal gravity waves or a magnetic field?

The same kind of data allows the study of gyrochronology, i.e., how stars slow down during their lifetime on account of the presence of winds, mass loss and magnetic fields. Sydney Barnes reviewed the prospects for and limitations of this technique. Interestingly enough, while a regular rotational period–age pattern is observed in open cluster stars, the results are not so clear for field stars with ages derived from asteroseismology. In general, the debate on whether gyrochronology is a viable way of measuring stellar ages appears to be quite lively. An associated question is whether the rotation of the Sun is anomalous for its mass and age. The answer appears to be: probably not.

For some stars even differential stellar rotation can be obtained, showing that, although the Solar case is not common, differential rotation behaviour generally agrees with models. Indeed, in his didactic review, Nuccio Lanza presented spectroscopic and photometric methods to measure surface differential rotation, also considering recent contributions from high-precision photometric time series from the MOST, CoRoT and Kepler space

missions. New, large, spectroscopic surveys are complementing the satellite data, producing precise stellar parameters and measured *V*sin*i*. Steve Kawaler and Kepler Oliveira reviewed the present status of methods for determining the rotation velocities of white dwarf stars via asteroseismology and spectroscopy, which will open up the study of rotation in the final stages of stellar evolution.

Stellar rotation and angular momentum evolution are also intimately coupled to proto-planetary discs and to the presence of planetary systems. The interaction between planets and stars is, however, not limited to the dynamics in the early stages, but continues all through the stellar lifetime. On the one hand, evidence is being sought for the presence of chemical abundance peculiarities in planet-hosting stars. R. Similjanic and A. Recio-Blanco reinforced the evidence for a link between rotation history and light-element abundances. This connection is not new, but in spite of the amount of data available, its nature is not yet fully understood.

On the other hand, rotation-induced magnetic activity of stars plays a key role in determining whether planets can retain a magnetosphere, which is essential for life as we know it. As Edward Guinan emphasised, "the Sun is still a dangerous star". In the same vein, Nuno Santos remarked on the analysis of rotation from the point of view of the research on exoplanets; he noted that "astronomers working on exoplanets don't like the fact that stars rotate", since the rotation–activity connection is the main source of stellar noise in planet searches.

Several talks (e.g., Reiners, Gouveia dal Pino, Vishniac and Lazarian) reminded us that while magnetic activity and magnetic fields can now be measured well in many stars and qualitatively understood, detailed modelling of the (Solar) dynamo still encounters several challenges in reproducing the observations. For binary stars in particular, as stressed by Klaus Strassmeier in his review, the situation is significantly more complex.

Acknowledgements

Galileo would likely have been delighted to discover the long trail that has been explored in Solar and stellar rotation since his time! The conference was superbly organised, and the attendees could enjoy the beautiful beach of Tabatinga, close to Natal, on the social trip (see Figure). The Local Organising Committee, and in particular Bruno Canto Martins, Sanzia Alves and Bia Pessoa, had a hard time making everything run smoothly, or perhaps more appropriately, "rotate swiftly", but succeeded admirably.

References

Molaro, P. 2012, AN, 333, 186
Righini, A. 2008, *Galileo. Tra scienza fede e politica*, (Bologna: Editrice Compositori)

Links

[1] Conference web page: http://www.dfte.ufrn.br/400rotation/index.htm

Report on the

ALMA Community Days: Preparing for Cycle 2

held at ESO Headquarters, Garching, Germany, 19–20 November 2013

Suzanna Randall[1]
Andy Biggs[1]
Tim Davis[1]
Claudia Lagos[1]
Thomas Stanke[1]
Leonardo Testi[1]
Martin Zwaan[1]

[1] ESO

ALMA has now been obtaining scientific observations for the astronomical community for over two years. While commissioning is still continuing, the upcoming Cycle 2 should allow for nearly 2000 hours of science observations. The Cycle 2 ALMA Community Days, summarised here, were designed to optimally prepare the European ALMA Community for proposal submission and were held just a couple of weeks before the Cycle 2 deadline.

The Atacama Large Millimeter/submillimeter Array (ALMA), is the world's leading observatory at millimetre and submillimetre wavelengths. It is the result of a global cooperation involving Europe (through the ESO Member States), North America and East Asia, as well as the host country Chile. Located at the unique site on the Chajnantor Plateau in northern Chile at over 5000 metres above sea level, the final array will comprise at least 66 high precision antennas equipped to observe in the 30 GHz to 1 THz frequency range. The antennas are grouped into the main array, comprising 50 12-metre dishes, and the Atacama Compact Array (ACA, also known as the Morita Array), containing 12 closely placed 7-metre antennas together with four total-power 12-metre antennas used to recover large-scale structures on the sky. By combining data obtained with different configurations of the main array and the ACA, complex and extended sources can be accurately imaged.

ALMA has been used, at least part of the time, for observations proposed by the

Figure 1. A clear statement from Wolfgang Wild, the ALMA Program Manager, on the status of ALMA was presented at the Community Days.

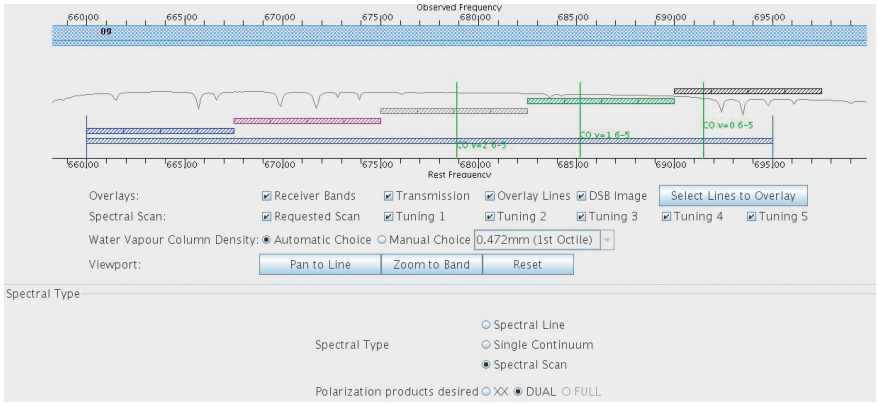

Figure 2. An example Observing Tool screen is shown for defining the spectral setup. In this example, a Band 9 spectral scan has been chosen, and the CO lines have been overlaid for visualisation.

international astronomical community since Early Science operations began with Cycle 0 in September 2011. It is currently obtaining data for Cycle 1, and the deadline for proposing Cycle 2 observations, scheduled to start in June 2014, was in December 2013. While construction has now officially ended, commissioning is still ongoing and the scientific capabilities of the array will continue to increase over the coming years. In Cycle 2, there will be at least 34 antennas available in the main array and nine 7-metre antennas together with two 12-metre antennas used in the ACA. The receiver bands offered are 3, 4, 6, 7, 8 and 9, corresponding to wavelengths of about 3.1, 2.1, 1.3, 0.87, 0.74 and 0.44 millimetres respectively. Polarisation observations will be possible for the first time for on-axis continuum observations in Bands 3, 6 and 7. Finally, antenna baselines of up to 1.5 kilometres are offered in Bands 3, 4, 6 and 7, while for Bands 8 and 9 baselines will be up to 1.0 kilometres.

One of the high-level goals of ALMA is that it should be accessible to the entire astronomical community, not just experienced submillimetre observers. This is facilitated by the comprehensive user support offered by the ALMA Regional Centres (ARCs), which have been set up in each of the three executives (Europe, North America and East Asia). The European ARC is made up of a network of nodes distributed across Europe that are coordinated by the ARC located at ESO. The ARCs make up the interface between the Joint ALMA Observatory located in Chile and the scientific community. Among other things they provide services for users, including extensive documentation (manuals, handbooks, video tutorials), an online Helpdesk facility and community events.

Community Days — presentations and tutorials

The ALMA Community Days held at ESO are part of a coordinated effort by the European ARC network to optimally prepare users for proposal submission, and similar events or presentation tours were organised by several of the ARC nodes for their local communities. They have so far taken place for every ALMA observing cycle (Randall et al., 2011; 2012); the Cycle 2 Community Days being the third such event. The format of the ESO Community Days has always been quite similar, starting off with a series of technical and scientific presentations followed by practical hands-on tutorials for the software most critical to proposal preparation. Held just a couple of weeks before the proposal deadline, the main aim is to help users finalise their scientific case and define a valid technical setup that will allow the proposed observations to achieve their aims.

In response to feedback received from the participants of previous ALMA Community Days, the Cycle 2 workshop focused more heavily on practical hands-on tutorials than previously. Only the morning of the first day was devoted to presentations, which gave attendees a quick overview of the ALMA status (see

Figure 1), recent science highlights and the user support services offered by the European ARC. The Cycle 2 policies and capabilities were also introduced, a special focus being placed on polarisation and single dish observations. After this, the participants were split into two groups (novice and advanced) according to their level of experience with submillimetre interferometry and started their hands-on tutorial sessions for the ALMA Observing Tool and the ALMA simulators.

The ALMA simulators come in two flavours: the Online Simulator Tool (OST), a web-based interface for simple simulations, and the simulation packages incorporated into the Common Astronomy Software Applications (CASA). Carrying out simulations for proposed observations is recommended, especially for spatially complex or extended sources in order to ascertain that the structure of interest can indeed be recovered. Simulations are also helpful in assessing whether ACA observations are needed in addition to those with the main array. While the novice group was given an introduction to interferometry concepts and focused mostly on the more intuitive OST, the advanced group spent more time working with the CASA-based simulation packages.

The ALMA Observing Tool (OT) is the main piece of software needed for proposal preparation. It is used to capture the scientific requirements of the observations, and contains a number of useful tools to help the user set up and visualise the required elements, e.g., the pointings and correlator modes, needed to achieve their science goal (see Figure 2). The OT also comes with an in-built time estimate and sensitivity calculator, and determines the needed array configuration(s) based on the user input. At the time of proposal submission, the OT runs a number of validation checks to ensure the technical setup of the proposed observations is sound. The OT is designed for intuitive use and comes with extensive documentation, but, due to the flexibility of the ALMA array and correlator, the technical setup of observations can be quite challenging.

The novice tutorial group therefore began with an introduction to submillimetre spectroscopy, where concepts such as basebands and spectral windows were explained. After this, a detailed demonstration was given on how to prepare a standard proposal; following that, participants were encouraged to work on their own projects under the supervision of tutors. The advanced tutorial featured a more concise demonstration covering mainly the changes made to the OT since Cycle 1, with more time available for individual work. The tutorials were truly interactive in that the information flow between the users and software experts went both ways, resulting not only in a better understanding of the tools on the side of the participants, but also yielding valuable feedback for the software scientists and developers. Many of the enhancements implemented for the ALMA software tools over the last year or two have in fact stemmed from user input, notably that given during face-to-face interactions such as practical tutorials.

Figure 3. The participants at the Cycle 2 ALMA Community Days collected together in the entrance hall of ESO Headquarters.

The ESO Cycle 2 ALMA Community Days were attended by 65 participants from all over Europe (see the photo in Figure 3), more than half of whom described themselves as novices to submillimetre interferometry. A large fraction of the novice participants had a background in optical/infrared observational astronomy, which is to be expected given the traditional ESO user community. More than two thirds of the participants were students or postdocs. Interestingly, a significant proportion (~ 1/3) of this year's participants had already attended one of the previous ESO ALMA Community Days, and stated that they would be interested in a similar workshop for future observing cycles. We can therefore conclude that these events are useful to the community and should be offered for at least as long as the scientific capabilities of ALMA are evolving.

Acknowledgements

Thanks to Izaskun Jimenez Serra and Evanthia Hatziminaoglou for helping with the general organisation, and to all the speakers for giving excellent presentations. The tutorials would not have been possible without the tutors: George Bendo, Andy Biggs, Bartosz Dabrowski, Liz Humphreys, Suzanna Randall, Anita Richards, Eelco Van Kampen and Martin Zwaan.

References

Randall, S. et al. 2011, The Messenger, 144, 39
Randall, S. et al. 2012, The Messenger, 149, 47

Fellows at ESO

David Jones

Unlike many of the other astronomers who have had their profiles printed on these pages, I had no "key moment" that turned my life towards astronomy, no childhood event which would turn my path towards the stars — rather it was a slow drift that I never noticed happening. I'd always been obsessed with understanding the world around me, asking "why?" even more often than a typical child (much to the frustration of my parents), which I suppose was the first sign of my inclination towards the sciences.

David Jones

By the time I reached 18 and had to choose what to do at university, I'd narrowed my path down to chemistry or physics and applied to study both at a variety of universities in the United Kingdom. Somehow, I ended up studying physics with astrophysics at the University of Manchester, home of the 76-metre Lovell Telescope and the Jodrell Bank Observatory. In spite of taking this course, I generally found the astronomy modules hard going and was frustrated by the astronomer's annoying habit of clinging to absurd nomenclature that makes little sense with our current understanding. However, I persisted and in my final year selected a project that involved the use of a 20-centimetre telescope to make your own observations (I'd been regularly accused of being more of an engineer than a physicist by my fellow classmates, and this project seemed to be the most hands-on one available).

Staying up all night beneath the cold and cloudy Manchester skies left a lasting impression; it was only then, at the age of 21, that I realised that I was doomed to be an astronomer and an observational astronomer to boot! After graduating, I continued in Manchester to study for my doctorate working with Myfanwy Lloyd and Tim O'Brien studying the effects of binarity on the late stages of stellar evolution, particularly on the formation of planetary nebulae. During my PhD, I was fortunate enough to spend a year working on the Spanish island of La Palma as a support astronomer for the 2.5-metre Isaac Newton Telescope. This experience, coupled with repeated observing trips to Chile, Mexico and South Africa, made it clear that an observatory was the place for me, and led me to join ESO as a Fellow with duties at the Paranal Observatory in March 2011. During my three years at ESO I've had the privilege of night work on two of the magnificent 8.2-metre Unit Telescopes, as well as supporting instrument operations as the FORS2 Fellow. Now entering my fourth and final year, I have moved to the Universidad de Atacama in Copiapó to help found an astronomy department in the heart of the desert which plays home to ESO and the world's most important telescopes.

Koraljka Muzic

I come from the small, historic town of Solin on the southern coast of Croatia. Nowadays it sounds surreal that someone still (relatively) young grew up in Europe without a phone and, for most of the time also without a TV. But maybe without today's omnipresent technology and with information more difficult to access, knowledge was more appreciated by the average kid. But maybe I'm just a bit old-fashioned... Anyway, our town simply didn't have the phone network until I turned 13 (and, citing my parents, why would anyone in their right mind want that noisy thing in the house?!) and the local TV mechanics were not able to make that device work for more than a month at a time.

So I grew up running around, making mud cakes and secret shelters, playing my guitar, and reading any book I could find along the way. From an early age, I remember being fascinated by nature in general, and spent a lot of time reading the ex-Yugoslavian classic *1000 zasto, 1000 zato* (1000 questions, 1000 answers), the only place to find answers to intriguing questions like: Why do we sweat and what happens while we sleep? Do elephants really fear mice? When did people start wearing clothes? Some questions turned out to be rather useful later in my life: What is smog? What are the Easter Island statues? Since when have people made beer and how did we invent coffee? And finally: What are the stars made of, and what exactly is the Milky Way?

As a teenager I was fascinated by Carl Sagan's *Cosmos* series, and tried to imagine the vast Universe from the perspective of our tiny planet (which resulted in a headache most of the time). But what I loved most was the natural and cultural diversity of this pale blue dot. I wanted to travel, and experience other places. The first small step was to start studying physics at the University of Zagreb in Croatia, where, during my final year, I had a taste of what astronomy really is about. This led me to start a PhD in astronomy at the University of Cologne and the Max-Planck Institute for Radioastronomy in Bonn. I chose to study the

Koraljka Muzic

very central parsec of the Milky Way, attracted by the beautiful images captured by NACO at the VLT, and the simple life philosophy of my soon-to-become supervisor. When I admitted that I was having trouble choosing between his project and another PhD project related to star formation, he just said: Don't worry, it's not a matter of life and death. And it obviously was not, not that time, and not at any time in my life after that. From time to time, I still find it healthy to remind myself of that.

After the PhD, I stayed for a short postdoc at the University of Cologne, until I got an opportunity to change not only the city I lived in, but also the science focus of my research. My old interest in star formation lead me to take up a postdoc dealing with brown dwarf formation at the University of Toronto. Two years later, I continued my continent-hopping tour, to land in Chile and start the ESO Fellowship.

My duty station is Paranal, and although we all like to complain about the tiring night shifts, it is a special and fascinating place to be. For me maybe even more special, since it is the first observatory I've ever been at, and Unit Telescope 1 is the first telescope I ever observed with (how spoiled that sounds)! I sit on my favourite spot near the mountain top, and look at that bare, calm, vast desert, and again the same old thought comes back of how small we are, and how preoccupied we are by insignificant things. Have I changed at all since I was 15?

Personnel Movements

Arrivals (1 Jan–31 March 2014)

Europe	
Aniyan, Suryashree (IN)	Student
Chira, Roxana-Adela (DE)	Student
Coccato, Lodovico (IT)	Astronomer
Csépány, Gergely László (HU)	Student
Lampinen, Mervi Johanna (FI)	Head of IT Unit
Saulder, Christoph (AT)	Student
Szécsényi, Orsolya (HU)	Contract Officer
Zahorecz, Sarolta (HU)	Student

Chile	
Perez, Maria Francisca (CL)	Procurement Officer

Departures (1 Jan–31 March 2014)

Europe	
Barbosa, Carlos Eduardo (BR)	Student
Bonzini, Margherita (IT)	Student
Bourtembourg, Reynald (FR)	Software Engineer
Gall, Elisabeth (DE)	Student
McPherson, Alistair (GB)	E-ELT Programme Manager
Michaleli, Anna (GR)	HR Advisor
Sirey, Rowena (GB)	Senior Advisor to the Director for Science

Chile	
Garrido, Hernan (CO)	Student
Grellmann, Rebekka (DE)	Fellow
Sippel, Anna (DE)	Student
Vera, Enrique (CL)	Dome Mechanic

ESO Studentship Programme 2014

The research studentship programme of the European Southern Observatory provides an outstanding opportunity for PhD students to experience the exciting scientific environment at one of the world's leading observatories for a period of up to two years.

ESO is the foremost intergovernmental astronomy organisation in Europe. Its approximately 110 staff astronomers, 40 Fellows and 50 PhD students conduct frontline research in fields ranging from exoplanets to cosmology, offering one of the most vibrant and stimulating scientific settings anywhere in the world.

ESO's studentship positions are open to students enrolled in a PhD programme in astronomy or related fields. Students accepted into the programme work on their doctoral project under the formal supervision of their home university, but they come to ESO to work and study under the co-supervision of an ESO staff astronomer, normally for a period of between one and two years. Studentships may be hosted either at ESO's Headquarters in Garching (Germany) or at ESO's offices in Santiago (Chile), where two additional positions per year are provided for students enrolled in South American universities.

Applicants and their home institute supervisors should agree upon and coordinate their research project jointly with their prospective ESO supervisor. For this purpose the ESO supervisor should be contacted well in advance of the application deadline (15 June 2014). A list of potential ESO supervisors and their research interests can be found at http://www.eso.org/sci/activities/personnel.html. A list of PhD projects currently being offered by ESO staff is available at http://www.eso.org/sci/activities/thesis-topics.html. It is strongly recommended that applicants plan to start their PhD studies at their home institute before continuing to develop their research projects at ESO.

ESO Chile students have the opportunity to visit the observatories and to get involved in small technical projects aimed at giving insights into the observatory operations and instrumentation. Such involvement is also strongly encouraged for Garching students. In addition, students in Garching may attend and benefit from the series of lectures delivered in the framework of the International Max-Planck Research School on Astrophysics.

Students who are already enrolled in a PhD programme in the Munich area (e.g., at the International Max-Planck Research School on Astrophysics or a Munich University) and who wish to apply for an ESO studentship in Garching, should provide a compelling justification for their application.

If you are interested in enhancing your PhD experience through an extended stay at ESO, then please apply by completing the web application form available at http://jobs.eso.org/.

Please include the following documents in your application:
– a cover letter;
– a Curriculum Vitae, including a list of publications, if any;
– copies of your university transcript and certificate(s) or diploma(s);
– a summary of your master's thesis project (if applicable) and ongoing projects, indicating the title and the supervisor (maximum half a page);
– an outline of the proposed PhD project highlighting the advantages of coming to ESO (recommended one page, maximum two);
– the names and contact details of your home institute supervisor and of the ESO local supervisor; these will be automatically invited to submit a recommendation letter, however, applicants are strongly advised to trigger these invitations (using the web application form) well in advance of the application deadline;
– a letter from the home institute that i) guarantees the financial support for the remaining PhD period after the termination of the ESO studentship, ii) indicates whether the prerequisites to obtain the PhD degree at the home institute have already been met.

All documents should be typed in English (but no translation is required for the certificates and diplomas).

The closing date for applications is 15 June 2014. Review of the application documents, including the recommendation letters, will begin immediately. Incomplete or late applications will not be considered.

Candidates will be notified of the results of the selection process during July–August 2014. Studentships will normally begin between August 2014 and March 2015.

Further information

For more information about the studentship programme please see:
http://www.eso.org/studentship

For a list of current ESO staff and fellows, and their research interests, please see:
http://www.eso.org/sci/activities/personnel.html

A list of PhD projects currently being offered by ESO staff can be found at:
http://www.eso.org/sci/activities/thesis-topics.html

Details on the employment conditions and benefits are available at:
http://www.eso.org/public/employment/student.html

For any additional questions please contact:
For Garching: Eric Emsellem, Email: eric.emsellem@eso.org
For Chile: Claudio De Figueiredo Melo, Email: cmelo@eso.org

Although recruitment preference will be given to nationals of ESO Member States (members are: Austria, Belgium, Brazil, the Czech Republic, Denmark, Finland, France, Germany, Italy, the Netherlands, Portugal, Spain, Sweden, Switzerland and United Kingdom) no nationality is in principle excluded.

The post is equally open to suitably qualified female and male applicants.

IC 2220, called the Toby Jug Nebula, is shown in a colour composite formed from FORS1 broad-band filter images (*B*, *V* and *R*) and narrow band images ([O III] and Hα). The dust in the ejected bipolar nebula is illuminated by its central red giant star HD 65750. See Release eso1343 for details.

Annual Index 2013 (Nos. 151–154)

Subject Index

Astronomical Science

Astronomical News

Author Index

ESO, the European Southern Observatory, is the foremost intergovernmental astronomy organisation in Europe. It is supported by 15 countries: Austria, Belgium, Brazil, the Czech Republic, Denmark, France, Finland, Germany, Italy, the Netherlands, Portugal, Spain, Sweden, Switzerland and the United Kingdom. ESO's programme is focused on the design, construction and operation of powerful ground-based observing facilities. ESO operates three observatories in Chile: at La Silla, at Paranal, site of the Very Large Telescope, and at Llano de Chajnantor. ESO is the European partner in the Atacama Large Millimeter/submillimeter Array (ALMA) under construction at Chajnantor. Currently ESO is engaged in the design of the European Extremely Large Telescope.

The Messenger is published, in hard-copy and electronic form, four times a year: in March, June, September and December. ESO produces and distributes a wide variety of media connected to its activities. For further information, including postal subscription to The Messenger, contact the ESO education and Public Outreach Department at the following address:

ESO Headquarters
Karl-Schwarzschild-Straße 2
85748 Garching bei München
Germany
Phone +49 89 320 06-0
information@eso.org

The Messenger:
Editor: Jeremy R. Walsh;
Design, Production: Jutta Boxheimer;
Layout, Typesetting: Mafalda Martins;
Graphics: Roberto Duque.
www.eso.org/messenger/

Printed by G. Peschke Druckerei GmbH,
Schatzbogen 35,
81829 München, Germany

ISSN 0722-6691

Contents

Front cover: VLT Survey Telescope (VST) colour composite image of part of M8 (NGC 6523), known as the Lagoon Nebula. The image was taken in the VST/OmegaCam Photometric Hα Survey of the Southern Galactic Plane and Bulge (VPHAS+), one of the VST Public Surveys. VPHAS+ surveys the stellar and ionised gas content of the southern Plane of the Milky Way with VST broadband images (*u, g, r, i*) and a dedicated Hα mosaic filter. M8 is a Galactic star-forming region at about 1.25 kpc containing hot stars, such as the O7V star Herschel 36 in the central Hourglass Nebula, which ionise the surrounding gas cloud producing the Hα emission prominent in this image. See Release eso1403 for further details.